Black Slate - Surface Alteration Due to Fungal Activity

Dissertation

zur Erlangung des akademischen Grades doctor rerum naturalium
(Dr. rer. nat.)

vorgelegt dem Rat der Chemisch-Geowissenschaftlichen Fakultät
der Friedrich-Schiller-Universität Jena

von Dipl.-Biol. Daniela Siegel

geboren am 22. Januar 1980 in Altenburg

Gutachter

1. Prof. R. Gaupp, Jena

2. Prof. E. Kothe, Jena

Tag der öffentlichen Verteidigung: 16.Juli 2010

Abstract

Black slates of different oxidation states and graphite samples as pure carbon source were incubated with the white-rot fungus *Schizophyllum commune* 4-39 for 3 months. Investigations by SEM showed fungal affinity to rough surfaces. Oxidatively weathered, bleached black slate samples have more micropores and increased surface roughness than unweathered samples. Unpolished and polished bleached black slate samples were colonized best by fungal hyphae. The hyphae often entered pores. Etch pits induced by fungal activity could be observed which were then quantified by vertical scanning interferometry (VSI). The etch pits measured 3 – 4 µm in width and 180 – 200 nm in depth. In contrast to black slate samples, more etch pits were found on graphite surfaces. Moreover, they showed a more elongated morphology and branches reminiscent of fungal growth morphology. Under laboratory conditions, *Schizophyllum commune* was able to degrade about 0.03 $\mu m^3/\mu m^2$ rock material during 3 months of incubation. It could be shown that collapsed hyphae material remained in their etch pits even after sample preparation which was caused by strong fungal fixation to the rock surfaces. The higher carbon content and the "softness" of pressed graphite thus allow for earlier fungal attachment and higher dissolution rates. Amounts of nitrogen could be proved by chemical analyzing techniques (x-ray photoelectron spectroscopy and electron microprobe) at all incubated rock samples. Nitrogen increased eminently on rock surfaces due to fungal colonization. Amounts of nitrogen were detected both on hyphae and former hyphae attachment areas. This indicates the presence of fungus and/or fungal excreted proteins such as hydrophobins for attachment or enzymes for degradation. The accumulation of iron within fungal hyphae, which were grown on iron containing black slates, demonstrates microbial influence on metal mobility during rock alteration. Furthermore, biomineralization on incubated black slate and graphite samples could be observed. The biominerals were often spatially associated with fungal hyphae. Biominerals with amorphous or crystalline shapes varied between 3 and 100 µm in mean size. Chemical analyses suggested magnesium phosphate and calcium rich biominerals. Additionally, small lateral structures occurred at fungal hyphae, some of which extended into elongated structures attached to the rock surface or to other hyphae.

Kurzfassung

Schwarzschiefer mit unterschiedlichen Verwitterungsgraden sowie Graphitproben wurden mit dem Weißfäulepilz *Schizophyllum commune* 4-39 für mindestens drei Monate bei Raumtemperatur inkubiert. Untersuchungen mit dem Rasterkraftelektronenmikroskop zeigten die Affinität des Pilzes zu rauen Oberflächen. Sowohl unpolierte als auch polierte, vor allem durch oxidative Verwitterung gebleichte Schwarzschieferoberflächen wurden am stärksten von Pilzhyphen besiedelt. Die Hyphen verblieben am häufigsten in Porenräumen oder tieferen Depressionen. Mit vertikaler Weißlichtinterferometrie (VSI) konnten pilzinduzierte Ätzgrübchen gemessen und quantifiziert werden. Die Ätzgrübchen waren zwischen 3 und 4 µm breit und im Durchschnitt 180 - 200 nm tief. Im Gegensatz zu den Schwarzschieferproben konnten auf den Graphitoberflächen mehr Ätzgrübchen erfasst werden, die zudem eine länglichere und verzweigte Morphologie, ähnlich der der Pilzhyphen, aufwiesen. Innerhalb von 3 Monaten konnte *Schizophyllum commune* unter Laborbedingungen etwa 0,03 µm^3/µm^2 (organisches?) Gesteinsmaterial entfernen. Desweiteren konnte nachgewiesen werden, dass die durch Trocknung kollabierten Pilzhyphen in ihren eigenen Ätzgrübchen verbleiben und dadurch besser auf bzw. in den Oberflächen haften können. Die „Weichheit„ der gepressten Graphitproben und ihr Gehalt an Kohlenstoff beeinflussen den mikrobiellen Materialabbau offensichtlich stärker. Mithilfe chemischer Oberflächenanalysen (Röntgen-Photoelektronenspektroskopie und Elektronenstrahl-Mikrosonde) konnte Stickstoff auf allen inkubierten Proben nachgewiesen werden. Im Zuge der Pilzbesiedlung nahm der Stickstoffgehalt auf den Gesteinsoberflächen sichtbar zu. Stickstoff trat an Hyphen, sowie verstärkt an ehemaligen Hyphen-Kontaktflächen, auf. Das weist einerseits auf die vormalige Anwesenheit von Pilzen auf den Proben, andererseits auch auf die Anwesenheit von extrazellulären Proteinen, wie Hydrophobine und Enzyme, hin. Die Anreicherung von Eisen in Pilzhyphen, die auf eisenhaltigen Schwarzschiefern gewachsen sind, zeigt deutlich den mikrobiellen Einfluss auf die chemische Gesteinsverwitterung. Nebenbei konnte die Bildung von Biomineralen auf Schwarzschiefer - und Graphitproben beobachtet werden. Diese waren fast ausschließlich an Pilzhyphen aufzufinden. Die amorphen und kristallinen Gebilde erreichten mit Ausnahmen durchschnittlich Größen von 3 – 100 µm. Chemische Analysen deuten auf

kalzium- bzw. magnesiumphoshatreiche Biominerale hin. Weiterhin konnten kleine laterale Strukturen auf den Hyphen beobachtet werden. Bei einigen kleinen lateralen Strukturen wurden längliche (organische) Ausscheidungen, die die Gesteinsoberfläche oder andere Hyphen berührten, entdeckt.

Content

List of Abbreviations

AFM	atomic force microscopy
AV	average value
BGI	Bayerisches Geoinstitut (Bavarian Research Institute)
BS	black slate sample with unbleached and bleached area on same sample
BSE	back-scattered electron
C_{org}	organic carbon
CYM	complex yeast media
DFG	Deutsche Forschungsgemeinschaft (German Research Foundation)
EDX	energy dispersive x-ray microanalysis
EMP	electron microprobe
IGW	Institut für Geowissenschaften (Institute of Earth Science)
IPHT	Institute of Photonic Technology
F	surface area ratio
FSU	Friedrich-Schiller-Universität
G	graphite sample (Plano GmbH, Wetzlar)
GZG	Geowissenschaftliches Zentrum Göttingen
H_2O_2	hydrogen peroxide
LA-ICP-MS	laser ablation inductively coupled plasma mass spectroscopy
MM	minimal medium
MPD	measuring point diameter
MPI BGC	Max Planck Institute for Biogeochemistry
M2	black slate sample, unbleached (Morassina mine, Schmiedefeld, Thuringia)
M3	black slate sample, bleached (dump, Schmiedefeld, Thuringia)
OM	organic matter
RIE	reactive ion etching
R_a	arithmetic average
R_q	root mean square
R_t	roughness depth
σ	standard deviation
S. c.	*Schizophyllum commune*
SE	secondary electron
SEM	scanning electron microscopy

List of Abbreviations

TOC   total organic carbon

TP   topography scan

VSI   vertical scanning interferometry

WDX   wavelength dispersive x-ray spectroscopy

wt. %   weight percent

XPS   x-ray photoelectron spectroscopy

ZELMI   Zentraleinrichtung Elektronenmikroskopie

List of Tables

List of Figures

List of Figures

List of Figures

1. Introduction

1.1   Aims and Objectives

Microbial colonies can develop on lithic surfaces depending on various parameters (Brehm et al., 2005; Brill, 1994; Chertov et al., 2004; Gadd, 2010; Kim et al., 2004; Phillips and LappinScott, 1997; Visscher and Stolz, 2005), but only limited knowledge exists for fungal-induced corrosion on multi-component rocks like fine-clastic sediments, such as claystones and shales or slates. Therefore, incubation experiments with the wood-rotting fungus *Schizophyllum commune* on controlled black slate surfaces were intended to investigate the influence of the microbial activity. *Schizophyllum* is able to excrete laccase, an unspecific oxidase that is able to degrade lignin. The structure of kerogen fractions within black slates suggests that similar components with structure comparable to lignin are present which might also be prone to degradation by laccase reactions (Catcheside and Mallett, 1991; Hofrichter et al., 1997a; Wengel et al., 2006). Furthermore the influence of unbleached and bleached (oxidized) slates to fungal activity will be investigated, because they contain different pore systems and different surface roughness (Fischer and Gaupp, 2005; Littke, 1993). Moreover graphite samples as pure carbon source shall prove to have a destructive effect on carbon compounds.

On this account the surface area will be investigated both by surface topology analyzing methods and by surface chemical analysis techniques. Incubated rock samples will be examined at the microbe-rock/mineral interface. Roughness analyses, presence and distribution of elements will contribute to elucidate fungal impact on black slate weathering.

This project will focus on the change of surface morphology and chemistry in weathering black slates of different oxidation states due to fungal activity.

1.2   State of the Research

1.2.1   Geological Background – Black Slate

Slates are low-grade, regionally metamorphosed rocks, which are highly fissile and fine grained. The fissility results from the parallel alignment of numerous fine phyllosilicate minerals (e.g. muscovite and chlorite) induced by compressive tectonic deformation (Allaby, 2008). Thus black slates are slates which are rich in sulfides, such as pyrite, and organic material deposited under barred basin conditions (McGraw-Hill, 2004). They often contain large amounts of heavy metals. Dark colored black shales and slates are defined to contain more than 0.5 wt. % organic carbon (Fischer et al., 2007).

Black slates, shales and other sediments enriched in organic matter are the most important crustal reservoirs of organic carbon. They are deposited in marine and continental settings under reducing conditions (Littke, 1993; Petsch et al., 2000; Petsch et al., 2005). Redox-sensitive elements such as carbon, sulfur, nitrogen, iron, phosphorus, molybdenum and uranium are often enriched in these sediments (Yamaguchi, 2003). Black slates experience several changes when they are exposed to oxygen. In the early stage of oxic weathering, pyrite breaks down and releases sulfurous acid to the environment (Alastuey et al., 1999; Craig et al., 1998; Evangelou, 1995; Littke et al., 1991). This may lead to acid mine drainage (AMD) (Dold et al., 2005; Evangelou, 1995). Organic matter (OM) is converted to carbon dioxide and/or released as dissolved or particulate organic matter to streams and groundwater. It has been estimated that weathering of black shale causes about 12% of the estimated annual CO_2 flux from oxidative weathering of sedimentary rocks (Jaffe et al., 2002). Oxidative weathering of OM in sedimentary rocks contributes significantly to the global cycling of carbon (Berner, 2003; Petsch et al., 2005). Several studies have shown an organic matter decrease in surface-exposed black shales (Littke et al., 1991). Quantifications of the pore-space area and the specific surface area of black and bleached slates suggested an isotropic degradation of OM during oxidation (Fischer and Gaupp, 2004; Fischer and Gaupp, 2005; Fischer et al., 2007). The internal rock surface area decreased dramatically during OM dissolution from ~15 m^2/g to ~5 m^2/g. A linear relationship was found between the decrease of internal rock surface

area and quantity of OM dissolved (Fischer and Gaupp, 2005). During dissolution, the total external surface area of black slates will increase by 0.2×10^6 m^2 for every cubic meter of black shale with total organic carbon content (TOC) of 10 wt. %. Oxidative weathering is an important rock alteration process at or near the earth's surface. Fischer et al. (2007) showed oxidative degradation within only a few decades. Roofing slates decreased from initially 0.73 - 1.7 wt. % to ~0.50 wt. % after almost 100 years, respectively. The organic carbon content of alum slate mining waste decreased from > 7.5 wt. % at the base (5 m below surface) to < 1 wt. % at the top of a dump during an exposure time of 53 years. In addition to natural processes, human-induced rock alteration processes contribute significantly to oxidative weathering of minerals and rock, often providing enhanced accessibility of oxygen to rocks through, for example, mining processes or the heaping up of mining waste (Fischer et al., 2007; Fischer et al., 2009; Fouad and El-Rakaiby, 2009). Redox-sensitive metals are mobilized to various extents and enter streams and groundwater, sometimes in high (toxic) concentrations (Fouad and El-Rakaiby, 2009).

Uranium producing companies are able to exploit uranium containing black slates and shales. Between 1954 and 1991, the SDAG Wismut produced about 113,000 t uranium, which originated from the Thuringian mining area around Ronneburg, Germany (Grawunder et al., 2009; Jakubick et al., 1997; Wismut, 1994). Leaching heaps were built up by waste rocks with a low grade of uranium mineralization (uranium content < 300 g/t; Grawunder et al., 2009). Until 1978, uranium was leached with acid mine drainage from underground mines (AMD; pH2.7 - 2.8) and subsequently with sulphuric acid (10g/l) (Wismut, 1994). During this leaching process, leachate infiltrated through the lining of the heap and accumulated in the sediments underneath. Later, leaching was stopped and during remediation processes the heaps were filled into the nearby open pit and the basement areas were re-contoured and covered with heterogeneous allochthonic soil substrate (Carlsson and Büchel, 2005; Grawunder et al., 2009). Now, different scientists investigated and investigate test sites to examine the effects of released heavy metals, such as uranium, in (ground) water, soils, microorganisms and plants. For example, most heavy metals are bound to the residual fraction and to Fe- and Mn-oxides (Grawunder et

al., 2009) and reductive microbial processes did not have a major impact on metal retention at this site (Burkhardt et al., 2009).

1.2.2   Microbial Background – *Schizophyllum commune*

The filamentous fungus *Schizophyllum commune* Fries is found worldwide (Cooke, 1961), except in Antarctica. The gills of basidiomycete split when the fungus dries out. Thus the names "Split Gill" (English) or "Gemeiner Spaltblättling" (German) were derived. *Schizophyllum* is investigated for its complex mating system consisting of thousands of "sexes" (Fowler et al., 1999; Raper and Fowler, 2004). The fungus occurs year round on wood as saprobic; solitary, scattered or in overlapping clusters on decaying hardwoods.

Schizophyllum is a very successful wood decaying fungus that causes white rot. The fungus is able to infect trees with spores liberated from fruiting bodies, as well as by mycelium that grows from injured onto healthy trees (Snieskiene and Juronis, 2001). As a wood-rotting fungus, *Schizophyllum commune* excretes wood decaying enzymes such as laccases. These laccases, copper-containing oxidases enzymes, are able to degrade lignin (Arora and Sharma, 2010; Boyle et al., 1992; De Vries et al., 1986; Zhao and Kwan, 1999). Lignin is a complex oxyphenyl propanoid polymer found in all vascular plants, including herbaceous species. Lignin provides rigidity, support, and protection to the plants (Arora and Sharma, 2010; Dean and Eriksson, 1992). It is synthesized by one-electron oxidation of the precursors; p-coumaryl alcohol, coniferyl alcohol, and sinapyl alcohol, generating phenoxy radicals which then undergo non-enzymatic polymerization. The biological degradation of lignin is one of the most important parts of the biospheric carbon and oxygen cycle (Hagedorn and Machwitz, 2007; Lundell et al., 2010). As the second most abundant organic compound, lignin continually contributes enormous amounts of organic carbon to the biosphere. In addition, lignin biosynthesized by plants is mineralized and returned to the atmosphere as CO_2 by the same degradative pathways (Crawford and Crawford, 1980).

However, substrates are not oxidized directly by laccases, due to their large size which restricts access to the enzyme active site or because of their particularly high redox potential. Thus the oxidized radical formed then are able to interact with the substrates (Arora and Sharma, 2010; Riva, 2006). Because of their high relative nonspecific oxidation capacity, laccases have been found as useful biocatalysts for diverse biotechnological applications. The application of laccases can be divided into industrial-technical, chemically synthetic, or environmental as far as food, medicinal, and personal care fields (Sharma and Kuhad, 2008).

Hydrophobins were first isolated from *Schizophyllum commune* (for review see Wessels, 1993). Hydrophobins are a remarkable class of small cysteine-rich proteins found exclusively in fungi (De Vries et al., 1993; Wessels, 1993). They self-assemble to form robust polymeric monolayers that are highly amphipathic (Wang, 2004; Wösten et al., 1995) and play numerous roles in fungal biology, such as in the formation and dispersal of aerial spores and in pathogenic and mutualistic interactions. The polymeric form can be reversibly disassembled and is able to reverse the wettability of a surface, leading to many proposals for nanotechnological applications (Sunde et al., 2008). The surprising properties of hydrophobins and their potential for commercialization have led to substantial efforts to delineate molecular structure and function (Scholtmeijer et al., 2004; Sunde et al., 2008).

Fungi also show evidence for the bioremediation of uranium and rare earth elements (Merten et al., 2005). High concentrations of uranium and rare earth elements in mine seepage water were significantly reduced by incubation with *S. commune* (Kothe et al., 2005)*. Schizophyllum commune* has also been shown to take up and concentrate cadmium from the environment (Lilly et al., 1992).

1.2.3   Bio-Geo Interactions

Studies of bio-geo interactions in recent years focused mainly on interactions between bacteria and minerals (Barker et al., 1998; Dong et al., 2000; Kalinowski et al., 2000; Lee

and Fein, 2000; Lower et al., 2001; Lüttge and Conrad, 2004; Roden and Zachara, 1996; Santelli et al., 2001). A few studies on fungal influence on minerals (Adeyemi and Gadd, 2005; Burford et al., 2006) or multi-component rocks (Burford et al., 2003; Hoffland et al., 2002; Hoffland et al., 2004; Hofrichter et al., 1999; Warscheid and Braams, 2000) were performed as well.

It could be demonstrated that certain basidiomycetes (white-rot and litter-decaying fungi) possess the ability to depolymerize coal humic substances effectively to lower molecular mass products (Fakoussa and Hofrichter, 1999; Hofrichter et al., 1999; Ralph et al., 1996). Hofrichter et al. (1999) showed that wood-rotting basidiomycetes are capable of degrading/depolymerizing macromolecular fractions of low-rank coal (lignite, brown coal). Figure 1 proposed a scheme for the degradation of low-rank coal (lignite) by ligninolytic basidiomycetes. Synergistic enzymes such as lignin peroxidases and laccases, chelating dicarboxylic acids, manganese peroxidases and additional mediating agents enable low-rank coal degradation.
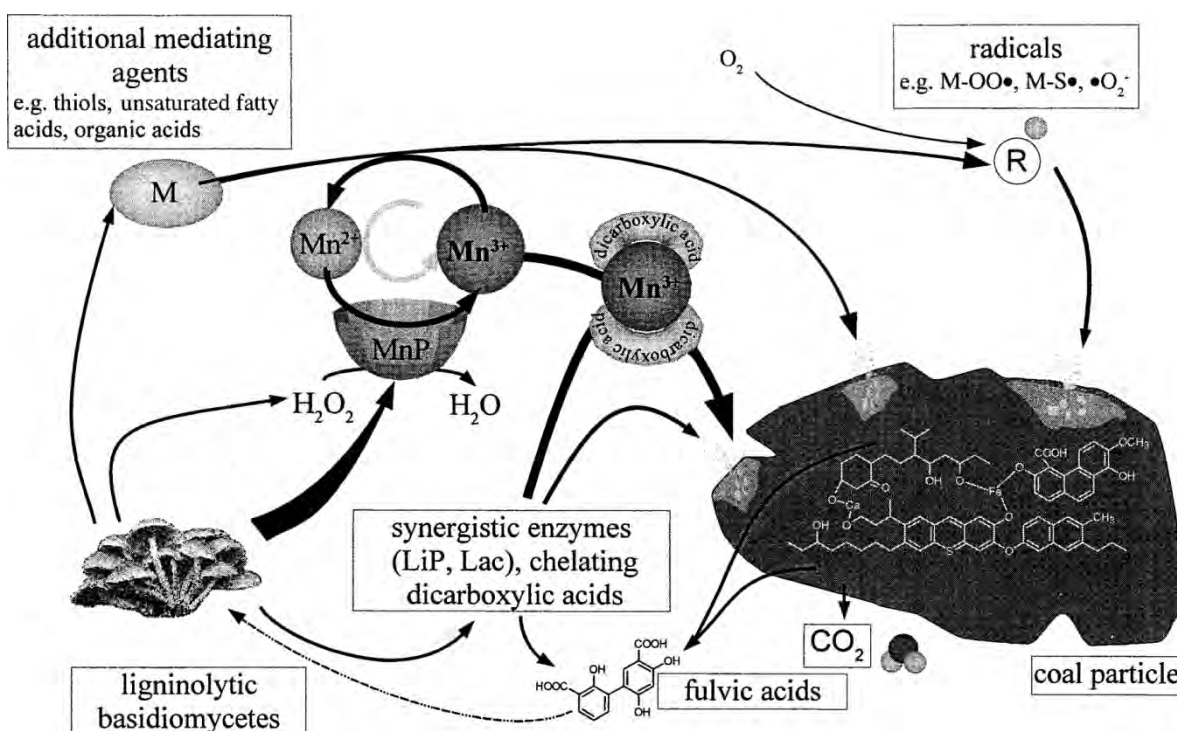
Figure 1: Proposed scheme for the degradation of low-rank coal (lignite) by ligninolytic basidiomycetes; MnP-manganese peroxidase, LiP-lignin peroxidase, Lac-laccase, M-mediator, R-radical (Hofrichter et al., 1999)

Wengel et al. (2006) focused on fungal influence on charcoal (CC) as short-time end product of high tempered wood in the absence of oxygen and black shales (BS) which were formed in an abiotic, geogenic long-time process. Incubation with *Schizophyllum commune* for 84 days caused carbon decrease in the solid fraction. It has been confirmed that this carbon was released as dissolved organic carbon (DOC) by the fungus. At the same time, biological oxidation processes increased iron and manganese concentrations in the aqueous phase significantly.

Other fungi have been reported from a wide range of rock types including limestone, soapstone, marble, granite, sandstone, andesite, basalt, gneiss, dolerite, amphibolite and quartz, even from the most harsh environments, e.g. hot and cold deserts (Gorbushina et al., 1993; Staley et al., 1982; Sterflinger, 2000). Fungi are an important component of lithobiotic communities (an association of microorganisms forming a biofilms at the microbe-mineral interface), where they interact with the lithic substrate, mainly laminar minerals, both geophysically and geochemically (Burford et al., 2003; Burford et al., 2006; de los Rios et al., 2009). Biomechanical deterioration of rocks is believed to occur through extensive penetration by fungal hyphae (e.g. into decayed limestone), and by burrowing into otherwise intact mineral material. Hyphal penetration, for example, can occur along crystal planes in calcitic and dolomitic rocks (Koestler, 2002; Sterflinger, 2000). To gain access fungal hyphae can exploit grain boundaries (Hoffland et al., 2002).

1.3   Strategy

To investigate black slate alteration due to fungal weathering, appropriate rock and microbial materials have to be selected. Bleached and unbleached black slate samples will be used to study oxidization effects upon microbial impact. Additionally, graphite samples shall demonstrate fungal influence on carbon surfaces.

Geochemical and petrophysical properties of black slates will be analyzed. In consequence of incubation experiments with *Schizophyllum commune* petrophysical and geochemical surface changes will be investigated.

Modifications of rock surface topology and roughness due to fungal incubation will be examined by scanning electron, atomic force and vertical scanning interferometric microscopy.

The determination of the total organic carbon content and distribution of elements, including nitrogen, silicium, aluminum, potassium, phosphorus, magnesium, iron, and sulfur will elucidate the influence of rock elements and mineral composition on *Schizophyllum commune* growth as well as the influence of the fungus on the rock components.

2. Material & Methodology

2.1 Used Material

Different types of rock material were used for incubation experiments. The main focus was set on black slates with different content of carbon (unbleached and bleached). Supplementary graphite was used as pure carbon source. The white-rot fungus *Schizophyllum commune* was used as rock colonizing microorganism.

2.1.1 Rock Samples

qh - Holozän
qp - Pleistozän
tB - Tertiär: Basalte
tS - Tertiär: Sedimente
kr - Kreide
j - Jura
ko - Oberer Keuper (Rät)
km - Mittlerer Keuper
ku - Unterer Keuper
mo - Oberer Muschelkalk
mu+mm - Mittlerer und Unterer Muschelkalk
sm+so - Oberer und Mittlerer Buntsandstein
su - Unterer Buntsandstein

z - Zechstein
ro - Oberrotliegend
co/ruS - Oberkarbon/Unterrotliegend: Sedimente
co/ruV - Oberkarbon bis Unterrotliegend: Vulkanite
cu - Unterkarbon
coP - Plutonite des Oberkarbon
doG - Diabase des Oberdevon
d+si - Devon und Silur
o - Ordovizium
cbo - Kambro-Ordovizium
np - Neoproterozoikum
pzKr - Metamorphite, mesozonal

Figure 2: geological map of Thuringia (TLUG), yellow circles mark sampling locations

The investigated black slate samples originate from the Morassina mine in Schmiedefeld (Thuringia, Germany). On the one hand the lower Silurian (Figure 2), low-grade metamorphic black slate samples (Fischer et al., 2007; Heuse et al., 1994; Schlegel, 1995) were collected unbleached freshly mined from the middle horizon of the subsurface mine (named M2, Figure 3) and on the other hand bleached and partly weathered from the waste dump (named M3, Figure 3) in front of the mine. The origin of geological setting of the bleached sample M3 is unknown.
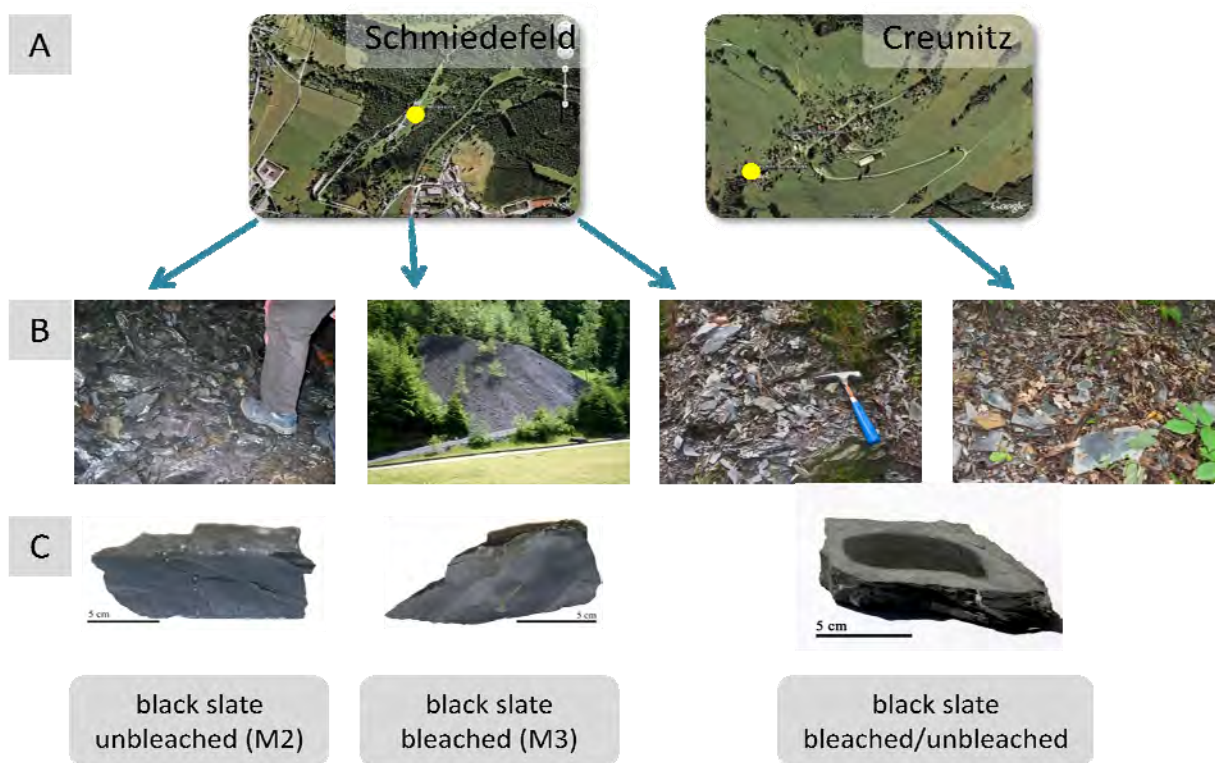
Figure 3: **A)** satellite picture (Google Earth) yellow circles mark the sampling places; **B)** mine, dump and outcrops; **C)** black slate samples

Furthermore samples with partly weathered and unweathered areas on each sample (named BS, Figure 3C) were collected from Schmiedefeld and Creunitz (Thuringia, Germany, Figure 3).

The utilized graphite samples were spectral clean graphite rods (6.4 mm in diameter, Plano GmbH, Wetzlar) which are, normally used for carbon coating. The impurity rate is less than 2 ppm.

The rock specimens were cut into 1 cm x 1 cm x 0.3 - 0.5 cm small pieces (Figure 4) with rock saws (Naicotec and Struers discoplan-TS, Institut für Geowissenschaften der Friedrich-Schiller-Universität Jena), washed with distilled water and polished afterwards on one side (black slate samples polished by T. Beckmann, Schwülper-Lagesbüttel and H. Schulze,
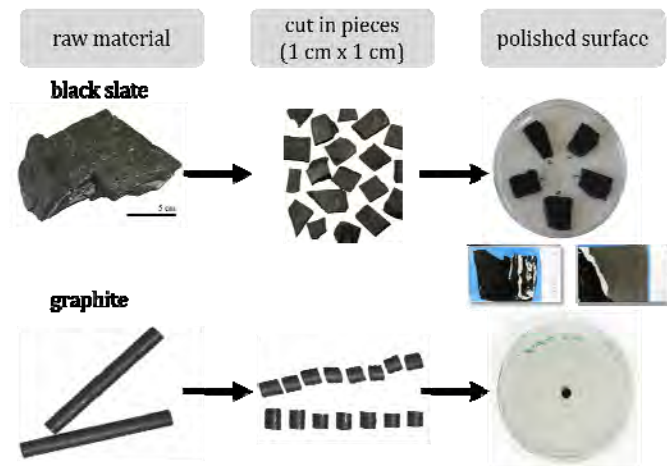
Figure 4: way of sample preparation

BGI Bayreuth, graphite samples polished by S. Bergmann, Institut für Geowissenschaften der Friedrich-Schiller-Universität Jena). Thin-slides without cover slips were made of the sample M2 and M3 (Figure 4).

The samples used for incubation experiments were labeled by laser (cross, 1 x 1 mm) in order to allow same orientation during different investigations.

2.1.2 Fungi

The white-rot fungus *Schizophyllum commune* (Figure 5) was used for microbial incubation experiments. The monokaryotic strains 4-40 and 4-39 (strain collection at the Fungal Reference Center Jena) were selected from the strain collection of the Institut für Mikrobielle Phytopathologie, Friedrich Schiller Universität Jena. Due to the "thin" mutation of strain 4-40 (Figure 7 C), only *Schizophyllum commune* 4-39 was used for main experiments with polished rock samples.

Figure 5: *Schizophyllum commune* growth on CYM solid media

For experiments minimal medium (MM: 2 g aspartate, 1 g K_2HPO_4, 0.5 g KH_2PO_4, 0.5 g $MgSO_4 \times 7H_2O$, 120 µg thiamine chloride, 5 N NaOH pH 6.3 and 15 g agar per liter of distilled water) and complex yeast medium (CYM: 2 g peptone, 2 g yeast extract, 20 g glucose, 0.5 g $MgSO_4 \times 7H_2O$, 0.5 g KH_2PO_4, 1 g K_2HPO_4 and 18 g Difco Bactoagar per liter of distilled water) were used.

In order to improve fungal growth, the main incubation experiments were done with CYM.

2.2   Incubation Experiments

To sterilize the black slate and graphite samples, they were treated with UV light for 24 hours. Sometimes it was necessary to supplementary sterilize the samples for two hours with ethanol (70 %). The sterilized samples were stored on CYM agar plates at room temperature on their own. If no contaminations were detected after one week, the samples were treated with *Schizophyllum commune* (Figure 6). Contaminated rock samples were discarded. The fungus, which was placed beside the samples, only came in contact with the rock surface through aerial hyphal growth. To minimize water evaporation, a flexible film (Parafilm) around the petri dishes was used for sealing. The chosen incubation conditions of 25 ± 1 °C were kept for 3 months. The control samples were cultivated without fungi (Figure 7 A).
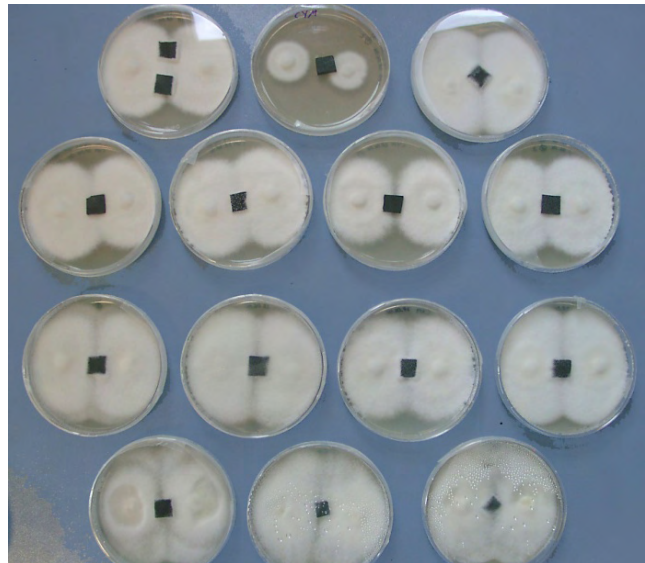
Figure 6: incubation experiments with *S. commune* and black slate

A few unpolished samples were incubated for one year. The fungal growth was observed by light microscopy (Zeiss Jenalab) and photographs taken weekly (Figure 13).

Figure 7: agar plates with black slate samples; **A)** control without the fungus; **B)** sample with *S. commune*, 4-39); **C)** "thin" mutation of *Schizophyllum commune* 4-40 with decreased aerial hyphae

2.2.1   Removal of Fungal Hyphae

To investigate the rock surfaces after incubation, the mycelial mat was removed by different methods. The best results were achieved by removing the hyphal mat by tweezers (Figure 8). Growing into each other, the hyphae were able to create a strong net which can be picked up on one side and completely peeled from the entire rock surface. Without scratching the surface, this method left an intact rock surface in contrast to other methods. Only a few hyphae still remained visible on the surface (in pores or depressions). The smoother the surface, the less hyphae remained (Figure 17 C).
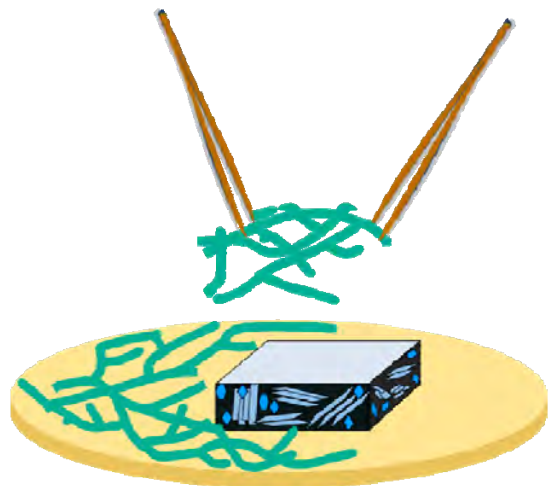
Figure 8: schematic of hyphae removal with tweezers

The method of plasma etching was also used to try removing hyphae from the surfaces. Reactive ion etching (RIE) uses chemically reactive plasma to remove material deposit on surfaces. The plasma is generated under low pressure by an electromagnetic field. Plasma high-energy ions attack the surface and react with it (Jafri and Hassan, 2008). Black slate (88) and graphite samples (119) were treated 20 minutes with oxygen RIE (W. Morgenroth, IPHT Jena). The changes of surface topology were detected by a surface profiler (DEKTAK 32) (W. Morgenroth, IPHT Jena). The graphite sample (119) lost about 2500 nm and the black slate sample 270 nm (appendix) in height. This loss of material seemed unacceptable to study surface topology. Additionally, the black slate sample was investigated by scanning electron microscopy (SEM, Figure 9). The hyphae were destructed but not removed completely. A longer plasma residence time is possibly more successful to remove fungi. But to examine surface changes due to fungal colonization, further rock material loss would influence the results negatively.
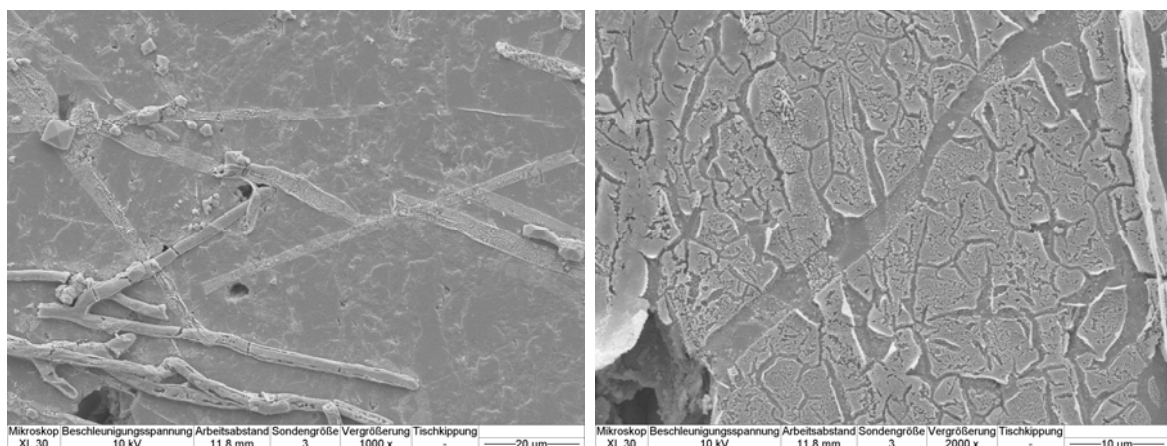
Figure 9: SEM image showing the influence of plasma etching to hyphae.

Further tests to remove the fungus were done with different chemicals. One graphite sample (101) was incubated 48 hours with hydrogen peroxide (30 %). The sample was investigated before and after H_2O_2 treatment with VSI (Rice University, USA). Minor amounts of organic matter were removed (Chapter 3.1.2, appendix) but the hyphae themselves resisted hydrogen peroxide.

The cell wall destroying enzyme caylase C3 (Cayla, Toulouse) was used to digest the hyphal walls. The enzyme mixture (0.2 g caylase C3 +2 ml 1M $MgSO_4$ + 2 ml distilled water)

was added to the rock sample (256). Then, the sample was shaken over night (13 hours) at 30 °C and subsequently rinsed with distilled water followed by 3 % Tween 20 solution which was added as detergent (5 minutes). Subsequently, the sample was flushed again with distilled water. All prepared samples (except the samples prepared for critical point drying) were dried and separately stored in small dry sterile plastic boxes.

2.3   Surface Topology

To investigate surfaces at micrometer to nanometer range, microscopy is necessary. Therefore, optical, scanning electron, atomic force and vertical scanning interferometric microscopy were used.

2.3.1   Optical Microscopy

The rock samples were examined before, during and after incubation with *Schizophyllum commune* by reflected-light microscopy (Zeiss, Jenalab). The fungal growth and thin section of black slate samples were obtained by transmitted-light microscopy (Zeiss Jenalab and Zeiss Axioplan).

2.3.2   Scanning Electron Microscopy (SEM)

To visualize microbe-rock interactions, scanning electron microscopy (SEM, Philips XL 30 ESEM, Institut für spezielle Zoologie, Friedrich-Schiller-Universität Jena) was used. The analyses ran with an acceleration voltage of 20 kV, a spot size of 3 and a working distance of 5 - 12 mm. Most samples were air dried at 38 °C, others were critical point dried to avoid collapsing or deforming of wet and fragile fungal structures. To these samples, 70 % ethanol was added. The ethanol was then replaced by increasing ethanol concentrations (70/80/90/96/100 %) and acetone (typically 30 minutes each, flushed 3 times) followed by liquid carbon dioxide replacement (critical point dryer EMI Tech K850, Institut für

spezielle Zoologie, Friedrich-Schiller-Universität Jena). For the SEM measurements, the samples were gold-plated by a sputter coater (EMI Tech K500, Institut für spezielle Zoologie, Friedrich-Schiller-Universität Jena). The pictures were processed by Scandium software. Selected black slate and graphite samples, as well as hyphal mats were investigated.

2.3.3 Atomic Force Microscopy (AFM)

Atomic force microscopy (AFM) is a high-resolution scanning probe microscopy with resolution at the nanometer scale. The used Dimension 2100 AFM (Veeco, J. Reichert, Institut für Materialwissenschaft und Werkstofftechnologie, FSU Jena) works by measuring the deflection produced by a sharp tip on a micron-sized cantilever as it scans across the surface of the specimen. Black slate samples (M3) were examined with different measuring fields (100 x 100 µm, 50 x 50 µm, 10 x 10 µm, 3 x 3 µm, 512 x 512 pixel); the data was analyzed and visualized by Gwyddion (free software) and SPIP (Image Metrology) software. However, the measuring time affected the fungal material which started to glue to the tip of the cantilever. Therefore, this method was not used for further analyses.

2.3.4 Vertical Scanning Interferometry (VSI)

To investigate the rock surface topography, vertical scanning interferometric microscopy (VSI, Micro XAM MP8, ADE Phase Shift, Institute of Earth Science at Rice University of Houston) was used in combination with white light. This method provided a field of view of 163 µm x 123 µm and in the z-direction of better than 2 nm (Lüttge et al., 1999). The lateral x-y resolution of VSI was approximately 250 nm (for a 50 x Mireau objective). Also, a 100 x Mireau objective was used to examine specific surface areas.

The obtained values of about 500 selected xyz-data sets were analyzed and visualized by Image Processing Software for Microscopy (SPIP, Image Metrology).

2.4 Surface Chemistry

To analyze surface chemistry different methods are available. But not every method is suitable for the used incubated rock samples.

2.4.1 Elemental Analysis of Carbon and Nitrogen (C, N)

The analytical principle is that solid substances (soils, rocks) are changed into gaseous combinations through quantitative high temperature decomposition (1100 °C). The gas mixture was cleaned, separated into its components (purge and trap principle) and determined by a thermal conductivity detector with a precision and accuracy of up to 0.1 % relative. Most important is the large dynamic range of detection, from < 0.01 to 100 %. This range is even possible when there is a great difference in relative concentrations (Elementar-Analysensysteme GmbH).

The elemental analyses of carbon and nitrogen with an elemental analyzer like the used vario MAX (Elementar-Analysensysteme GmbH, MPI BGC Jena) required a definite amount of material (sample weight 250 mg in general, but 5 mg up to 2000 mg were possible). In this investigation about 250 mg powdered rock material per sample was used (appendix). The detection limit (vario MAX) of carbon ranges between 0.400 - 180 mg and 0.120 - 84 mg for nitrogen.

Samples of unbleached (M2) and bleached (M3) rock material were analyzed. Although direct carbon and nitrogen analyses are not applicable on rock surfaces, the results can be used to conclude on surface C and N ratios due to homogeneity of rock samples.

2.4.2 Laser Ablation Inductively Coupled Plasma Mass Spectroscopy (LA-ICP-MS)

Laser ablation inductively coupled plasma mass spectroscopy as a micro-analytical technique for trace elements determination of solid sample surfaces was used. The sample is directly analyzed by ablating a small quantity of sample material with a pulsed

laser beam. The created aerosols are transported into the core of inductively coupled argon plasma (ICP), which generates very high temperatures. The plasma in ICP-MS is used to generate ions that are then introduced to the mass analyzer. These ions are then separated and collected according to their mass to charge ratios. The constituents of an unknown sample can then be identified and measured. ICP-MS offers extremely high sensitivity to a wide range of elements (EAG Labs).

The analyses were performed with Quadrupol-ICP-MS X Series II (Thermo Electron) and laser ablation (Nd: YAG; λ = 266 nm) microprobe II (Merchantek). As the ablation areas are very small, complete surface analyses are not possible with this method. The laser was used to label the rock samples before incubation experiments started (Figure 10).
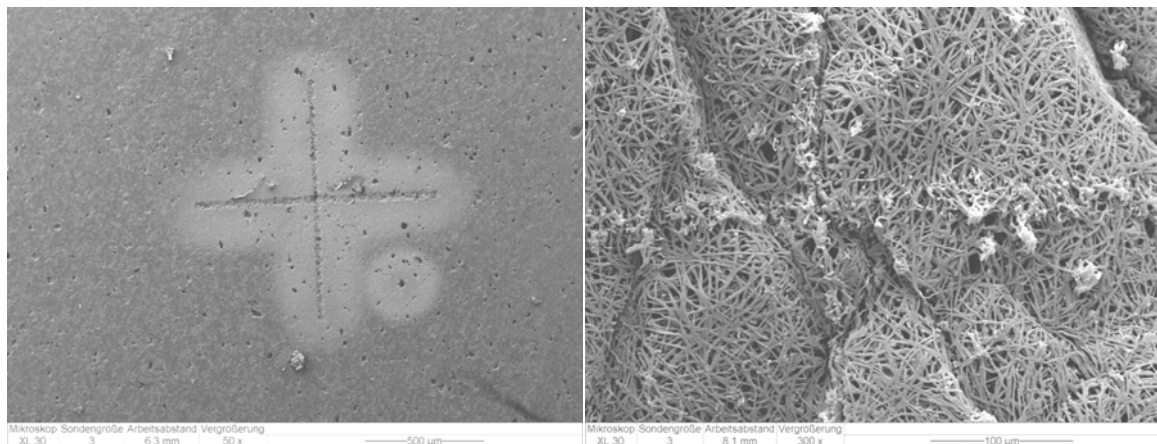
Figure 10: SEM image of labeled rock surface and fungal hyphae grown on labeled surface

2.4.3   X-Ray Photoelectron Spectroscopy (XPS)

X-ray photoelectron spectroscopy (XPS), also known as electron spectroscopy for chemical analysis (ESCA), is a quantitative spectroscopic technique that measures the elemental composition in a surface (Siegbahn, 1982). XPS spectra are obtained by irradiating a material with mono-energetic x-rays while simultaneously measuring the kinetic energy and number of electrons that escape from the top 2 to 30 nm of the material being analyzed (Quantum 2000, Physical Instruments). The determination of

element identity, chemical state, and quantity of an element requires ultra high vacuum conditions (Mikushkin et al., 2004).

Analyses were realized by Quantum 2000 (Physical Instruments, R. Wagner, Institut für Materialwissenschaften und Werkstofftechnik, FSU Jena). Surveys of black slate (M2 and M3) and graphite samples were created with a measurement period of 60 minutes, a pass-energy of 117.4 eV, and measuring point diameters of 100 µm and 10 µm. The elements found were identified by means of their binding energy; the counts on y-axis show their intensity.

2.4.4 Electron Microprobe (EMP)

An electron microprobe (EMP) is an analytical tool used to determine the chemical composition of small volumes of solid material surfaces. The operating mode of an electron microprobe like the used JEOL JXA 8900 RL (A. Kronz, Universität Göttingen) accelerates thermally activated electrons by means of high voltage and magnetic electron lenses focus the beam on the specimen. The resulting focal spot has a diameter of less than 1 micron. Electrons impinging on the solid sample give rise to a variety of interactions and secondary and backscattered electrons, as well as x-rays characteristic for each element which allows identifying elements of the specimen. For the qualitative x-ray analysis, two different types of detectors are available: the energy-dispersive (ED) and the wavelength-dispersive (WD) system. Both types of spectrometers disperse the characteristic x-ray lines and the intensity of each x-ray signal is measured. Elemental concentration is derived by comparing sample intensities with standard sample signals. Mathematical corrections take all influencing physical variables into account, resulting in exact analytical concentrations. Analytical errors lower than 1 % are feasible (Kronz, Universität Göttingen).

To determine the element distribution element mappings were created. With the JEOL JXA 8900 RL the element distributions of aluminum, iron, potassium, phosphorus and sulfur were measured by wavelength-dispersive system (M2 and M3 black slate control samples). Areas of 1000 x 1000 µm were mapped. Incubated graphite (G) and black slate (BS) samples were mapped with an area of 120 µm x 120 µm and 30 µm x 30 µm

respectively. The distribution of nitrogen, titanium, iron, sulfur, phosphorous (WDX) and magnesium, aluminum, silicium (EDX) were analyzed. Titanium was measured to distinguish it from light nitrogen signals. On graphite sample 259, single scans and a line scan (Figure 53) were performed.

Incubated black slate samples (M2 and M3) were examined by Cameca Camebax Microbeam (F. Galbert, ZELMI TU Berlin). Element mappings of aluminum, calcite, iron, magnesium, nitrogen, phosphorus, potassium, silicium and titanium were created. The measured areas had a size of 120 x 120 μm.

To investigate newly formed minerals (on black slate surfaces) due to incubation experiments a Cameca SX50 (R. Schöner, Institut für Geowissenschaften, FSU Jena) was used for EDX measurements.

3. Results and Discussion

3.1 Surface Topology

3.1.1 Optical Microscopy

Results: Black Slate

Comparing rock specimens of unbleached (M2) and bleached black slates (M3) with reflected-light microscopy, bleached samples showed a lighter color (Figure 11) and the surfaces of bleached samples contained larger pores. In some cases, pyrite as small crystals was found in bleached black slates, with an exceptionally large pyrite aggregation measuring a few centimeters (Figure 12, dark area on the left side of M3 thin section) occurred in one sample. Small single quartz veins crossed both black slate materials. Bigger quartz veins (Figure 12) appeared less frequently and did not occur in any of the incubated samples. Investigations of thin sections by transmitted-light microscopy show few indications of laminae (Figure 12, M3). In contrast to unbleached rocks (M2), bleached samples (M3) contained more micro quartz minerals.
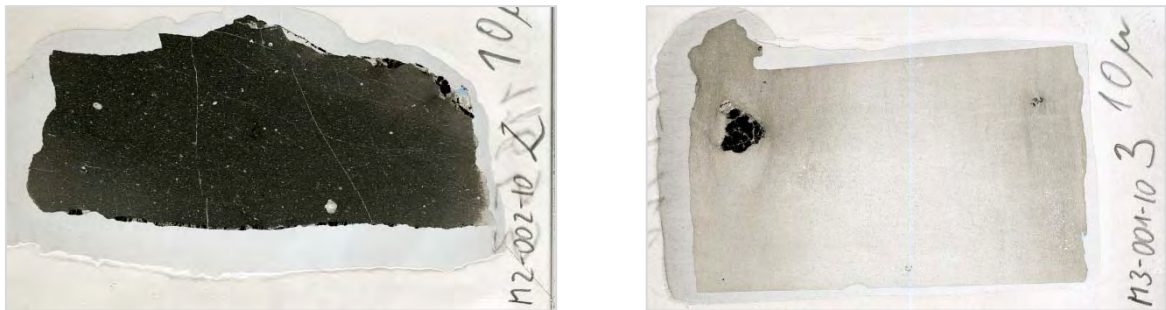
Figure 11: thin sections (10 µm) of unbleached (M2, left) and bleached (M3, right) black slates
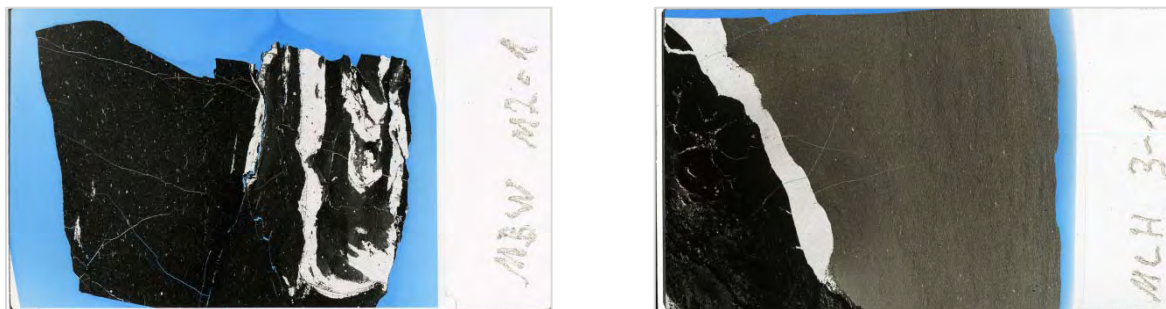
Figure 12: thin sections (30 µm) of unbleached (M2, left) and bleached (M3, right) black slates

The used black slate samples with unbleached and bleached areas on the same sample (BS) showed similar color and porosity characteristics described for M2 and M3 samples. The dark unbleached areas were less porous while light grey colored bleached areas showed more and larger pores. Both unbleached and bleached areas showed small quartz veins while pyrite aggregations were not detected.

Discussion:

The analyzed black slate samples differ from each other in their color and porosity. Organic matter colors sedimentary and metamorphic rocks black. During oxidative weathering, black slates and shales lose organic carbon (Bolton et al., 2006; Fischer and Gaupp, 2005; Fischer et al., 2007; Littke, 1993; Schlegel, 1995). Black slates with total organic carbon content (TOC) of more than 6 % have a characteristic black color. Within carbon loss, the rock color switches to lighter grey and even white colors (Fischer and Gaupp, 2005). The porosity increases due to oxidative weathering (Fischer and Gaupp, 2004; Littke et al., 1991; Tugrul, 2004) as well. The stronger silicification of bleached black slate sample M3 indicates siliceous slate or an intermediate state between alum and siliceous slate respectively. Fischer (2002) referred to the occurrence of alum slates and siliceous slates at Schmiedefeld. Pyrite in bleached black slates is uncommon. Bolton et al. (2006) described that pyrite reacts faster with oxygen than organic matter does. They found the pyrite front generally deeper than the organic matter front. Pyrite weathering is supposed to happen earlier than carbon weathering (Bolton et al., 2006; Littke, 1993; Schlegel, 1995). In contrast to this statement, the used bleached black slate samples (M3) contain amounts of pyrite. However, Littke et al. (1991) described small amounts of pyrite in weathered black shales too. This leads to the conclusion, that pyrite and organic matter weathering were not completed up to the time of investigation. The used bleached samples (M3) are interpreted as a state between unweathered and completely weathered rock materials. Schüring (1996) demonstrated that under waterlogged conditions with oxygen as oxidant treated anthracite (to the exclusion of atmospheric oxygen) no pyrite weathering was noticed. According to that, pyrite weathering can be

influenced or avoided. It is not excluded that ranks of silicification have further influence on pyrite weathering.

The absence of pyrite in partly weathered black slate samples (BS) indicate an earlier pyrite weathering than organic matter weathering (Bolton et al., 2006; Littke et al., 1991; Schlegel, 1995).

It is unclear how long the used bleached sample M3 was exposed to weathering on the over 50 year old waste dump. Over the years freshly broken subsurface rock material from the mine was also transferred and distributed on the waste dumps.

On the basis of using and investigating only one hand specimen per rock weathering type (unbleached M2 and bleached M3 rock specimens) conclusions do not have to be representative to other black slate samples.

Results: *Schizophyllum commune*

The samples were incubated with the white-rot fungus *Schizophyllum commune* 4-39. After transferring the fungus to agar plates with rock samples, aerial mycelia grew within seven to ten days covering the entire rock surface (Figure 13). After two weeks, the petri dishes were completely colonized. Up to the end of the incubation period of three months, the aerial mycelium increased in height and density (Figure 13). During incubation, substrate hyphae as well as aerial hyphae grew with elongated side branches forming a mycelial network. At the end of the incubation period mycelial mats on rock surfaces were about two to three millimeters in thickness. Exceptions were observed with *S. commune* strain 4-40. The air mycelia decreased after two to four weeks (Figure 7 C) and substrate hyphae grew curled.

Figure 13: incubated culture after 3, 7, 26 and 75 days

S. commune incubated with unpolished black slate samples for one year was still viable on the rock surface, in contrast to hyphae on the dried agar medium. The hyphae which grew on the rock sample did grow after plating on fresh CYM agar plates. After removing the hyphal network from the surface, a lightly moist rock surface was determined with all rock samples. Furthermore, newly formed minerals were found on the dried agar and on the rock samples after one year of incubation between mycelia and rock surface (Figure 20). The minerals had a whitish transparent color and sizes varying between 2 - 12 millimeters.

Discussion:

The complex yeast media (CYM) as nutrient media initialized fungal growth. The colonization of black slate or graphite surfaces excludes negative fungal chemotropism due to toxic metals (Fomina et al., 2000). That leads to the conclusion that used rock materials are not hostile for *Schizophyllum commune*. Fungal rock colonization was able to be observed (Burford et al., 2003; Catcheside and Mallett, 1991; Gleeson et al., 2005; Hoffland et al., 2002; Hofrichter et al., 1997a; Hofrichter et al., 1997b; Kolo et al., 2007; Ralph et al., 1996; Wengel et al., 2006). Both rock surface topology (Hoffland et al., 2004) and chemical substances like various elements and minerals (Burford et al., 2003; Gadd, 2010; Hoffland et al., 2004; Jongmans et al., 1997) are reasons for fungal attack. It must be assumed that organic compounds containing rocks are attractive for organic matter degrading fungi (Catcheside and Mallett, 1991; Wengel et al., 2006). This fact is supported by fungal viability after one year of incubation; on the one hand the availability of organic matter and nutrient elements and on the other hand fungal water storing in rock pores were responsive to survive. Water availability is an important factor to create aerial hyphae (Wessels, 1993). In contrast to agar media, rock samples are able to save fluids like water in their pores. Additionally, the fungal hyphae prevented water evaporation from the rocks due to creating a strong mycelial mat.

The decreasing of air mycelia and curled morphology of hyphae of *S. commune* 4-40 was caused by a spontaneously occurring mutation called "thin". This mutating phenotype, commonly seen in some *Schizophyllum commune* strains, is caused by mutation of the

thn1 gene (Fowler and Mitton, 2000; Raper and Miles, 1958). Thin hyphae were distinguished microscopically by their characteristic corkscrew morphology (Schwalb and Miles, 1967) as contrasted to the relatively smooth morphology of wild-type hyphae (Fowler and Mitton, 2000). The decreasing of air mycelia inhibits the fungal surface colonization which is important to explore fungus-rock interaction. Only hyphae, which are able to grow over rock surfaces, are suiTable for surface interaction researches.

Newly formed minerals were found on incubated dried agar plates and on black slate samples (Figures 19, 20, 21). One opportunity is the precipitation of mineral composition of CYM agar plates. Contrary to that, dried agar plates without microorganisms had no visible signs of crystallization. Thus a fungal participation is supposed. The occurrence of newly formed minerals on black slates can be explained by precipitation from solutions that derived from material degradation during the incubation experiments. No newly formed minerals were found on control samples. Fungal participation on forming new minerals is supposed as well (Ehrlich et al., 2008; Gadd, 2007). Both elements of rock minerals and elements of nutrient media were accumulated potentially by fungus. Ensuing they were transported to other hyphae lying on agar or black slate respectively. Wessels (1993) described that the efficacy of spreading is enhanced by the ability of the hyphae to continue apical growth in nonnutritive substrata by translocation of water and nutrients from a food base (Rayner, 1991). Mycelia of higher fungi consist of interconnected hyphae that are compartmentalized by septa. These septa contain large pores that allow streaming of cytoplasm and even organelles. The cytoplasm of such mycelia is, therefore, considered to be continuous (van Peer et al., 2009; Weber, 1993) which ensures exchange of nutrients (Madigan et al., 2001). The found minerals are interpreted as biominerals that precipitated due to microbial activity (Gadd, 2010; Perry et al., 2009; Perry et al., 2007; Skinner, 2005) and were analyzed by SEM (Figure 20) and EDX (Table 1).

3.1.2 Scanning Electron Microscopy (SEM)

The fungal morphology and growth, the resulting rock surfaces and newly formed minerals (biominerals) were examined by scanning electron microscopy.

Results: Fungal Morphology

With light microscopy the elongated morphology of hyphae was detected. Scanning electron microscopy provided a higher resolution and additionally a clear hyphal morphology. The network of hyphae (Figure 14) showed typical branching and septation pattern and a smooth surface. The diameter of most hyphae varied between 2 to 5 μm (Figure 14, appendix), with some hyphae showing a wavy and creased form (Figure 14 E). In addition, small lateral structures were detected (Figure 15). These lateral structures occurred single (Figure 15 D, G and K) or in groups (Figure 15 A and I). The small outgrowths differed in their morphology. They existed with basic structures without any features (Figure 15 A), with bubble-like structures on their tips (Figure 15 B), with crumpled structures on their tips (Figure 15 F and G), and with filamentous structures (Figure 15 C, D, E and K) and included aborted examples (Figure 15 H). The lateral structures were about 1 - 2 μm in length and 400 - 500 nm in width. The filamentous outgrowths had a length of few hundred nanometers to one micrometer and a width of 50 - 70 nm (see appendix). The presence of lateral appendices was recognized on incubated cultures (prior to one month) of *Schizophyllum commune* strains 4-39 and 4-40. The different sample preparation methods for SEM analyses (air drying and critical point drying) showed distinct varieties of hyphal forms. The air dried hyphae showed flat and smooth morphology (Figure 14 A, 15 A and K). In contrast to this, critical point dried hyphae were circular and seemed vivid (Figure 14 B-D). However, small particles were often determined on critical point dried hyphal surfaces (appendix).
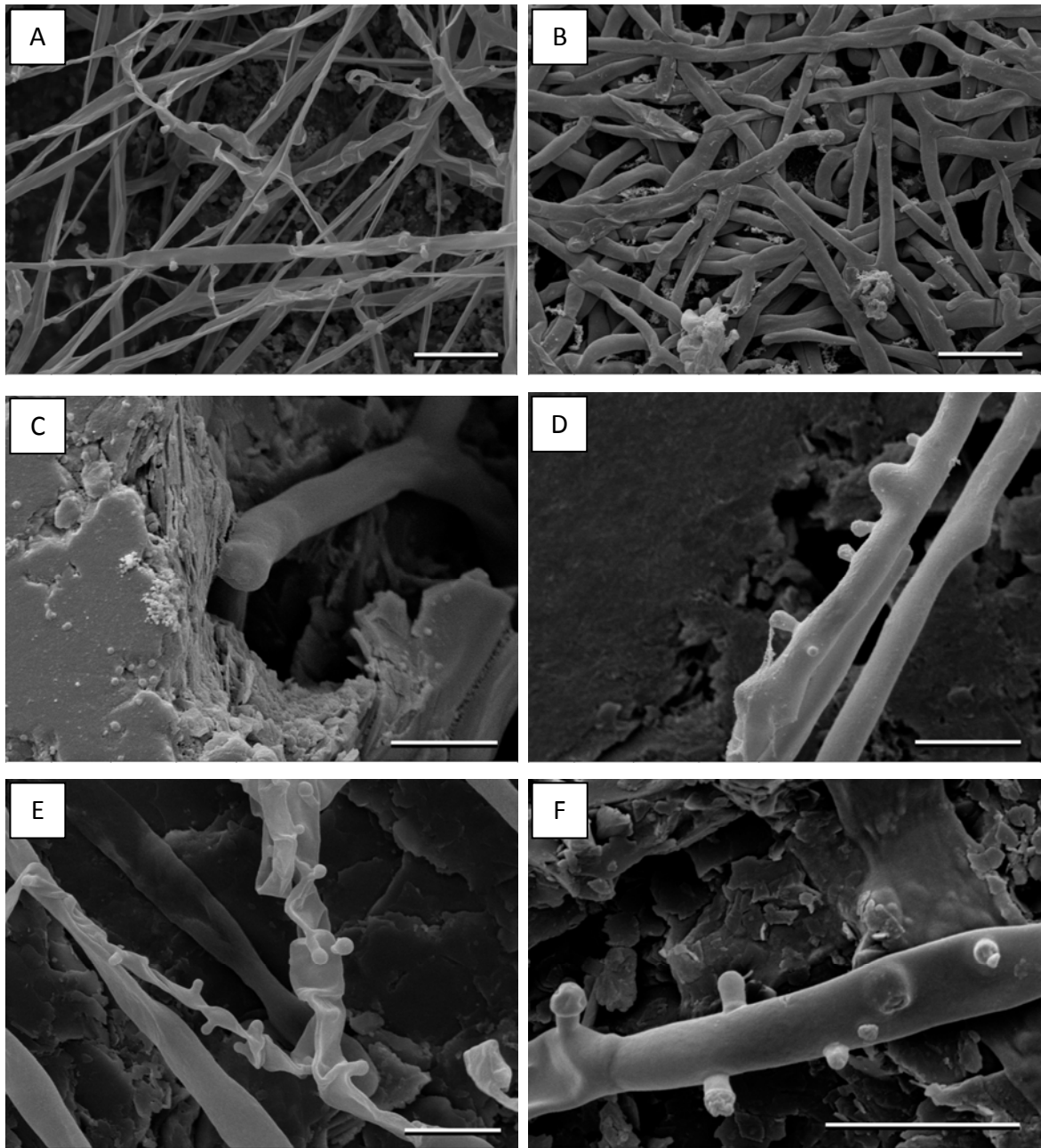
Figure 14: fungal growth morphology on rock surfaces; **A)** hyphal network (air dried sample), scale bar = 10 µm; **B)** hyphal network (critical point dried sample), scale bar = 10 µm; **C)** hyphae tip, scale bar = 5 µm; **D)** hyphae with starting side branch and lateral structures (critical point dried sample), scale bar = 5 µm; **E)** hyphae with and without lateral structures (air dried sample), scale bar = 5 µm; **F)** lateral structures with different morphology (critical point dried sample), scale bar = 5 µm
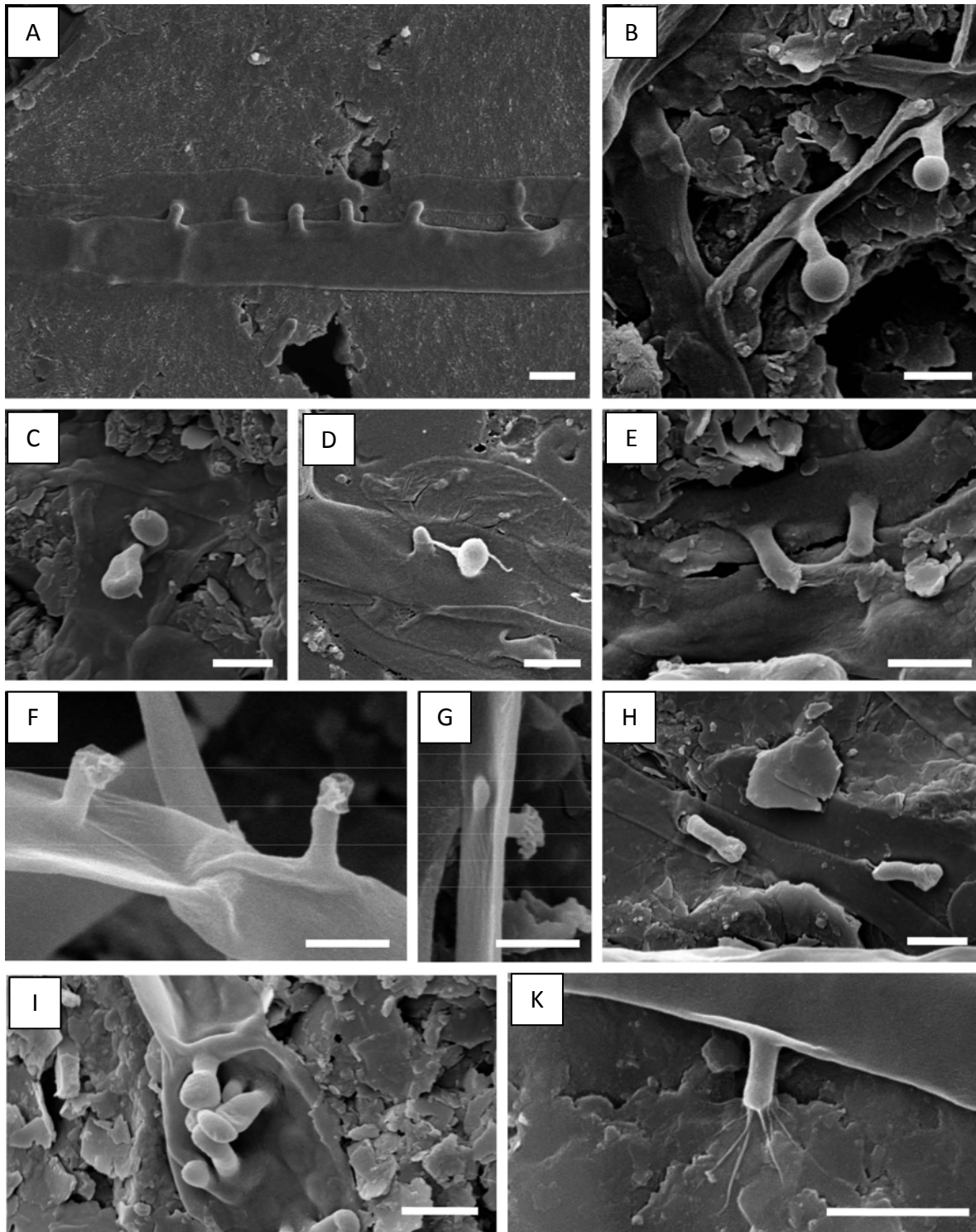
Figure 15: lateral structures of *Schizophyllum commune* with different types of morphology; **A)** group of lateral structures; **B)** with bubble like morphology on top; **C)** with small excretions; **D, E, K)** excretions sticking on their environment; **F, G)** with altered top morphology; **H)** aborted lateral structures; **I)** groups; scale bars = 2 µm

Discussion:

The fungal hyphae grew with elongated morphology and side branches (Essig, 1920; Weber, 1993). Essig (1920) differed between two types of hyphal widths with 1 - 2 µm and 3 - 5 µm in diameter which coincides with the measured hyphal width of this study. Due to using a monokaryotic strain of *S. commune,* fungal clamp connections (Essig, 1920; Kothe, 2007) at vegetative hyphae could not be observed. The growth of all fungi occurs at the hyphal tip (Bartnicki-Garcia and Lippman, 1972; Sanchez et al., 2004). The sample preparation (air drying, critical point drying) had a distinct influence on hyphal exterior. In contrast to air drying, critical point drying prevented hyphae from collapsing. Impacts of alcohol and acetone concentrations caused changes on extracellular microbial organics (Fratesi et al., 2004). Thus, the particles located on hyphal cell walls are interpreted as denaturized organics.
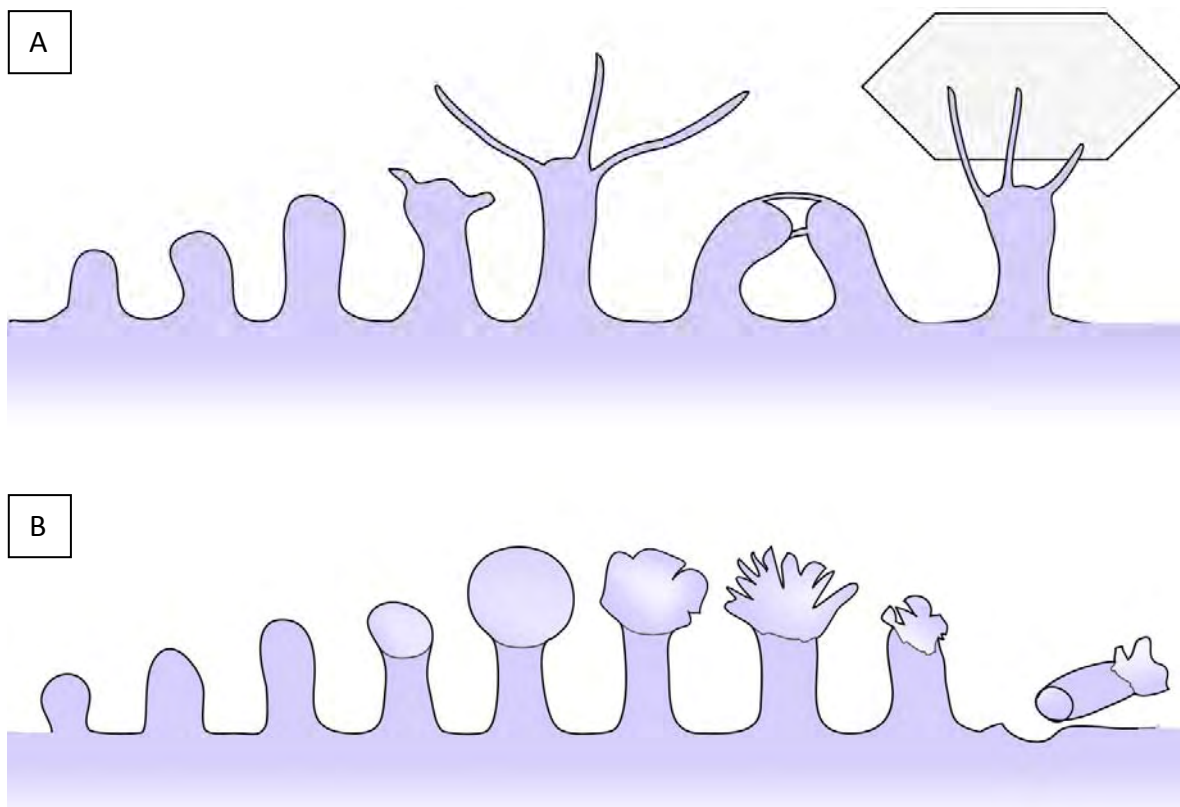
Figure 16: schematic of development of small lateral fungal structures (Figure 15); **A)** lateral structures grow, forming elongated excretions and attach afterwards their environment (other hyphae or further lateral structures, minerals, rock surface); **B)** lateral structures grow and create bubble-like structures on their tip, later the bubble-structures shrivel and finally the altered lateral structures break down

The observed small lateral structures (Figure 15) were also described by Essig (1920) as lateral projections which were present upon the walls of some of the hyphae. Furthermore he cited Rumbold (1910) who described lateral structures as lateral tubercles in *Schizophyllum commune*. However none of them described either the size or the morphology more precise. With higher resolution of SEM analyzes, the lateral structure morphology can be characterized clearly. The schematics in Figure 16 show the proposed development of the lateral appendices.

On one side the structures created various numbers of elongated excretions and attached their environment like rock surface or other hyphae (Figures 15 K and 16 A). This leads to the conclusion that these structures are important for fungal interaction with their proximity. It might be that they make food sources accessible auxiliary. The small lateral structures were discussed by Essig (1920) as aid in the absorption of food materials, since they closely resemble haustoria in shape and are found only on those hyphae which are purely vegetative. If elongated excretions did not act parasitical to other hyphae, an exchange of chemical information is thinkable. The frequency of lateral structures is insufficient to enhance fungal adhering with their environment.

Otherwise the lateral structures are able to form bubble-like structures on their tips (Figure 15 B and 16 B). These bubbles shrivel and collapse. The obvious altered lateral structures break up finally. It is assumed that the bubbles might be excretions as well. If the distance between lateral structures and their environment is too far, excretions are not able to establish a connection with minerals or fungus. In this case, they create bubbles instead of filamentous structures. Afterwards the bubbles shrivel due to disuse and the whole lateral structures secede.

The excretions occurred independent due to sample preparation methods (air drying or critical point drying) and are not preparation artifacts (Fratesi et al., 2004).

The appearance of lateral structures after one month of incubation, suggest that they are not necessary for spreading but convenient and helpful to support fungal live. Essig (1920) described lateral projections without any rock material presence. This implies that black slates or graphite are not the only critical factor to induce lateral structures. The nutrient

availability of environment (e.g. nutrient agar media, wood, nutrient containing rocks) may, however, play a role.

Results: Rock Surface and Fungal Colonization

Regarding all investigated rock samples, unpolished black slate samples (Figure 17 A) featured the roughest surfaces. Sheet silicates and quartz minerals were found most frequent. Pore diameters ranged from few nanometers to several hundred micrometers. A few pores were arranged in a circular pattern, which could resemble a radiolarian test (appendix). Despite removing the mycelia mat from rock surfaces, remaining hyphae were found most of which adhering to unpolished black slates. The hyphae covered large areas (Figure 17 B), coated quartz, clay and other minerals and grew into nearly all pores bigger than the hyphal diameters (appendix). Pores and valleys were colonized very frequently. Some hyphae occurred cumulative and formed a homogenous mat which coated the surface tightly and directly. Single hyphae seemed to be assembled to these flat nets. A few lateral structures (Figure 15) had direct contacts to the rock surface. These structures excreted filamentous structures which attached the surface (Figure 15 K).

Sheet silicates, quartz minerals and other minerals on polished unbleached (M2, Figure 17 C) and bleached black slates (M3, Figure 17 E) were hardly recognizable. Rock forming minerals could only be detected inside bigger pore areas. A few small pores, which were arranged in a circle (appendix), were also found on polished samples. In contrast to unbleached samples (M2, Figure 17 C), the bleached samples (M3) showed a rougher surface with more and bigger pores (Figure 17 E). On both rock samples (M2 and M3) fungi attached more often to rough than to smooth areas. In relation to each other, more hyphae remained on bleached black slate samples (M3). Pore colonization was detected on all black slate samples. Flat net assembles were not observed. Small lateral structures (Figure 15) and some excretions occurred (appendix). Elongated excretions were found on the rock surface, on other hyphae or at other lateral structures. Visible changes of black slate rock surfaces due to fungal colonization could not be detected.
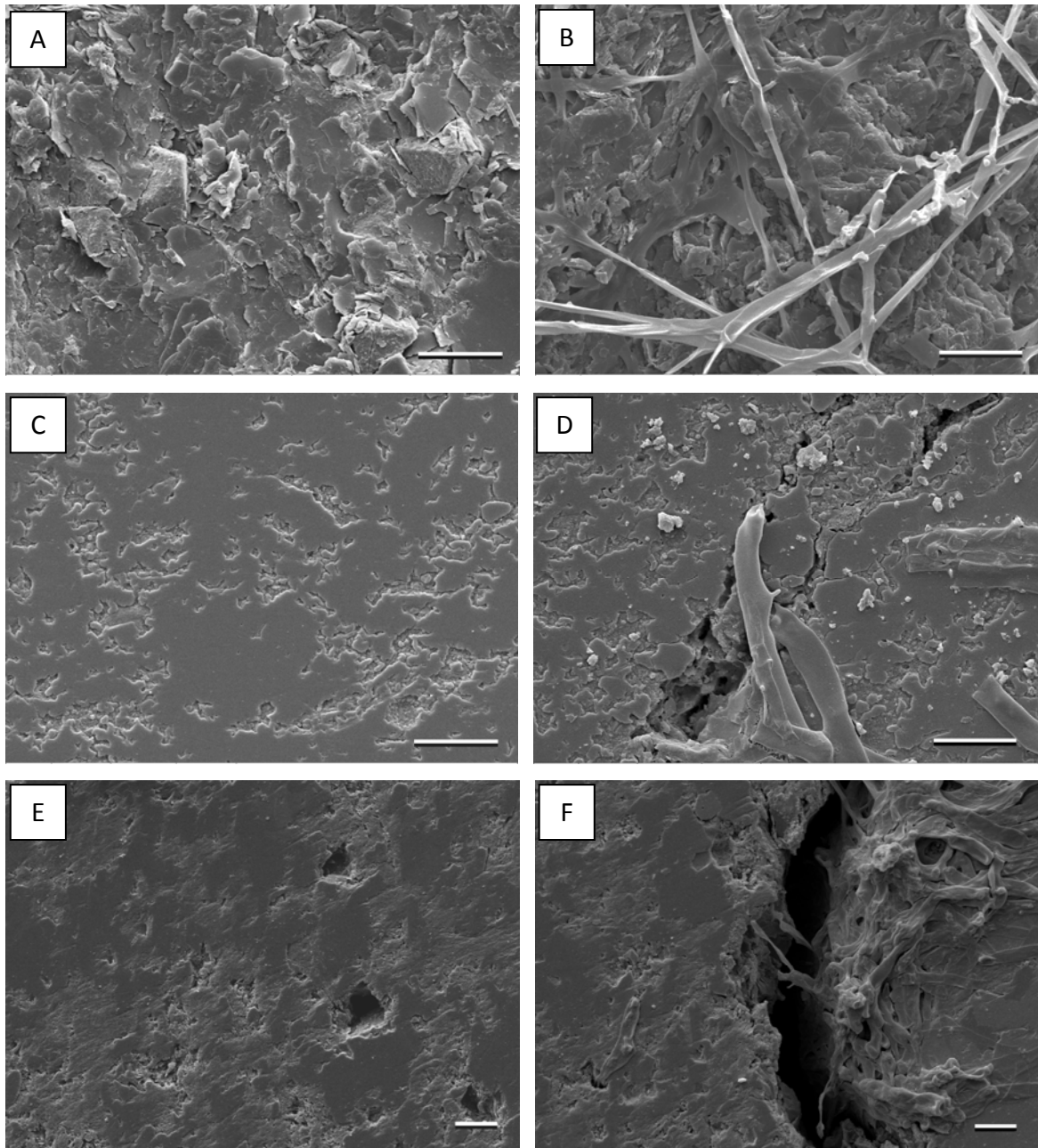
Figure 17: black slate controls (A,C,E) and incubated samples (B,C,F); **A, B)** unpolished bleached black slate; **C, D)** polished unbleached black slate; **E, F)** polishes bleached black slate; scale bars = 10 µm

Polished graphite samples were also colonized by *Schizophyllum commune* (Figure 18). Comparing black slate and graphite surfaces, graphite surfaces were characterized by a smoother surface. In contrast to black slate pores, graphite pores occurred less frequently and in smaller sizes. Graphite pores were colonized by hyphae similarly to black slates and hyphae remained again mostly on rough, pore containing areas.

Populating graphite surfaces, fungal hyphae also created small lateral structures (Figure 15), partly with excretions, as seen with black slate. The filamentous excretions were able to adhere to graphite, to hyphae and to other lateral structures. Again, obvious changes of graphite surfaces due to fungal influence could not be detected (Figure 18 A and B).
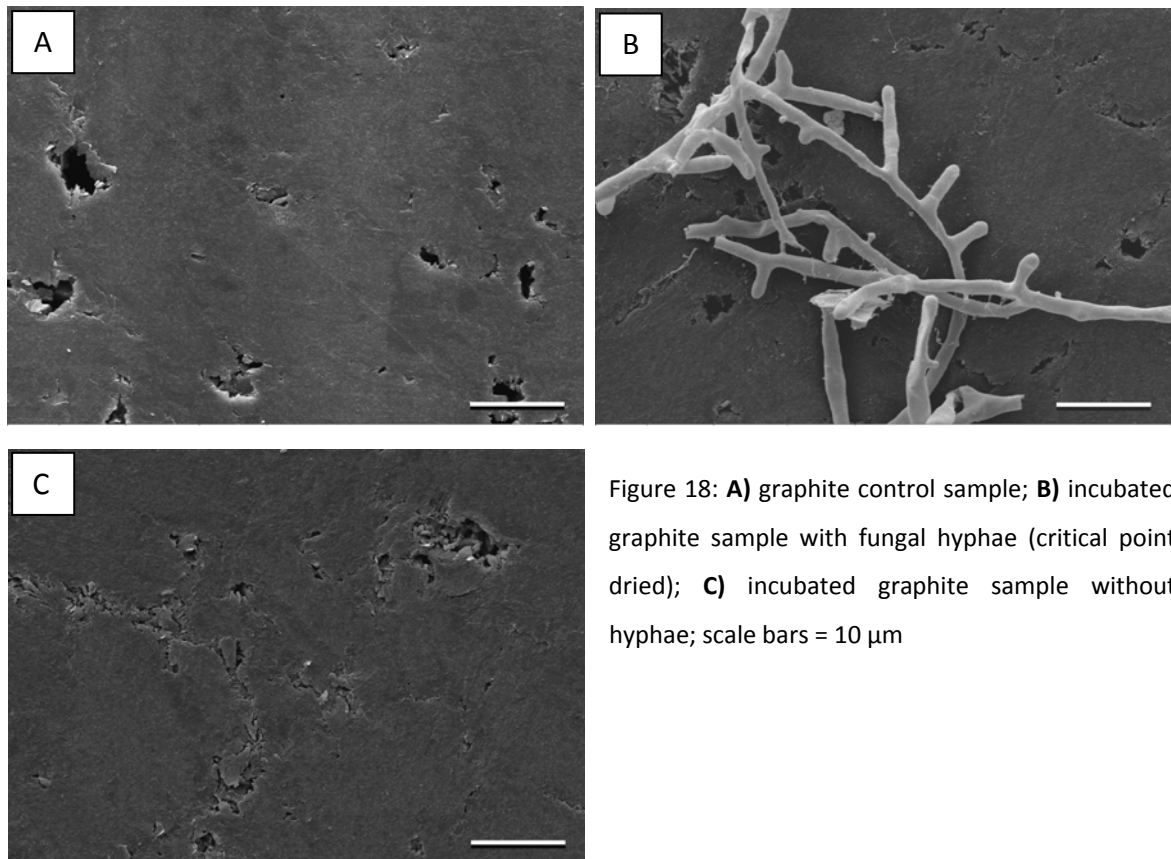
Figure 18: **A)** graphite control sample; **B)** incubated graphite sample with fungal hyphae (critical point dried); **C)** incubated graphite sample without hyphae; scale bars = 10 μm

Discussion:

The unpolished black slate samples naturally featured the roughest surfaces. This is caused by sampling preparation (sawed material) and existing sizes of mineral grains (e.g. quartz and sheet silicates) which cause large peaks and valleys. The determined minerals are main components of black slates (Fischer, 2002; Schmidt, 2004; Szurowski, 1985). Due to polishing the rock surface, near-surface minerals were modified by material removal to create a smooth surface. Thus mineral grains identification based on surface topology is hardly possible. Polished unbleached (M2, Figure 17 C) and bleached black slate samples

(M3, Figure 17 E) differed in their surface roughness in spite of polishing. Generally, rock weathering is associated with material loss (Alastuey et al., 1999; Berg and Banwart, 2000; Littke et al., 1991; Tugrul, 2004; Tuttle et al., 2009; White and Brantley, 2003). The larger pores and higher pore frequency of bleached black slates (M3) was caused by organic matter loss due to oxidative weathering (Bolton et al., 2006; Fischer and Gaupp, 2005; Fischer et al., 2009; Littke, 1993). While no organic matter aggregations were determined by SEM, Fischer (2002) suggested an organic matter coating of minerals (Mayer, 2005; Modl et al., 2007; Zhuang and Yu, 2002). Among others pyrite dissolution is a known process during oxidative weathering (Alastuey et al., 1999; Fischer et al., 2007; Littke et al., 1991; Petsch et al., 2000; Tuttle et al., 2009). Pore structures which are arranged in a circle (appendix) are indications of former radiolarian test or pyrite weathering. Small pyrite minerals arranged in a round complex are known as framboidal pyrites (Alastuey et al., 1999; Folk, 2005; Tuttle et al., 2009; Wilkin and Barnes, 1997; Wilkin et al., 1996). The presence (observations by light microscopy) and absence (observations by SEM) of pyrites in both black slate weathering types (M2 and M3) indicates incomplete pyrite dissolution. Arising pore volume and permeability due to pyrite weathering leads to higher influx of oxygen and oxygen containing surface water (Schmidt, 2004). Thereby oxidative weathering can be accelerated.

The successful fungal colonization of all black slate samples could be determined by SEM analyses, as well. The fungal preference to grow and stick on rougher surfaces was clearly recognizable (Figure 17 B, D, F). Comparing incubated unbleached (M2) and bleached black slate samples (M3), more hyphae remained on bleached samples due to more intense roughness. After removing mycelial mats, hyphae remained on minerals, at pore areas (Figure 17 D, appendix) and in pores (Figure 14 C). This indicates the higher fungal affinity to adhere on rough surface structures. A direct correlation between hyphal adhering on rough surfaces and occurrence of lateral structures could not be observed. Thus, the formation of lateral structures is not responsible for hyphal adhering on surfaces. The rock surface morphology with edges, corners and pits, which is caused by minerals and pores, supports microbial adhesion. The occurrence of microbes on smooth surface areas is obviously subject to adhesive forces (Emerson et al., 2006). Barbour et al.

(2007) demonstrated that polishing does not necessarily reduce oral bacterial colonization. Furthermore, organic excretions can benefit microbial attachment. *Schizophyllum commune* is known to excrete hydrophobins (Wessels et al., 1991). These cysteine-rich fungal proteins of about 10 kDa in size are surface active proteins. Hydrophobins, with amphiphilic nature and self-assembly properties, have a role in fungal growth as structural components and in the interaction of fungi with their environment (Linder et al., 2005; van Wetter et al., 2000; Wang, 2004; Whiteford and Spanu, 2002). Wosten et al. (1994) proved the binding of hydrophobins to Teflon surfaces as an important aspect of the function of hydrophobins. The hydrophilic parts of the proteins can form specific and stable intermolecular interactions (van der Vegt et al., 1996). Studies have shown that hydrophobin coated biomaterials enhance cell growth (Scholtmeijer et al., 2004). It must be assumed that surface roughness, adhering forces and organic excretions like hydrophobins enable the fungal attachment on rock surfaces. Further on, nutrient availability as hyphae adhering factor should be discussed. A lot of studies have proved the importance of nutrients and trace elements (Chertov et al., 2004; Eger, 1970; Giannantonio et al., 2009; Heilmann-Clausen and Boddy, 2005; Lilly et al., 1992). Heterotrophic fungi use carbon for growth (Fuchs and Schlegel, 2007; Madigan et al., 2001). Carbon containing soils or rock materials seem to act as carbon source for many microbes (Huang et al., 2005; Matlakowska and Sklodowska, 2009; Petsch et al., 2005; Petsch et al., 2001; Rezacova et al., 2006; Wengel et al., 2006). Especially fungi colonize and influence carbon rich rocks like lignite, coal or black shales (Fakoussa and Hofrichter, 1999; Fritsche et al., 1999; Glombitza et al., 2009; Hofrichter et al., 1997a; Hofrichter et al., 1997b; Hofrichter et al., 1999; Pokorny et al., 2005; Ralph et al., 1996; Silva-Stenico et al., 2007; Wengel et al., 2006). Fungal rock degradation was proved by material loss (Glombitza et al., 2009; Hofrichter et al., 1997b; Silva-Stenico et al., 2007), transforming of carbonaceous fractions (Glombitza et al., 2009; Hofrichter et al., 1999; Ralph et al., 1996), and dissolved organic carbon (DOC) (Wengel et al., 2006). Oxidative enzymes (peroxidases, laccases), hydrolytic enzymes (esterases), alkaline metabolites and natural chelators are responsible for microbial coal degradation/ liquefaction (Fakoussa and Hofrichter, 1999). *Schizophyllum commune,* which excretes laccases, was able to

degrade charcoal and black shale (Wengel et al., 2006). This suggests promotional influence of rock containing organic nutrients on fungal growth. However, SEM analyses did not show any visible surface changes either on unbleached (M2) or on bleached black slate samples (M3) due to fungal incubation. On the one hand patchy occurring organic coatings are too thin to be recognized by SEM and with it organic removal. On the other hand it is possible that fungal hyphae remain over these areas and cover modified surfaces (see Chapter 3.1.4).

Polished graphite samples (G) presented the smoothest surface (Figure 18) of all investigated rock samples. Because a great amount of very small graphite flakes and granules were compressed to graphite rods, single minerals or crystals were not identifiable. Since the investigated graphite samples were not monocrystals but pressed material of small crystals, pores occurred. These pores allowed fungal hyphae to remain on the surface in spite of the removal of mycelia. This phenomenon was seen on incubated black slates which were discussed before, as well. The pores support fungal attachment. The occurrence of some hyphae on smooth polished areas could be caused by adhesion forces (Emerson et al., 2006). It is easily conceivable that fungal hyphae not only adhere but rather stick into modified surfaces (see Chapter 3.1.4). Because graphite consists only of carbon an equal carbon distribution existed. Although an adequate nutrient supply remained hyphae occurred unbalanced. Thus fungal attaching seems to be a selective process which depends on surface roughness, nutrient availability and competence of the fungus to stick on surfaces. The excretion of hydrophobins and exoenzymes are supposed to play an important role in hyphal adhesion. Small lateral structures of hyphae occurred with similar frequency on graphite as well as on black slate samples. It may be excluded that numbers of lateral structures increase due to stronger carbon availability of graphite samples.

Results: Biominerals

During preparation and during SEM analyses, newly formed minerals were found on black slate and graphite surfaces which were incubated with *Schizophyllum commune* for at least three months. The minerals resided between hyphae and rock surfaces. Some minerals grew directly on fungal hyphae (Figure 21).
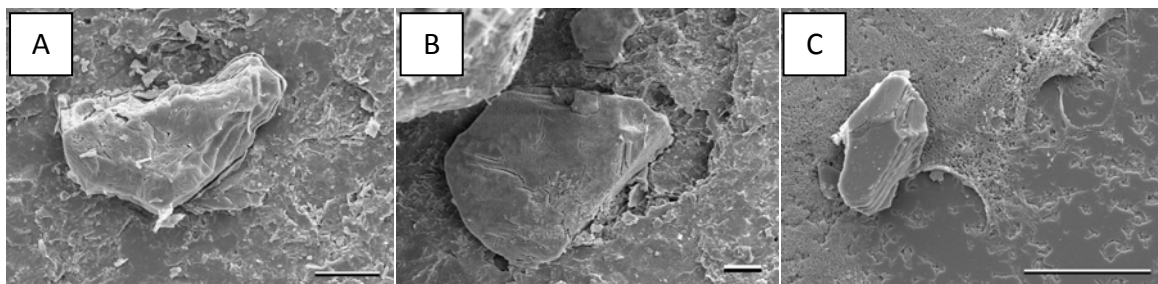
Figure 19: **A, B)** biominerals on unpolished bleached black slate with pattern shown in Figure 20 E; **C)** biomineral (?) on polished unbleached black slate; scale bars = 20 μm

The biominerals had crystalline or amorphous shapes (Figure 21 and 19) and occurred as simple (Figure 21 A, B and D) or assembled (Figure 21 E and F) minerals. Their sizes varied between 3 μm and 100 μm. Some minerals even achieved a size of a few millimeters (Figure 20). These larger minerals were found on black slate samples which were incubated for more than six months. None of the control samples showed newly formed minerals on their surfaces.

Measurements with energy dispersive x-ray spectroscopy (Table 1), of the mineral shown in Figure 20, revealed a magnesium (~38 wt. %) and phosphorous (~59 wt. %) composition with low amounts of potassium (> 1 wt. %) and sodium (> 1 wt. %). Other minerals on black slate samples containing calcium as the major constituent could be detected by electron microprobe measurements (e.g. crystal depicted in Figure 21 A; for EMP measurement see appendix).
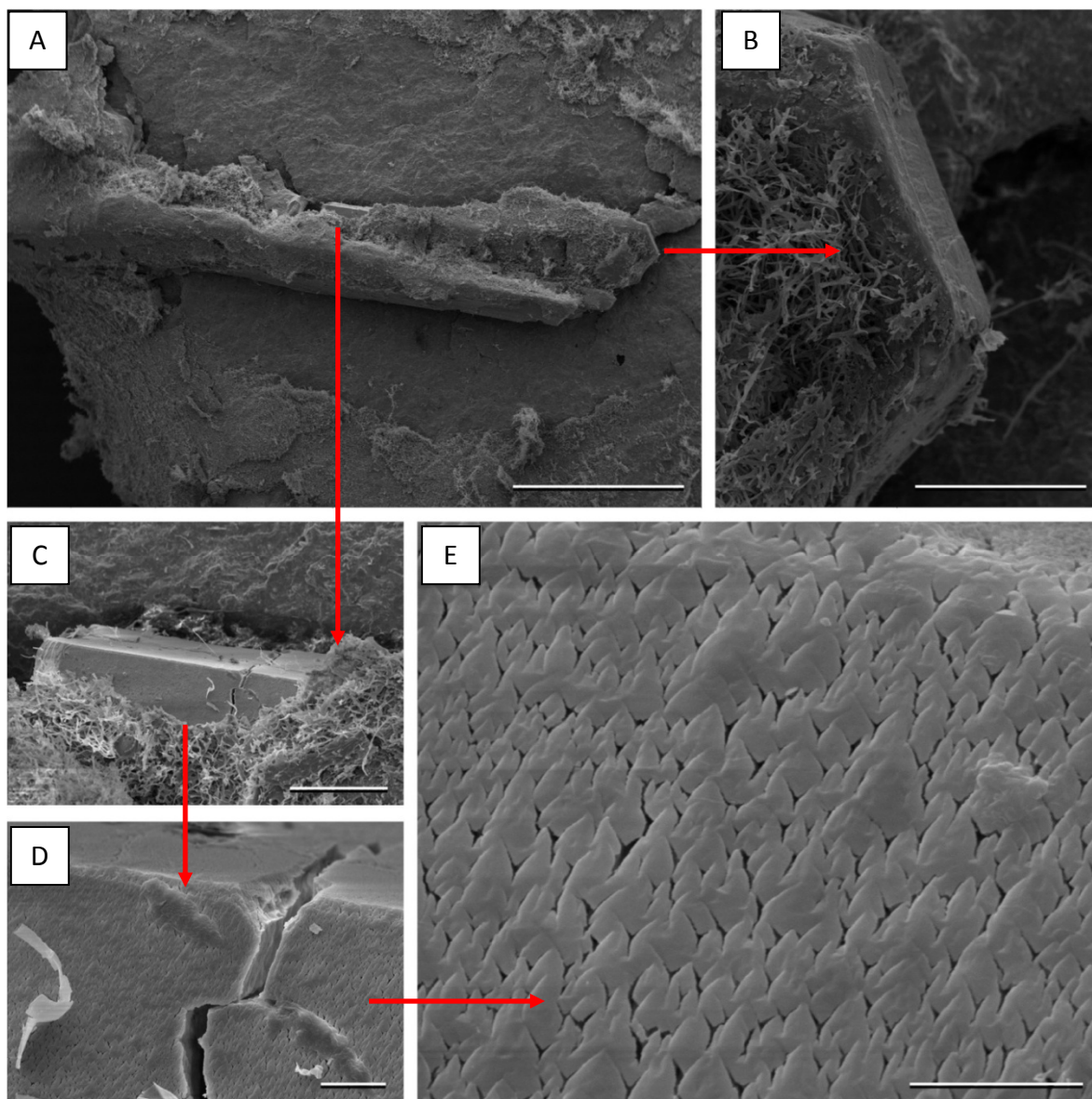
Figure 20: biomineral between fungal hyphae and unpolished black slate surface; **A)** scale bar = 1 mm; **B)** scale bar = 100 μm; **C)** scale bar = 100 μm; **D)** scale bar = 10 μm, **E)** scale bar = 5 μm

Table 1: three EDX analyses of the biomineral shown in Figure 20

Element	wt. %	wt. %	wt. %
Mg	38.87	38.08	37,91
P	58.60	59.25	59.33
K	1.24	1.18	1.31
Na ?	?	?	1.45
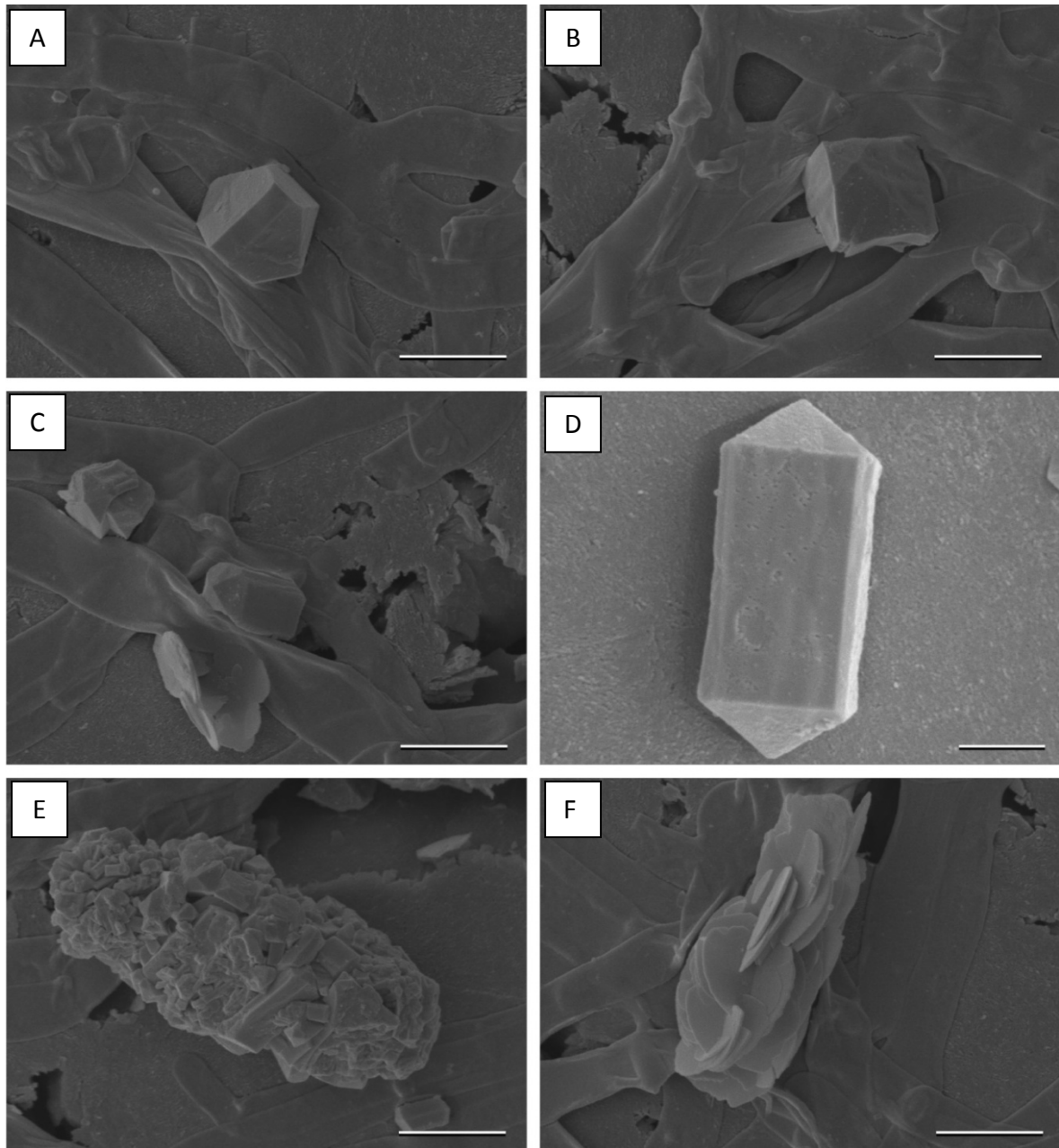
Figure 21: simple and assembled biominerals on polished and incubated graphite samples; **A, B, C, E and F)** scale bars = 5 μm; **D)** scale bar = 2 μm

Discussion:

In contrast to control samples, newly formed minerals were found on incubated rock surfaces. Minerals which are formed from the remains; or as a result of the metabolic activity of organisms are described as biominerals. Skinner (2005) defined biominerals as a subset of the mineral kingdom, created through the actions and activity of a life form.

Biominerals are widely formed by bacteria, single-celled protists, plants, invertebrates and vertebrates including humankind (Perry et al., 2009). They consist of an inorganic phase or phases (usually simple salts or oxides) and a range of biomolecules that are often proteins, carbohydrates or lipids (Mann, 2001). Perry et al. (2009) wrote that biominerals or organominerals (Perry et al., 2007) are always formed from an aqueous environment that is globally undersaturated with respect to the required mineral or mineral phase and yet is rich in ions and biomolecules. The formation of a biomineral requires the transport and concentration of the required element(s), nucleation, growth and aggregation/assembly of the mineral building blocks, together with possible phase transformations.

On one side, the found minerals (Figure 20) consisted of phosphorus, magnesium and small amounts of potassium (Table 1). In one case small amounts of sodium were found also. The measured mineral seemed to be a kind of magnesium phosphate with further minor elements such as potassium and sodium. As the phosphorus and magnesium rich biominerals were found between rock surface and hyphae it must be assumed that biomineralization took place outside fungal cell walls. Critical detoxification as described by different authors (Haferburg et al., 2008; Saul, 2009; Simkiss, 1977) as reason for biomineralization is implausible due to late development (after 6 months) and fungal requirements of phosphorus, magnesium and potassium. Instead dead fungal cells or hyphal excretions are suggested to be initiators of biomineralization (Altermann et al., 2009; Boßelmann, 2007; Mann, 2001; Skinner, 2005). Maybe the term 'organomineral' which describes minerals as affected by organics, mostly life-related, but not directly produced by living cells (Perry et al., 2007) should be applied. As magnesium, phosphorus and potassium occur both in CYM and black slates, it is vague to determine the precise elemental source(s). Only sodium did not originate in CYM agar plates. This indicates that fungal hyphae are involved in rock weathering due to mineral dissolution and accumulating released nutrients.

On the other hand calcium containing biominerals were found (Figure 49, appendix). Calcium bearing biominerals occur commonly in nature as carbonates, sulphates or

phosphates (Davis et al., 2003; Ehrlich et al., 2008; Mann, 2001; Skinner, 2005). With EDX measurements investigated minerals (on black slate surfaces) consisted of calcium only. Thus, calcium carbonate or calcium oxalate is suggested as a mineral. Wood decaying fungi are able to produce oxalic acid. Calcium extracted from materials by fungi affects oxalate solubility and effects development of calcium oxalate crystals on fungal hyphae (Dutton et al., 1993; Gadd, 2007; Jarosz-Wilkolazka and Gadd, 2003; Kolo et al., 2007; Schilling and Jellison, 2007). Kolo et al. (2007) described fungal reshaping of calcium carbonate into newly formed minerals like weddellite and whewellite which are mineral forms of calcium oxalate. Therefore fungal dissolution of calcium carbonates (Li et al., 2009) rather than formation is more likely. However, calcium oxalate can be degraded to calcium carbonate as well (Verrecchia et al., 1993). Calcification of microbes is a well known and common process (Burford et al., 2006; Gadd, 2007; Riding, 2000; Visscher and Stolz, 2005). Calcification may proceed intracellular and/or extracellular. It is interesting that the analyzed minerals contained calcium, but no calcium was added to the CYM growth media. This indicates fungal dissolution and accumulation of calcium that may occur within black slates as well. To establish calcium bearing minerals a calcium surplus regarding fungal requirements is necessary. To detoxify calcium overflow calcium containing minerals may be created (Simkiss, 1977). Because calcium was detected in black slates in small amounts, it is more likely that newly formed calcite minerals may occur as calcium reservoirs than as detoxifying minerals. As no further precise chemical measurements were done with other calcium bearing biominerals, the minerals found remain incompletely determined.

The found minerals on graphite surfaces were not chemically analyzed. As graphite samples consisted only of carbon, the biominerals are suggested to be composed of minerals which occurred in growth media. Further investigations on biomineral components, biomineral generation conditions and mechanisms of biomineral development are necessary and should be done.

Results: Influence of Hydrogen Peroxide, Plasma Etching and Caylase

To clean rock surfaces of mycelia a few rock samples were treated with hydrogen peroxide (graphite, Figure 22 A and B), plasma etching (graphite and black slate, Figure 22 C and D), and caylase (graphite, Figure 22).
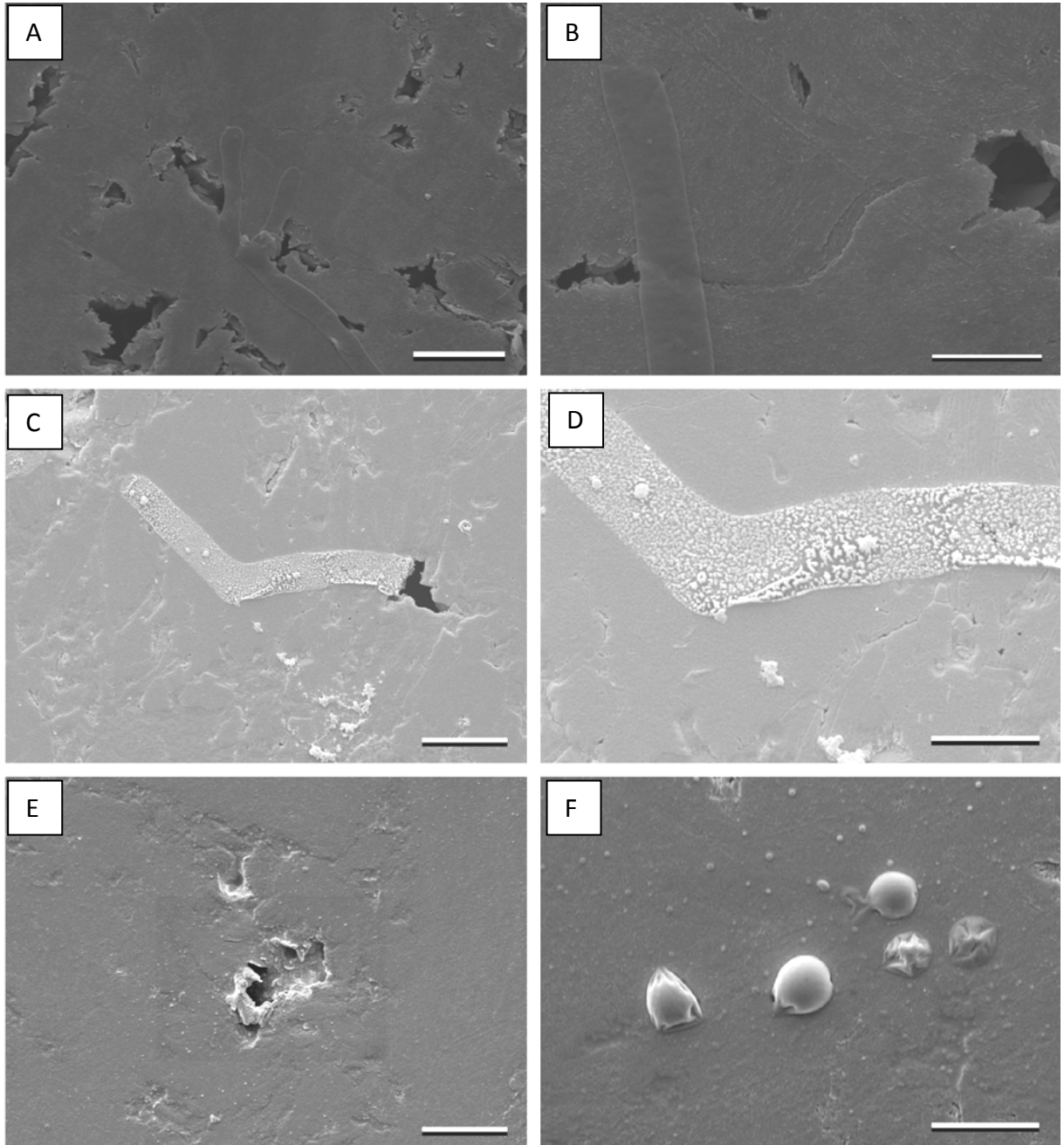

Figure 22: surface treatment with **A, B)** hydrogen peroxide (graphite sample); **C, D)** plasma etching (black slate sample); **E, F)** caylase (graphite sample); **A, C, E** scale bars = 10 μm; **B, D, F** scale bars = 5 μm

Hydrogen peroxide influenced neither graphite nor fungal hyphae conspicuously. Cell walls were not destroyed (Figure 22 B). Plasma etching caused material loss. The graphite sample (119) lost 2541.8 nm and the black slate sample (88) 269.4 nm after 20 minutes of treatment (see appendix). The hyphae were partly destroyed but not removed completely (Figure 22 D). Caylase treated graphite samples showed no remaining hyphae on smooth surfaces nor at pores. Only a few globules of organic material remained (Figure 22 F).

Discussion:

Chemical treatment with hydrogen peroxide (H_2O_2) was only done with graphite due to its high resistance to chemicals. Hydrogen peroxide with its strong oxidizing properties is commonly used for sterilization and bleaching organics. Wood-rotting fungi are able to produce hydrogen peroxide (Koenigs, 1974) as well. Thus fungal cell walls should be protected against hydrogen peroxide influence. By obvious physical integrity of fungal hyphae the H_2O_2 resistance of *Schizophyllum commune* is confirmed. Hence treatment with hydrogen peroxide is not successful in removing wood-decaying fungi.

The reactive ion etching (RIE) uses chemically reactive plasma to remove material deposits on surfaces. Solis-Fernandez et al. (2010) demonstrated effects of graphite etching. But due to reason of material hardness the used compressed graphite material (carbon rods) is not adapted on this method. The treated graphite sample lost too much material. Here the determinations of fungal caused surface changes are impossible. The black slate sample was less modified due to less carbon availability. The hyphae were partly destroyed but not removed completely (Figure 22 D). This indicates that the used parameters were not satisfactory to remove hyphae from the surface. Maybe a longer plasma residence time is more successful to remove fungi. But to examine surface changes due to fungal colonization, further rock material loss would influence the results negative.

An incubated graphite sample was treated with cell-wall degrading enzyme caylase. After this procedure, no further hyphae were determined on rock surface or in pores (Figure 22 E). Thus, the enzyme was able to attack cell walls and eliminated the bonds between hyphae and graphite surface. The found globules may be residues of fungal protoplasts

(Schuren, 1999). Devries and Wessels (1972) described released protoplasts as spheres whose sizes ranged from 2 to 10 μm. They seem to resist cleaning procedures with Tween solution and distilled water. However, the cleaning technique by using caylase was and is the most successful method to remove fungal hyphae. The influence of caylase to other rock samples should be investigated.

3.1.3 Atomic Force Microscopy (AFM)

Incubated bleached black slate (M3) and bleached control sample (M3) were analyzed by atomic force microscopy.

Results:

In contrast to control sample 92, the incubated black slate sample 85 showed a rougher surface (Figure 23 and 24, appendix). Lines caused by polishing were visible on all samples;
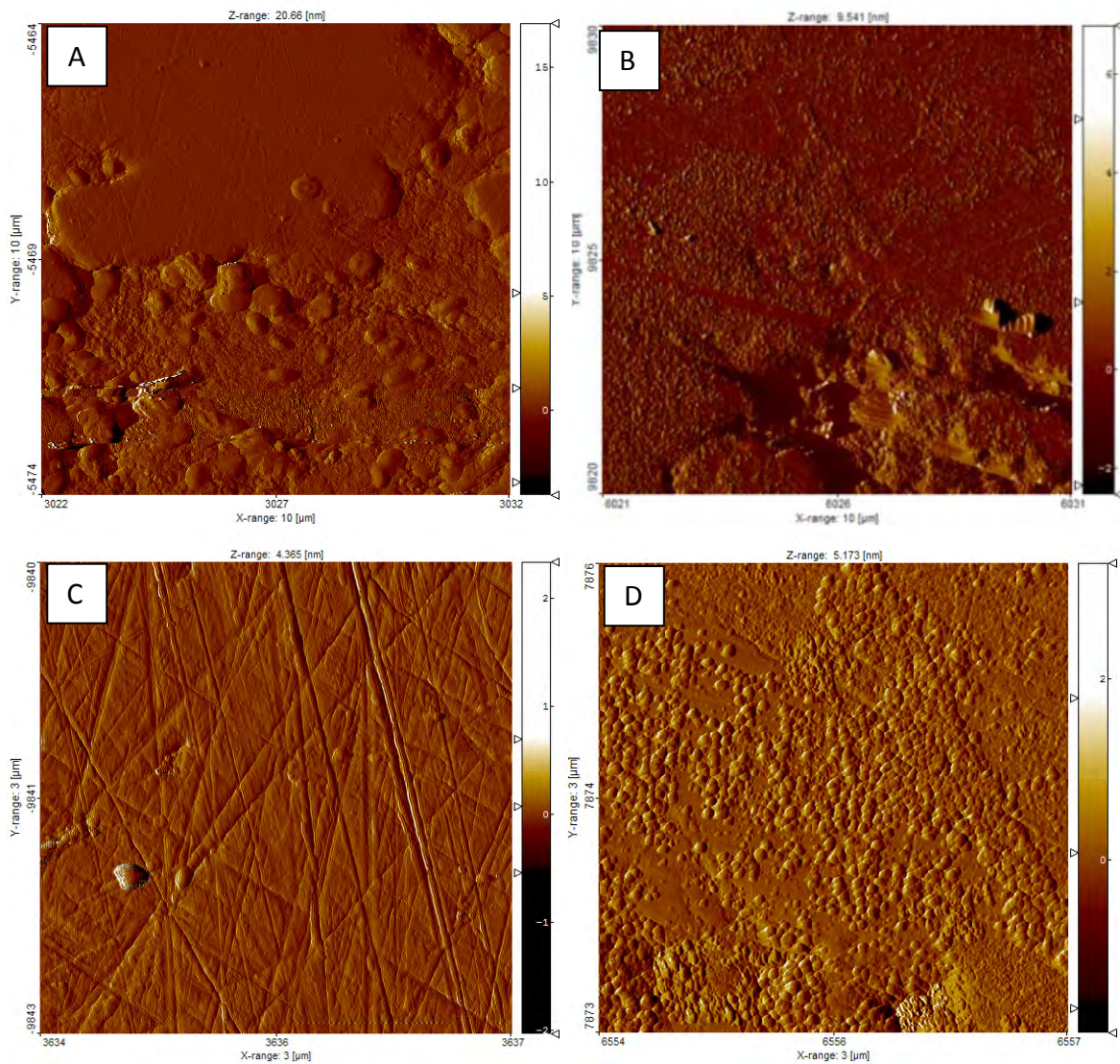

Figure 23: AFM topography images of bleached black slates (M3); **A, C)** control sample; **B, D)** incubated sample;   **A, B)** measured area = 10 x 10 µm; **C, D)** measured area = 3 x 3 µm

small spherical structures covered the surface of the incubated sample. These structures were about 50 to 150 nm in width and 8 to 15 nm high. In contrast to the control sample the measured roughness parameters (description see Chapter 3.1.4) of incubated samples increased (Table 2). The amplitude parameter (R_a), the root mean square (R_q) and the roughness depth (R_t) doubled due to fungal colonization. The roughness factor (F) was more than quadrupled (Table 2).

Table 2: roughness parameters (R_a, R_q, R_v, R_p, R_t and F) of black slate control (M3, Figure 23 C) and incubated (M3, Figure 23 D) sample surfaces

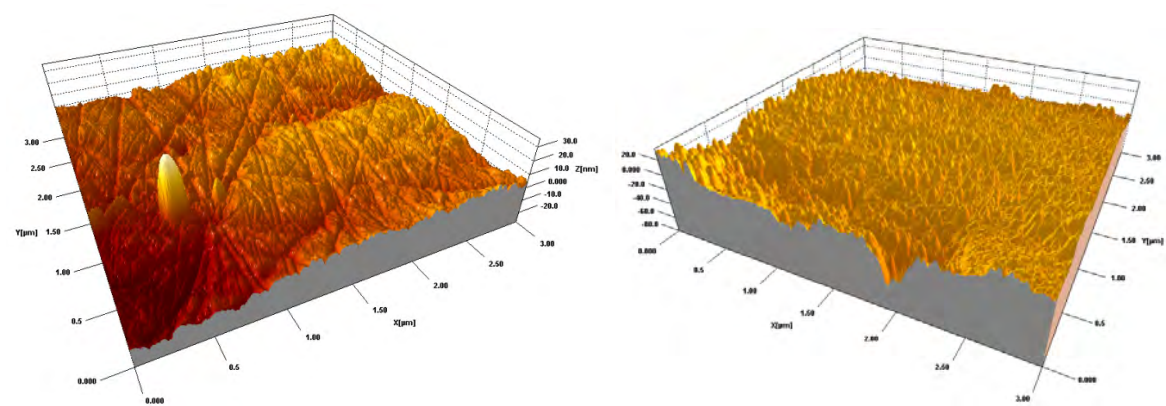|	R_a [nm]	R_q [nm]	R_v [nm]	R_p [nm]	R_t [nm]	F [%]
black slate (M3) control (3 x 3 µm)	5.27	7.23	-27.9	35.8	63.7	0.90
black slate (M3) sample (3 x 3 µm)	13.60	16.80	-80.4	34.8	115.2	4.64

Figure 24: 3D models of AFM measurements of black slate (M3) control sample (left, Figure 23 B) and incubated sample (right, Figure 23 D); **A, B)** measured area 3 x 3 µm
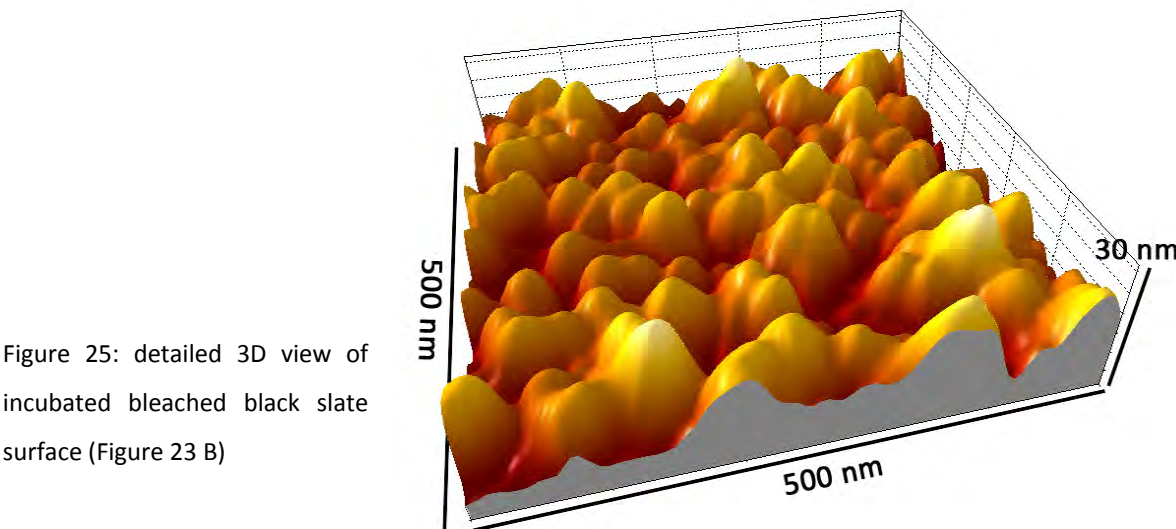

Figure 25: detailed 3D view of incubated bleached black slate surface (Figure 23 B)

Discussion:

Due to fungal incubation roughness parameters increased (Table 2). This indicates microbial impact on rock alteration (Johnson et al., 2007; Kulkarni et al., 2008; Ranogajec et al., 2008). The found spherical structures may be fungal excretions. Literature describes sizes of hydrophobins from 2.5 Å to 10 nm (Paananen et al., 2003; Sunde et al., 2008; Torkkeli et al., 2002; Wösten and de Vocht, 2000). Observed hydrophobin rodlets have a diameter of ~10 nm and visible lengths ranging between 35 and 240 nm (Dempsey and Beever, 1979; Sunde et al., 2008; Wösten and de Vocht, 2000). As found structures had spherical forms, hydrophobin rodlets can be precluded. In contrast to uniform patterns of assembled hydrophobins (Sunde et al., 2008; Wösten and de Vocht, 2000) the found spherical structures are unequally distributed. This allows for the assumption that spheres may not be hydrophobins. Extracellular enzymes were also described as fimbric structures (Green et al., 1992). Thus further investigations are necessary to determine spheres.

However, measurements of incubated bleached black slate samples were done near a laser carved cross (Figure 10). It might be that deposited laser removed material was analyzed (Figure 25). Chemical surface investigations would clarify microbial or laser induced spheres.

One disadvantage of this method was the susceptibility to fungal hyphae. The cantilever was contaminated with hyphae (they stuck on them after analysis) and led to damaged or incorrect results.

3.1.4 Vertical Scanning Interferometry (VSI)

Roughness Parameters

The roughness of a solid surface is a measure of its texture, which can be quantified by the vertical deviations of a real surface from its ideal form. The larger the deviation, the rougher the surface is. A lot of parameters are necessary to describe roughness (Thomas, 1999). The used parameters are shown in Table 3. The amplitude parameter (R_a) as average surface roughness, the root mean square (R_q), the maximum valley depth (R_v), the maximum peak height (R_p), the roughness depth (R_t) which results from maximum distance between the highest peak and the lowest valley over a distance, and the roughness factor (F), which is the ratio of measured surface area to geometric surface area (Thomas, 1999), were analyzed.

Table 3: overview of determined surface roughness parameters, their description and formula

Parameter	Description	Formula
R_a	Arithmetic average of absolute values	$R_a = \dfrac{1}{n}\sum_{i=1}^{n} |y_i|$
R_q	Root mean square	$R_q = \sqrt{\dfrac{1}{n}\sum_{i=1}^{n} y_i^2}$
R_v	maximum valley depth	$R_v = z_{min}$
R_p	maximum peak height	$R_p = z_{max}$
R_t	maximum distance between the highest peak and the lowest valley over a distance /roughness depth	$R_t = R_p - R_v$ $= z_{max} - z_{min}$
F	Roughness factor / Surface Area Ratio	$F = \dfrac{A_{measured}}{A_{geometric}}$

Results:

The arithmetic roughness average (R_a) of graphite surfaces (G, Table 4) increased due to fungal colonization from 77.6 ± 19 nm (G control) to 125.0 ± 29.5 nm. Also, an increase of R_q from 169.7 ± 24.3 nm to 308.5 ± 98.8 nm, R_t from 9449.9 ± 1588.9 nm to 10395 ± 2575.3 nm, and F from 359 ± 0.3 % to 20.8 ± 20.4 % was detected.

The unbleached black slate (M2, Table 4) surfaces showed a decrease of R_a from 116.2 ± 34.7 nm to 85.0 ± 14.4 nm, R_q from 213.7 ± 71.9 nm to 172.4 ± 29.6 nm, and F from 17.80 ± 21.3 % to 10.87 ± 8.5 %. Only the maximum distance between the highest peak and the lowest valley (R_t) increased from 7913 ± 4476.5 to 9805 ± 602.4 nm.

The surface roughness of bleached black slates (M3, Table 4) decreased in R_a from 235.1 ± 22.7 nm to 199.3 ± 38.9 nm, R_q from 477.8 ± 7.9 nm to 378.0 ± 119.8 nm, R_t from 12165 ± 417.5 nm to 10612 ± 2905.5 nm, and F from 47.91 ± 4.5 % to 36.44 ± 27.0 % due to incubation with *Schizophyllum commune*.

Table 4: roughness parameters of graphite (G) and black slate (M2, M3) surfaces

|	Ra [nm]	σ	Rq [nm]	σ	Rv [nm]	σ	Rp [nm]	σ	Rt [nm]	σ	F [%]	σ
G control AV	77.6	19.0	169.7	24.3	-5133	487.9	4316	1101.0	9449	1588.9	3.59	0.3
G sample AV	125.0	29.5	308.5	98.8	-5601	1267.4	4794	1448.0	10395	2575.3	20.81	20.4
M2 control AV	116.2	34.7	213.7	71.9	-4690	1681.5	3223	2795.0	7913	4476.5	17.80	21.3
M2 sample AV	85.0	14.4	172.4	29.6	-5241	365.4	4564	268.1	9805	602.4	10.87	8.5
M3 control AV	253.1	22.7	477.8	7.9	-6200	368.2	5965	49.4	12165	417.5	47.91	4.5
M3 sample AV	199.3	38.9	378.0	119.8	-5448	1463.1	5164	1700.4	10612	2905.5	36.44	27.0
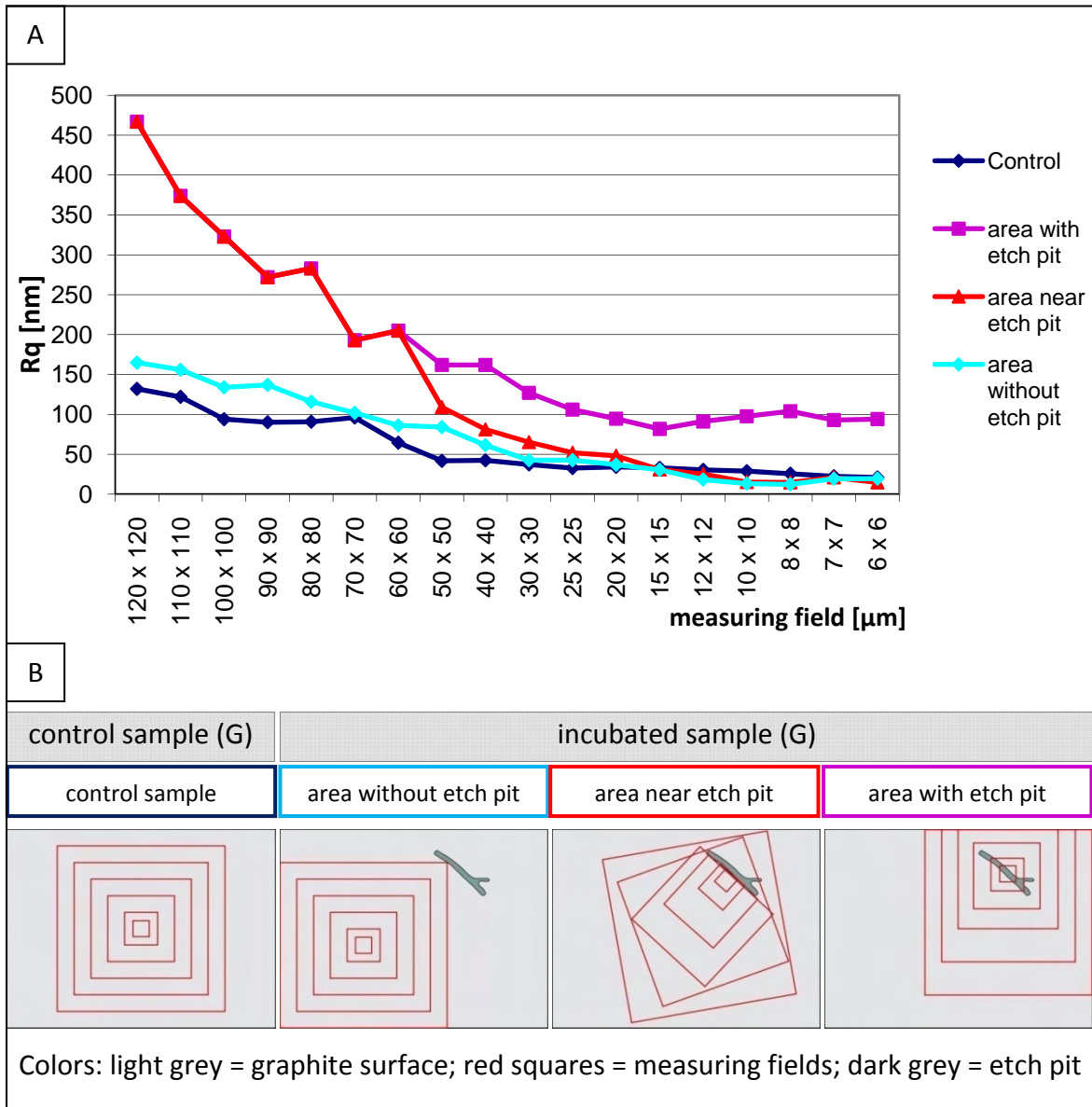
Figure 26: **A)** influence of measuring field size to roughness parameter R_q; **B)** scheme of measuring

Analyses of the graphite samples showed the influence of various measuring field sizes to roughness parameter R_q (Figure 26). With decreasing measuring field size, R_q decreased as well. Comparing the control with the incubated sample without etch pits, the R_q values were similar. The measuring fields (< 60 x 60 µm) of areas near etch pits showed values similar to the control samples. Only measuring fields with etch pits showed higher R_q values.

Discussion:

The roughness parameter R_a is often used to describe surface alteration, but Thomas (1999) demonstrated that similar R_a values can be derived from surfaces showing completely different characteristics of their peak and valley configuration. The significance of amplitude parameters for direct interpretation of surface features is valid only for surfaces built up by a periodical structure. The root mean square R_q is more strongly sensitive to minima and maxima of surface (Fischer and Lüttge, 2007). A careful interpretation of R_a values combined with comparison of R_q and F are useful to describe changes of surface roughness.

The increasing roughness parameters R_a, R_q, R_t and F of graphite samples show the fungal impact due to incubation experiments. Because of the presence of single hyphae, a clear conclusion on rock material loss is not possible. Newly formed pores (etch pits) due to fungal activity have an influence on surface roughness, but hyphae also remained on the surface due to roughness increase.

Except for R_t, all determined roughness parameters (R_a, R_q and F) of unbleached black slate samples (M2, Table 4) decreased due to fungal colonization. One reason is that the fungal hyphae attach to the surface, grow and stick into pores (Figure 17 D). In pores and on rock surface remaining hyphae form a smoother surface and cause a decrease in roughness values. The increased R_t parameter supports this theory. The other reason is that the fungus removes rock material without creating new pores. Possibly *Schizophyllum commune* is able to erode the rock surface from the top or degrades rock micro-roughness. Fischer and Lüttge (2007) described that black slate surface area and roughness were decreased during further weathering. They concluded that those parts of the OM that did not directly adjoin to the slate's clay minerals had a higher reactivity. This means that during ongoing OM weathering the rock surface reactivity and topography are controlled by the extent of OM degradation (Fischer and Lüttge, 2007). To conclude, a combination of both reasons is most plausible due to detected hyphae remained on the surface.

In contrast to bleached black slate control samples (M3, Figure 17 E), the incubated samples show decreasing roughness parameters (R_a, R_q, R_t and F). As discussed for unbleached black slates, a combination of fungal removal, fungal remaining and sticking into pores is most likely a reason for changing parameters. Figure 27 shows a schematic of fungal influence on roughness parameters (R_q and F), which is discussed above.
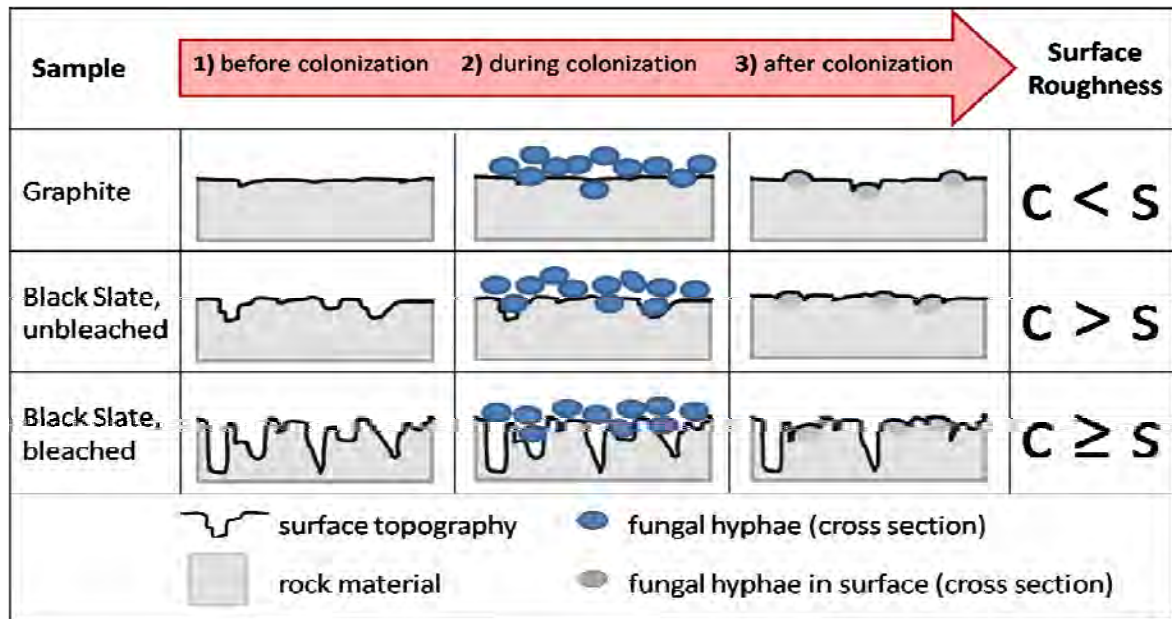

Figure 27: change of roughness parameters (R_q, F) due to fungal colonization (c = control, s = sample)

Comparing graphite and black slate samples, fungal induced depressions on black slates did not increase the roughness parameters. That implies that the frequency of fungal induced depressions was very low. Thus, lower carbon availability of black slate may influence the frequency of *Schizophyllum commune* caused depressions. Using the example of graphite and different measuring field sizes (Figure 26), the influence of fungal etch pits on roughness parameters, such as R_q, is visible. With decreasing measuring field size R_q decreased as well. The roughness values decreased less with measuring field sizes ≤ 25 x 25 μm. Therefore, appropriate measuring field sizes should be used to determine and interpret roughness parameter due to uneven distribution of fungal induced etch pits and some pores.

Fungal Etch Pits

With equal weathering influence, like oxidative weathering of black slates (Fischer and Gaupp, 2005), roughness parameters describe surface changes precisely. However, biological life did not follow the same constant rules like chemical reactions. Diverse parameters (i.e. temperature, pH-value, nutrient supply, food competitors) influence biological life and growth (Madigan et al., 2001). Observing rock surfaces at a micrometer scale, microbial impact can be detected in the form of etch pits (Hiebert and Bennett, 1992; Hoffland et al., 2002; Lüttge and Conrad, 2004).

Results:

The xyz-data set showed the determined rock surface area, with dark colors illustrating lower regions and lighter colors for higher regions of the surface. Detecting the rock surface of black slate and graphite samples, new structures (Figure 28) were found on incubated samples in contrast to control samples. These hole-like structures had similarities to hyphal morphology (Figure 14) interpreted to be fungal etch pits.
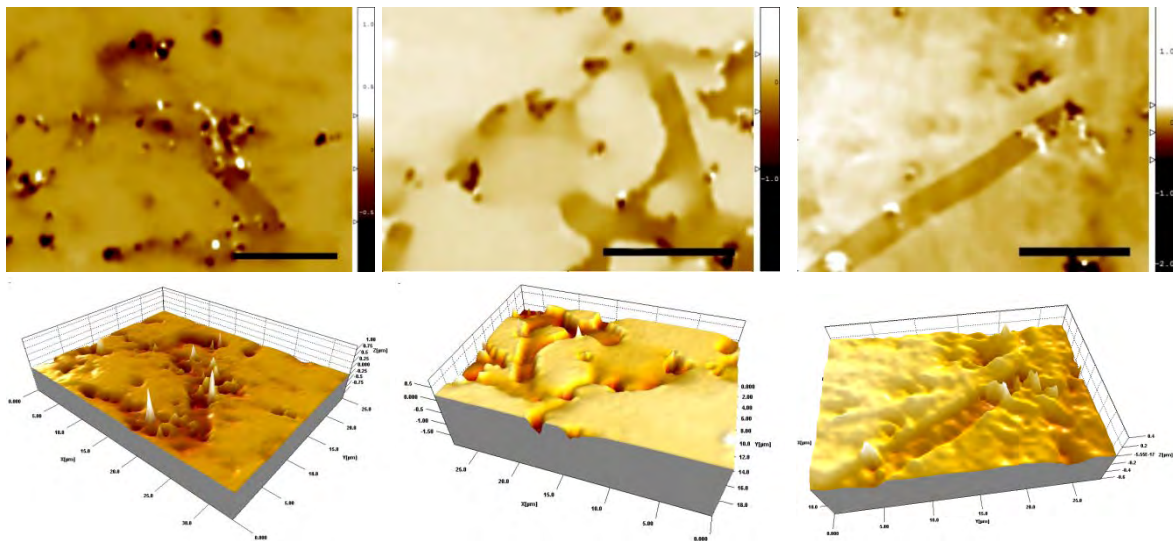

Figure 28: etch pits on unbleached black slate (M2), on bleached black slate (M3) and on graphite, scale bars = 10 µm

Comparing black slate and graphite surfaces, more etch pits were found on graphite samples. In contrast to etch pits on black slates (Figure 30 and 31), etch pits on graphite (Figure 29) had a more elongated morphology which is comparable to hyphal structures. These etch pits were up to 30 µm in length with interruptions up to 150 µm (Figure 29).
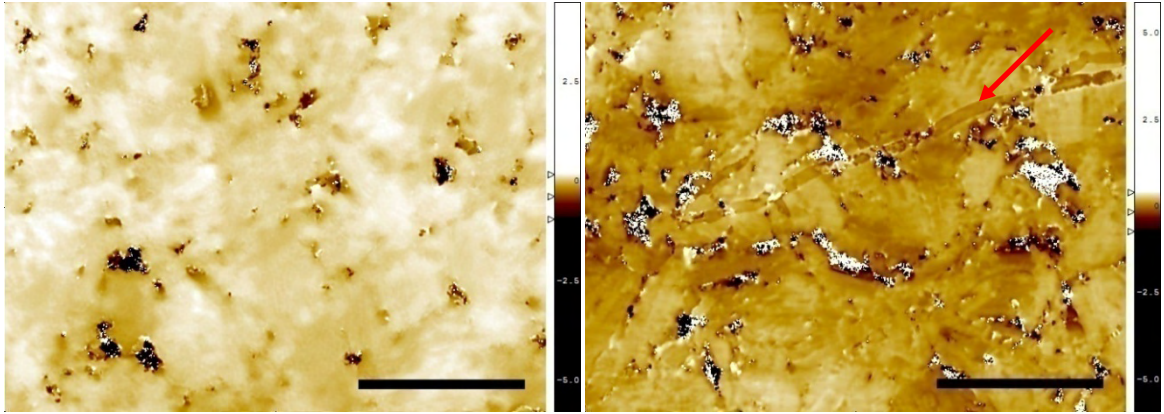
Figure 29: VSI xyz data set of graphite control sample (left) and incubated graphite sample (right); scale bars = 50 μm
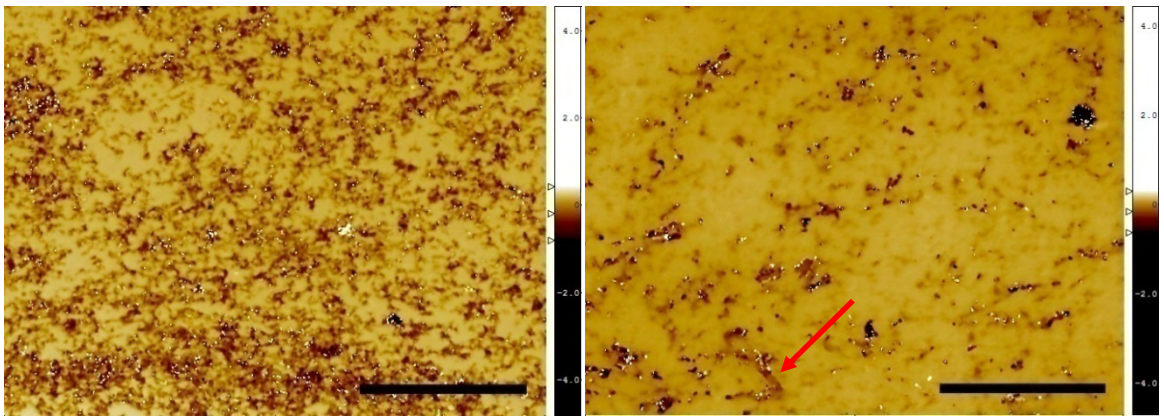

Figure 30: VSI xyz data set of black slate control sample M2 (left) and incubated black slate sample M2 (right); scale bars = 50 μm
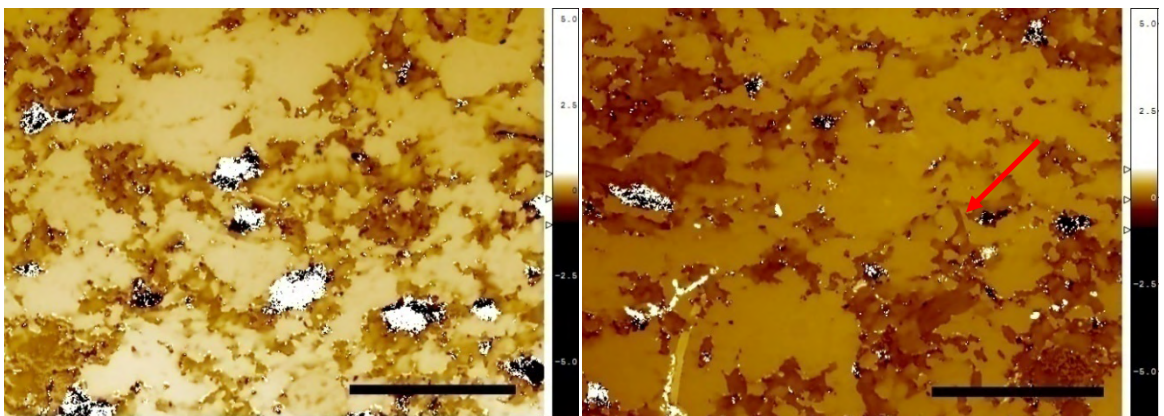

Figure 31: VSI xyz data set of black slate control sample M3 (left) and incubated graphite sample M2 (right); scale bars = 50 μm

On graphite surfaces, etch pits with lateral branches (Figure 32) occurred more frequently than on black slates. The etch pit tip areas were often deeper than the main etch pit area. At regular intervals, small elongated slots (Figure 32 and 38 D) occurred within the etch pits. Some etch pits seemed to be filled with fungal revenants (Figure 32). Other hyphae were found stuck on the surface surrounded by etch pits (Figure 38 B).
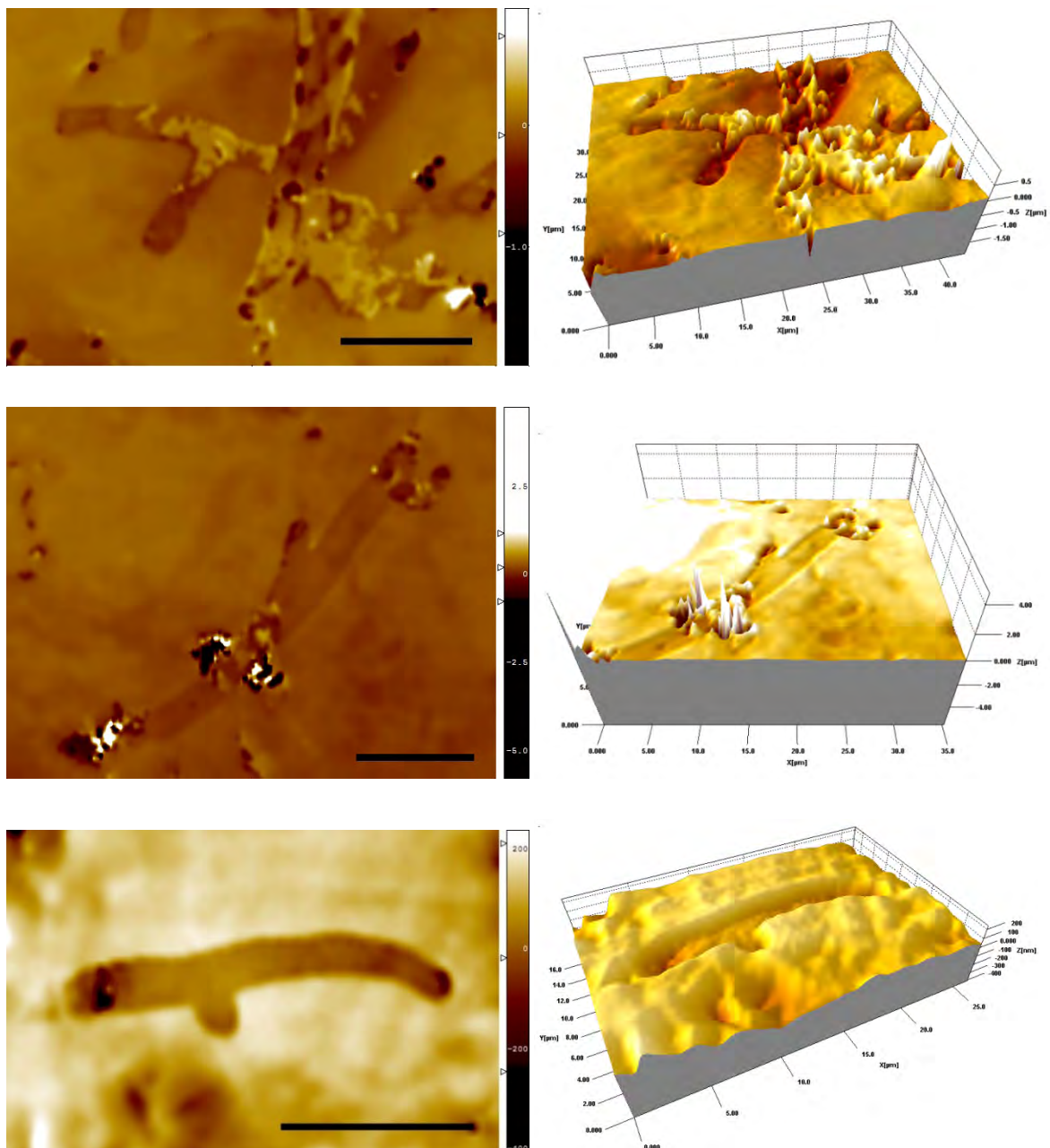

Figure 32: VSI xyz data sets (left) and 3D view of elongated etch pits with side branches on graphite surfaces; scale bars = 10 µm

Measurements of etch pit width (Figures 33 and 36) and depth (Figures 34 and 36) were performed on 45 etch pits on black slate and 249 etch pits on graphite. Figure 33 shows the frequency of etch pit width. The average value for black slate samples was 4.19 ± 1.37 μm and 3.81 ± 0.71 μm for graphite samples. The frequency of etch pit depth is shown in Figure 33. Etch pits on black slate samples were 200.6 ± 91.8 nm deep and 182.6 ± 75.4 nm deep on graphite samples.
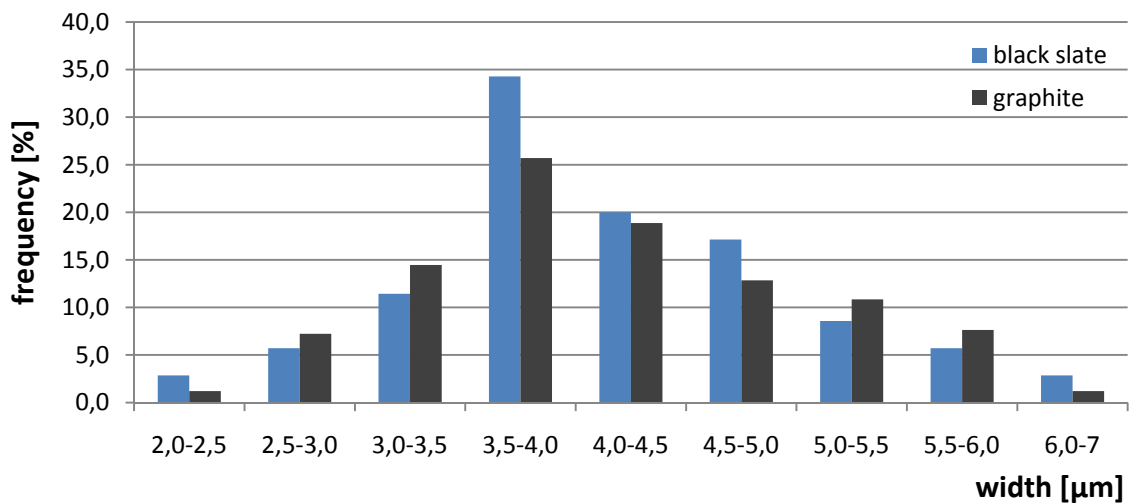

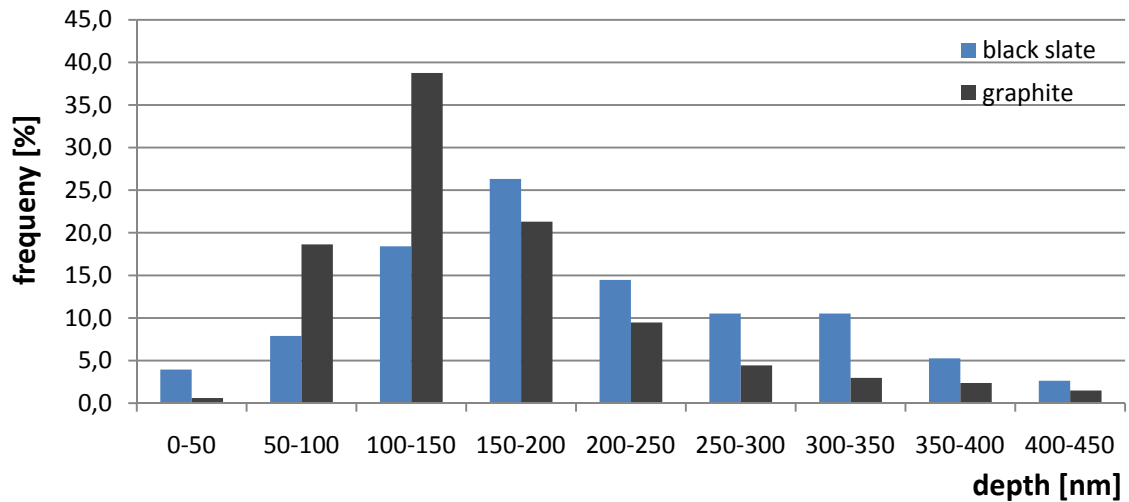Figure 33: frequency of width of etch pits on black slate and graphite sample

Figure 34: frequency of depth of hyphae etch pits on black slate and graphite surfaces

As a result of a stronger etch pit frequency and length, volumes of dissolved graphite material (Figures 35 and 36) were determined. The average volume of dissolved graphite was $3 ± 0.3 × 10^7$ nm^3/μm^2 (Figure 35).
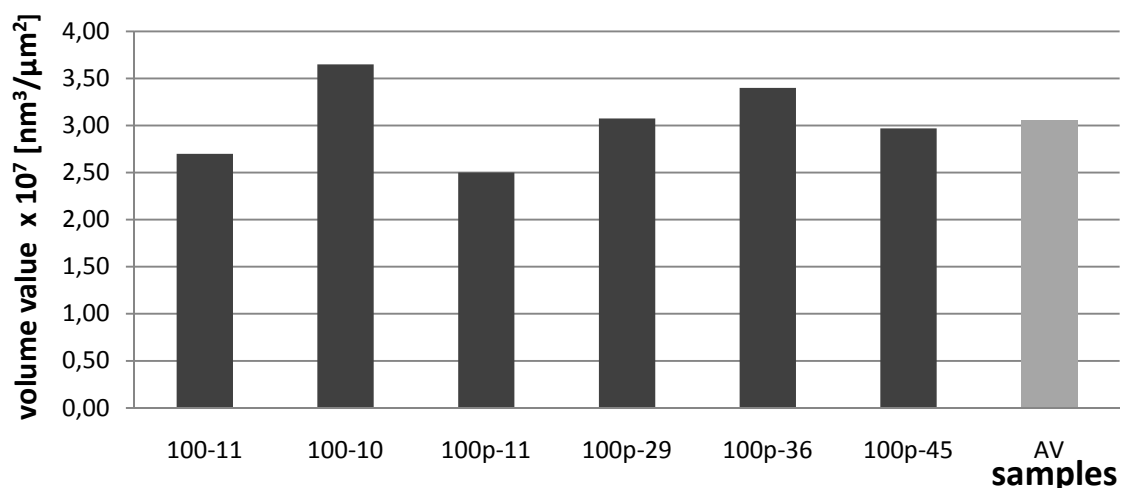
Figure 35: dissolved volume value of fungal etch pits on graphite surfaces
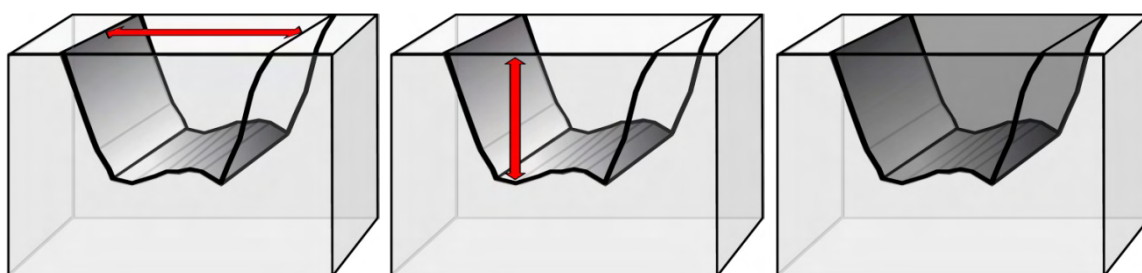
Figure 36: schematic of etch pit measurement (width, depth, volume)

A direct comparison of the same area (Figure 37) with scanning electron microscopy and vertical scanning interferometry showed strengths and weaknesses of each method. With SEM measurements complete hyphae were visible, but information about depth could not be obtained. VSI analyzes showed both peaks and valleys of hyphae and etch pits, but not the texture and physical situation of hyphae. The measured hyphal width of 2.68 µm was equal with both surface analyzing methods. The valley, measured by VSI, was approximately 145 nm deep and the peaks were about 260 nm high. The distance between valleys and peaks was about 405 nm (Figure 38 A). The super elevated illustration of z-scale was used to visualize the size of nanometers. All 3D models show super elevated z-scales as well.
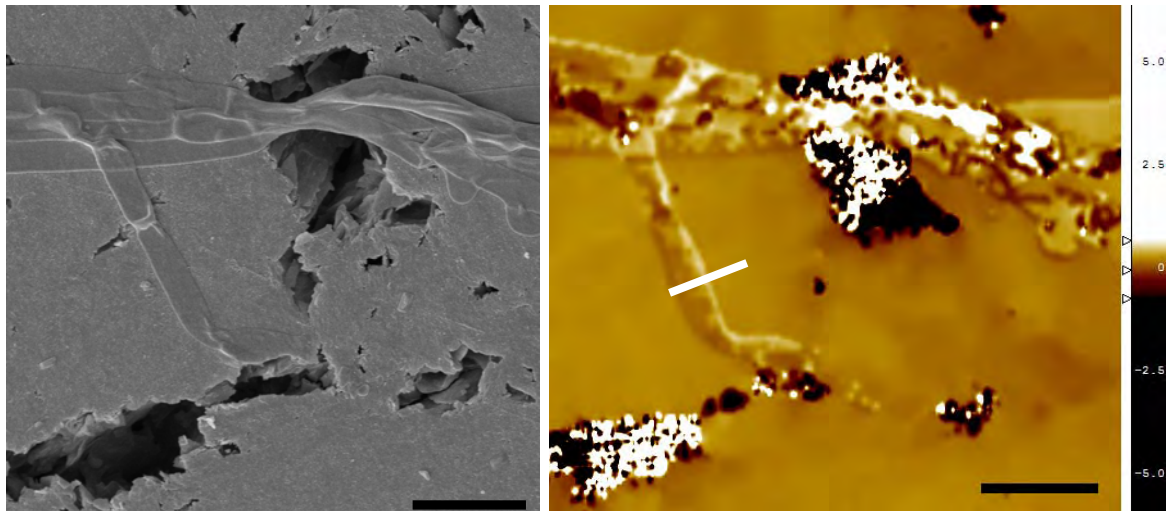
Figure 37: comparison of one area with SEM (left) and VSI (right) measurements; scale bars = 10 µm
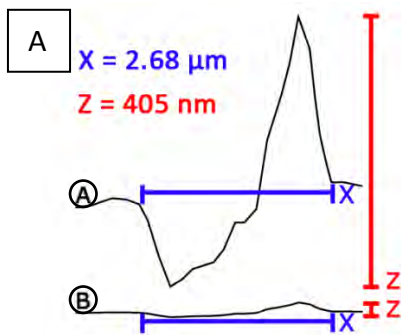
Figure 38: **A)** same profile of etch pit (white bar Figure 37) with different graph scaling properties, Ⓐ super elevated z-scaling, Ⓑ x- and z-scaling are equal; **B** (graphite)**, C** (black slate)**)** hyphae sticking on surface surrounded by etch pits; **D)** VSI xyz data set of graphite surface with etch pit (scale bar = 10 µm); **E)** 3D view of etch pit with hyphae inside
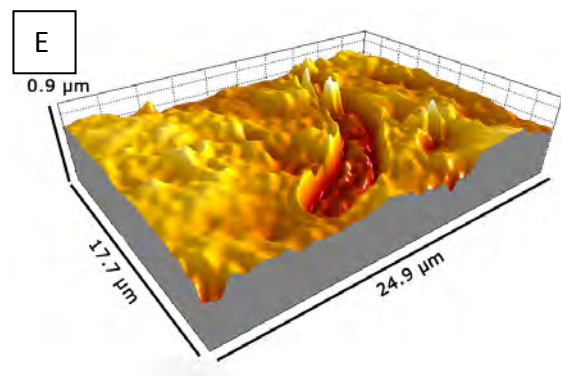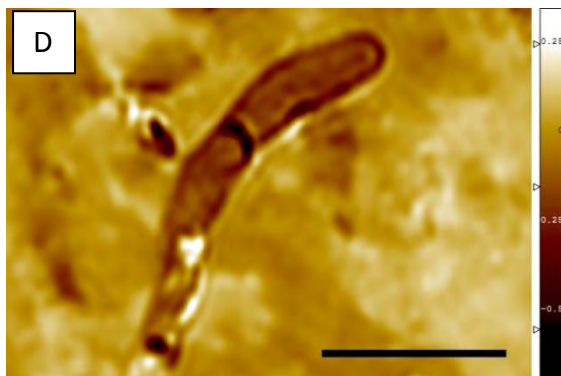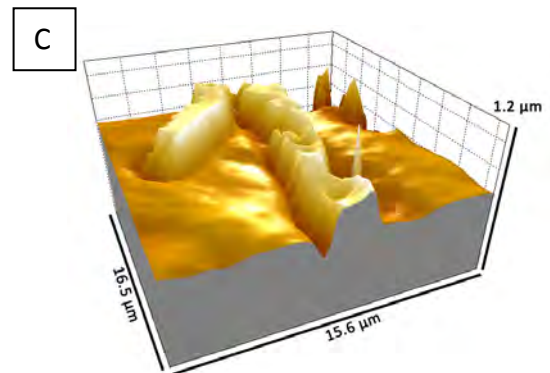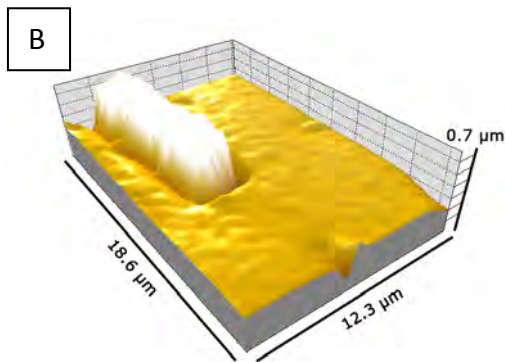
Discussion:

Etch pits were found on all incubated rock samples. This proves microbial impact on rock alteration (Bennett et al., 1996; Buss et al., 2007; Davis and Lüttge, 2005; Hoffland et al., 2002; Lüttge and Conrad, 2004). The higher etch pit frequency on graphite surfaces is caused on the one hand by higher carbon availability and on the other hand by softness of pressed graphite rods (Figure 39 B). The softness of graphite surfaces and carbon availability allow fungal hyphae to grow into the surface over longer distances (Figure 29, 39 B). In contrast to used graphite samples black slate material consists of minerals like quartz and sheet silicates (Fischer, 2002; Fischer et al., 2009; Szurowski, 1985) which are coated by carbon (Mayer, 2005; Modl et al., 2007; Zhuang and Yu, 2002). The less carbon ratio of black slates prevented uniform carbon degradation by fungus (Figure 39 A).
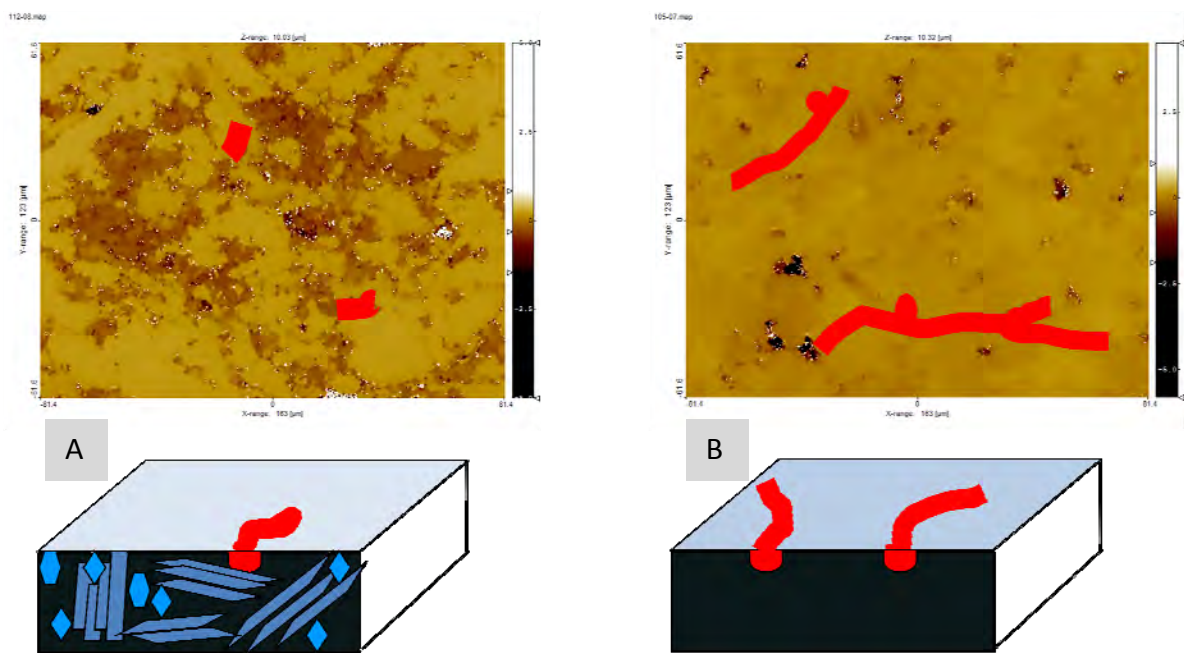
Figure 39: schematic comparison of etch pit frequency on **A)** black slate and **B)** graphite surfaces; material homogeneity in graphite allowed more continuous etch pit formation; black color = carbon; blue colors = minerals like quartz and sheet silicates; red colors = fungal etch pits

There are two possibilities how and why *Schizophyllum commune* created etch pits. On the one hand with mechanical alteration of rock material the fungus created new living space. The "softness" of graphite samples encouraged stronger material depletion in contrast to "harder" minerals of black slate surfaces. But neither on black slate nor on

graphite surfaces was fungal mechanically removed rock material observed. Thus mechanical alteration by *S. commune* is hardly probable. On the other hand, the fungus removed rock material by chemical reactions. It is assumed that enzymes like fungal laccases are able to dissolve carbon fractions of rocks. Scientists proved degradation of carbon containing rocks due to activity of wood-decaying enzymes (Hofrichter et al., 1997a; Hofrichter et al., 1999; Silva-Stenico et al., 2007). Lignin decomposing laccases are supposed to degrade kerogen fractions of black shales or slates due to similarities of carbon structures of lignin and kerogen fractions (Wengel et al., 2006). White-rot fungi, as most efficient lignin degraders, mineralize lignin to carbon dioxide and water (Boyle et al., 1992). As lignin cannot be used as sole carbon and energy source, further carbon sources (like cellulose or glucose) are necessary (Boyle et al., 1992; De Vries et al., 1986). Ligninolytic fungi need additional carbon sources to produce laccases. Further laccase production depends on various conditions like light and temperature availabilities (De Vries et al., 1986). Thus high temperature and darkness support laccase production. De Vries et al. (1986) determined that under specific conditions dikaryotic strains show much higher laccase production than monokariotic strains. This indicates that rock degradation and etch pit frequency depends both on carbon content of rocks and enzyme producing conditions.

The etch pit morphology showed similarities to hyphal morphology (Figure 14). Especially etch pit widths are suited for to fungal hyphae diameters. Etch pits with lateral branches and small etch pits around hyphae, which remained on rock surfaces, were further evidences of fungal induced etch pits. The elongated morphology of some etch pits conclude to an equal degradation due to enzymatic activity. Hence, rock carbon availability seem to influence etch pit morphology. The comparison of a characteristic area showed that etch pits were not empty (Figures 32 and 38). Apparently empty etch pits were filled with hyphae (Figure 38 E). They lay collapsed in their own etch pits. Thus fungal hyphae are able to create their own roughness which leads to better surface adhesion. It is supposed that in spite of mechanically removing mycelia, remaining hyphae stuck in the rock surface. This suggestion is supported by found etch pits surrounding remaining hyphae. Figure 40 illustrates etch pits with hyphae inside.

Therefore, determined depth and volume values are minimum values. To determine entire depth and volume values in future, it is necessary to make sure that all hyphae were removed from surface without modifying the rock surface.
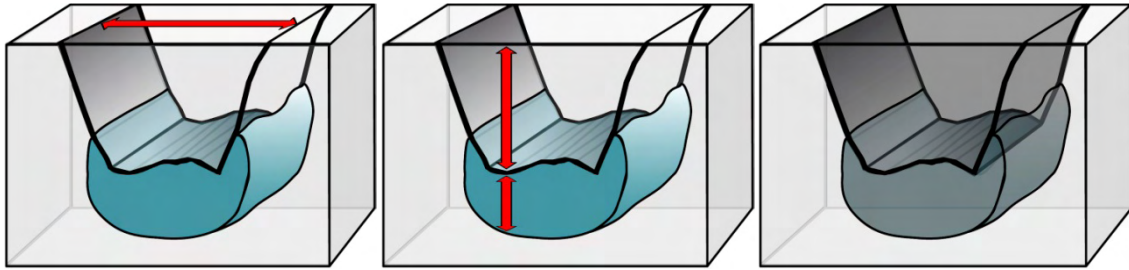

Figure 40: schematic of fungal etch pits with hyphae (blue color) inside; measured depth and volume values are minimum values

Differences between fungal induced etch pits on unbleached (M2) and bleached black slate (M3) surfaces were hardly visible. The etch pit frequency and morphology are similar to each other. Because unbleached and bleached black slates differed in their carbon content and grade of silicification comparisons are difficult. The found etch pits are supposed to be caused by carbon loss. However, it may well be other organics (kerogen) or minerals like quartz or clay minerals were altered due to fungal activity as well (Adeyemi and Gadd, 2005; Buss et al., 2007; Gadd, 2007; Hoffland et al., 2002; Hofrichter et al., 1997a; Hofrichter et al., 1999; Lüttge and Conrad, 2004; Rezacova et al., 2006; Wengel et al., 2006).

Comparing etch pits on black slate and graphite samples, etch pit frequency and morphology differ from each other. As discussed before, etch pits occur more frequently and with a more continuous elongated morphology on graphite surfaces (Siegel et al., 2009). In contrast to black slate, carbon loss of graphite samples is verifiable. Carbon availability and rock material consistence of used graphite samples is suggested to facilitate etch pit frequency and length. On the other hand determined etch pit widths (Figure 33) and depths (Figure 34) seemed to be less influenced by carbon availability. The minimum and maximum values are equal. Interestingly the average value of etch pit depth of black slates were higher than graphite etch pit depth. But due to less etch pit frequency, fewer etch pits could be determined on black slate samples than on graphite

samples. Maybe this influences the statistical statement. Due to their frequency and lengths, volume measurements were only done with etch pits which occurred on graphite surfaces.

During three months of incubation about 0.03 $\mu m^3/\mu m^2$ rock material was removed. But this value was achieved under laboratory conditions. In nature, fungi are addicted to environmental conditions like temperature, water and nutrient availability, and other rival organisms (Madigan et al., 2001).

3.2 Surface Chemistry

3.2.1 Elemental Analysis of Carbon and Nitrogen

Results:

Carbon and nitrogen element analyzes show that the bleached black slates (M3) contained less total organic carbon (0.48 wt. %) than the unbleached samples (M2, 6.17 wt. %). The rate of nitrogen with 0.13 wt. % was equal for both black slate specimens (Table 5) before incubation according to element analyses for C and N.

Table 5: content of total organic carbon (TOC) and nitrogen

Sample	C_{org} [wt. %]	N [wt. %]
black slate unbleached (M2)	6.17	0.13
black slate bleached (M3)	0.48	0.13

Discussion:

The different organic carbon content of the investigated black slate samples was caused by oxidative weathering (Bolton et al., 2006; Fischer and Gaupp, 2005; Fischer et al., 2009; Littke, 1993). Oxidative weathering of organic matter rich sediments and rocks induces carbon loss. Fischer et al. (2007) described organic matter degradation within only a few decades. In contrast to freshly mined unbleached black slate sample (M2) the bleached sample (M3) was collected from a waste dump. The bleached rock specimen (M3) was deposited for at least 53 years (personal communication with K. Müller, Schmiedefeld).

The equal nitrogen content indicates that nitrogen is not affected by oxidative weathering. It might be that nitrogen is incorporated as ammonium (NH_4^+) into clay minerals such as illite or illite/smectite and feldspars (Mingram et al., 2003; Mingram et al., 2005; Stevenson, 1961). The found nitrogen content with < 0.2 wt. % was similar to other black slates (Fischer, 2002). As no microorganisms were found on black slate surfaces (SEM investigation of controls) microbial fouling as nitrogen source can be nearly excluded.

3.2.2 X-Ray Photoelectron Spectroscopy (XPS)

Results:

The surfaces of polished unbleached and bleached black slate, as well as graphite samples (Figure 41) were analyzed by x-ray photoelectron spectroscopy. Survey analyses (Figure 42, appendix) were done with control and incubated samples. The data is shown in Figure 43 and 44.
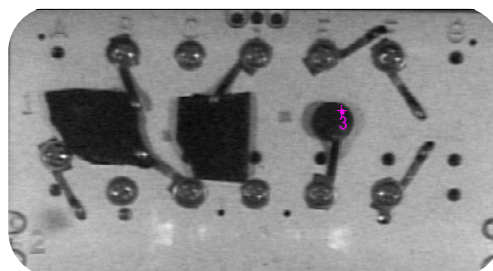
Figure 41: investigated black slate (M2, M3) and graphite sample (G)
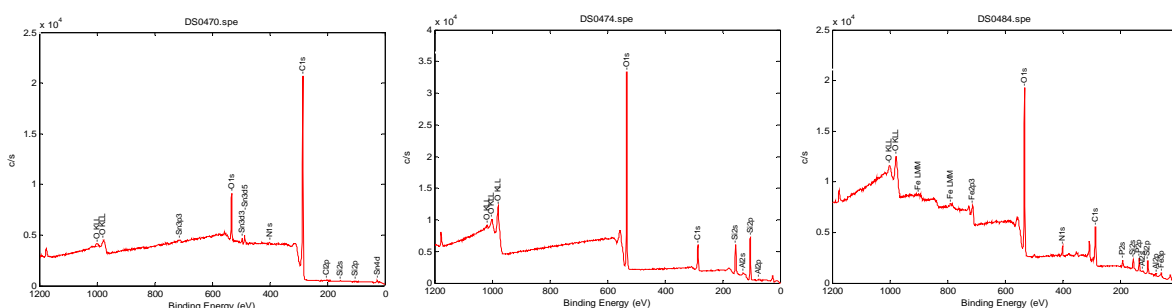
Figure 42: examples of XPS spectra of graphite, unbleached black slate (M2) and bleached black slate (M3)

The graphite sample consisted of ~90 % carbon, ~10 % oxygen and <0.02 % nitrogen (Figure 43). Upon incubation with the fungus, the concentration of nitrogen increased up to 2.32 % (Figure 43). By using a smaller measuring point diameter (MPD) of 10 μm, a nitrogen content of 1.75 % was determined.

Unbleached black slate (M2) control samples consisted of ~20 % carbon, ~57 % oxygen, < 0.5 % aluminum, ~22 % silicium (Figure 44), with nitrogen increasing upon incubation to 6.87 % (Figure 44). The carbon concentration with ~40 % was doubled due to fungal incubation, while silicium changed slightly (18.37 %) or even dramatically (10.18%) and oxygen concentration decreased to ~41 %. With one exception (0.92 %), the atomic concentration of aluminum was equal for both control and incubated samples. No amounts of iron, phosphorus, sodium and magnesium were detected.

	control #1	control #2	sample #1	sample #2	sample #3
■ C1s	87,99	90,09	88,16	90,86	89,92
■ N1s	0,02	0,01	2,32	1,51	1,75
■ O1s	11,31	9,54	9,48	7,62	8,21

Figure 43: atomic concentration of measured elements (C, N, O) on graphite surfaces; control #1, control #2, sample #1 and sample #2 = 100 μm MPD; sample #3 = 10 μm MPD
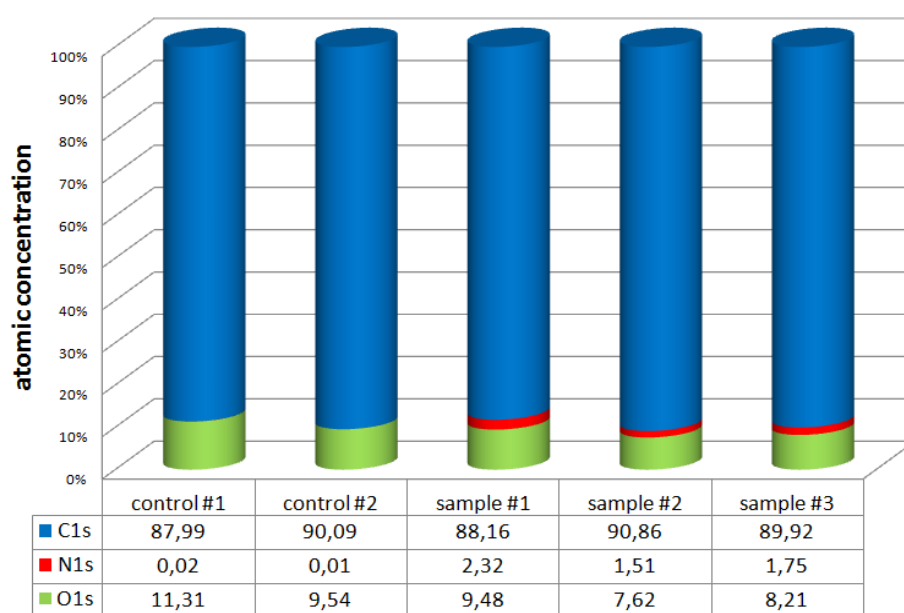

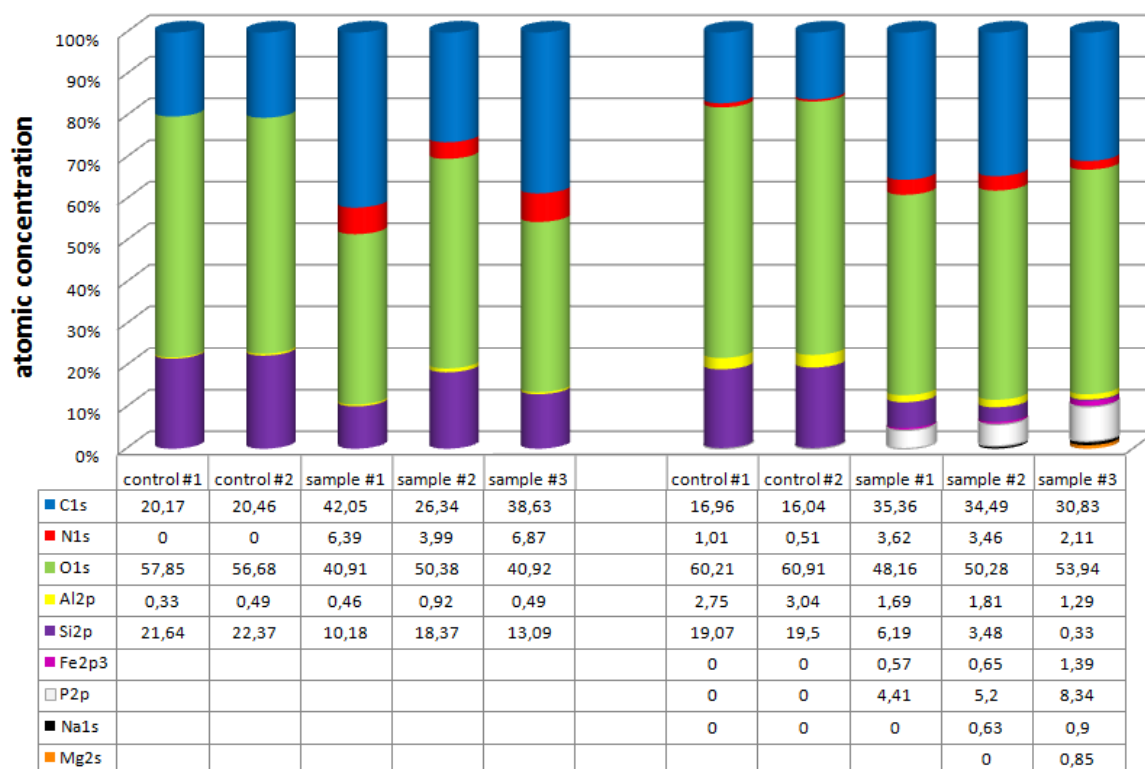|	control #1	control #2	sample #1	sample #2	sample #3		control #1	control #2	sample #1	sample #2	sample #3
■ C1s	20,17	20,46	42,05	26,34	38,63		16,96	16,04	35,36	34,49	30,83
■ N1s	0	0	6,39	3,99	6,87		1,01	0,51	3,62	3,46	2,11
■ O1s	57,85	56,68	40,91	50,38	40,92		60,21	60,91	48,16	50,28	53,94
■ Al2p	0,33	0,49	0,46	0,92	0,49		2,75	3,04	1,69	1,81	1,29
■ Si2p	21,64	22,37	10,18	18,37	13,09		19,07	19,5	6,19	3,48	0,33
■ Fe2p3							0	0	0,57	0,65	1,39
□ P2p							0	0	4,41	5,2	8,34
■ Na1s							0	0	0	0,63	0,9
■ Mg2s										0	0,85

Figure 44: atomic concentration of measured elements (C, N, O, Al, Si, Fe, P, Na, Mg) on unbleached (M2, left) and bleached (M3, right) black slate surfaces; samples #3 = 10 μm MPD; all other samples = 100 μm MPD

Bleached black slate (M3) control samples consisted of ~16 % carbon, ~60 % oxygen, ~3 % aluminum, ~19 % silicium, and 0.5 – 1 % nitrogen (Figure 44). No amounts of iron, phosphorus, sodium and magnesium were detected. The atomic concentration of nitrogen increased up to 3.62 %, the carbon concentration doubled due to fungal incubation (Figure 44). Proportions of silicium decreased dramatically to an average value of ~3%. The atomic concentration of oxygen decreased to ~50 %. Aluminum (1.28 – 1.81 %) decreased as well. Iron (0.57 – 1.39 %), phosphorus (4.41 – 8.34 %) and sodium (0.6 – 0.9 %) were detected only on incubated samples. One measurement with MPD of 10 µm (M3, sample #3) showed amounts of magnesium (0.85 %).

Discussion:

As expected the graphite control sample consisted only of carbon (Allaby, 2008). The very small amounts of nitrogen (<0.02 %) suggest surface contamination with organics (probable microbes). Due to fungal colonization the ratio of nitrogen increased clearly. The surface areas were measured without knowing hyphal presence or absence. Thus, nitrogen presence can be caused by hyphae and/or fungal organic excretions (Ralph et al., 1996; Sinsabaugh and Findlay, 1995; Theuerl and Buscot, 2010). The fungal cell wall is a complex structure composed of chitin, glucans and other polymers (Adams, 2004; Takano et al., 2008; van Wetter et al., 2000; Wessels, 1993). In contrast to fungal cell wall extracellular excretions such as hydrophobins and laccases are protein assemblings (De Vries et al., 1993; Hatamoto et al., 1999; Liers et al., 2007; Linder et al., 2005; Scholtmeijer et al., 2004; Whiteford and Spanu, 2002). Proteins are polypeptides that are created by nitrogen containing amino acids (Madigan et al., 2001). Therefore, fungal peptides (on fungal cell walls or as excretions) are supposed to cause nitrogen increase on graphite surface.

Atomic concentrations of carbon, oxygen, aluminum and silicium were found on unbleached black slate control sample (M2, Figure 44). Silicium is the main component of quartz minerals. Aluminum and silicium are basic components of clay minerals that are hydrous aluminum silicates (Allaby, 2008). Black slates are characterized by carbon as well (Fischer et al., 2007; Fischer et al., 2009). After incubation with *Schizophyllum commune*

chemical modifications were determined on black slate surface (Figure 44). The increase of carbon and nitrogen indicates fungal presence and fungal excretions (Adams, 2004; De Vries et al., 1993; Hatamoto et al., 1999; Liers et al., 2007; Linder et al., 2005; Scholtmeijer et al., 2004; van Wetter et al., 2000; Wessels, 1993; Whiteford and Spanu, 2002). It is suggested that hyphae and their excretions covered the rock surface and inhibited XPS analyses. Iron, phosphorus, sodium and magnesium were not detected. But this is no indication of mineral absence due to small measuring fields of 100 µm and 10 µm respectively.

Atomic concentrations of carbon, oxygen, aluminum and silicium were found on bleached black slate control sample (M3, Figure 44). This indicates that quartz and clay minerals are mixed with carbonaceous fractions as discussed above (Fischer et al., 2009; Littke, 1993). After incubation with fungus, chemical modifications were also determined on bleached black slate surface (Figure 44). The clear increase of carbon and nitrogen proves fungal presence and fungal excretions as well (Adams, 2004; De Vries et al., 1993; Hatamoto et al., 1999; Liers et al., 2007; Linder et al., 2005; Scholtmeijer et al., 2004; van Wetter et al., 2000; Wessels, 1993; Whiteford and Spanu, 2002). Silicium and aluminum decrease can be explained by fungal coating of quartz and clay minerals. Additionally iron, phosphorus, sodium and magnesium increased due to fungal colonization. Phosphorus and magnesium were components of fungal growth media. It is possible that fungal biominerals were detected (Figure 20, Chapter 3.1.2). But neither iron nor sodium was added to CYM. Thus, fungal hyphae solved iron and sodium from black slate material. Baldrian (2003) described the ability of white-rot fungi to adsorb and accumulate metals. As only a few small areas (100 µm and 10 µm) were investigated it is possible that amounts of iron and sodium which occur within black slates (Fischer, 2002; Littke et al., 1991) were not determined on control samples.

Comparing incubated rock samples it is conspicuous that nitrogen content increased on all surfaces. Both nitrogen and carbon increase indicate fungal impact on chemical composition of surfaces. Further fungal adsorption and accumulation of elements such as iron and sodium contained in rock material seem possible.

3.2.3 Electron Microprobe (EMP)

Results: Black Slate

To allow for a spatially resolved element determination, EMP measurements were performed. Silicium, aluminum and potassium were most frequently existent in all investigated unbleached (Figure 45) and bleached black slate samples (Figure 46). As minor elements sulfur, iron, calcium, phosphorus and titanium were determined by single spot EDX analyses, some pyrites were detected in M3 samples. Comparing the element mappings of unbleached (M2) and bleached (M3) rock samples, determined amounts of aluminum, potassium, iron and sulfur were higher in bleached samples. Phosphorus was not detectable at all. Counts of aluminum and potassium were clearly higher than iron or sulfur. Iron and sulfur occurred more frequently on bleached black slate.

Incubated black slate sample areas with hyphae remaining on the rock surface were specifically investigated (Figures 47 - 50). Figure 47 shows a composition scan (BSE) of a black slate (BS) surface with hyphae. Element mappings showed nitrogen, titanium and iron distributed at the hyphal area. Sulfur, magnesium, phosphorus, aluminum, and silicium showed no visible signals. On bleached black slate sample (M3) with remaining hyphae (Figure 49 SE), aluminum and silicium did not occur at the area of fungal growth (Figure 48 Al and Si), while minor amounts of potassium and magnesium could be detected (Figure 49 K and Mg). Calcium accumulations (biominerals) were found near hyphae (Figure 49 Ca). In contrast to the black slate surface, the hyphae showed high amounts of phosphorus, as well as some iron (Figure 50 P and Fe). Nitrogen was found at hyphal area and areas where hyphae had been removed (Figure 50 N). Titanium showed no signals on hyphae (Figure 50 Ti). Further element mappings are attached in the appendix. EDX measurement of fungal hyphae (Figure 51) determined large amounts of phosphorus, some iron and potassium, and low amounts of magnesium, sulfur, sodium and aluminum.
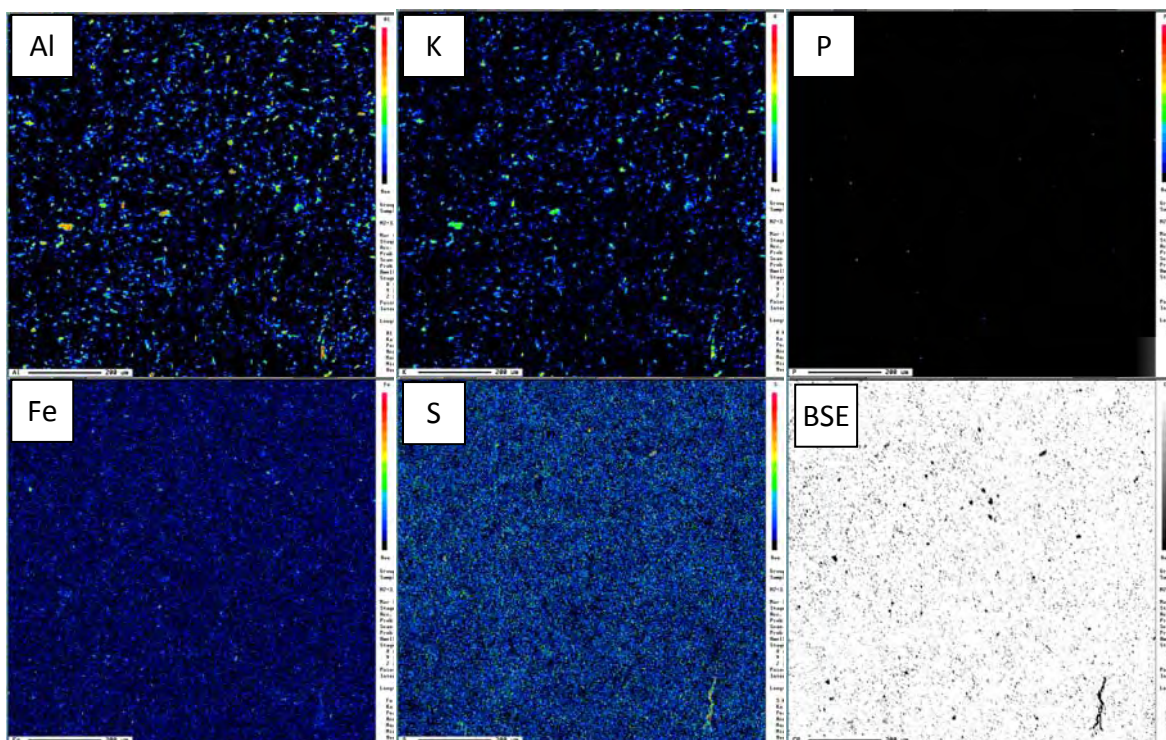
Figure 45: EMP element mapping (Al, K, P, Fe, S, and BSE) of unbleached black slate (M2) control sample
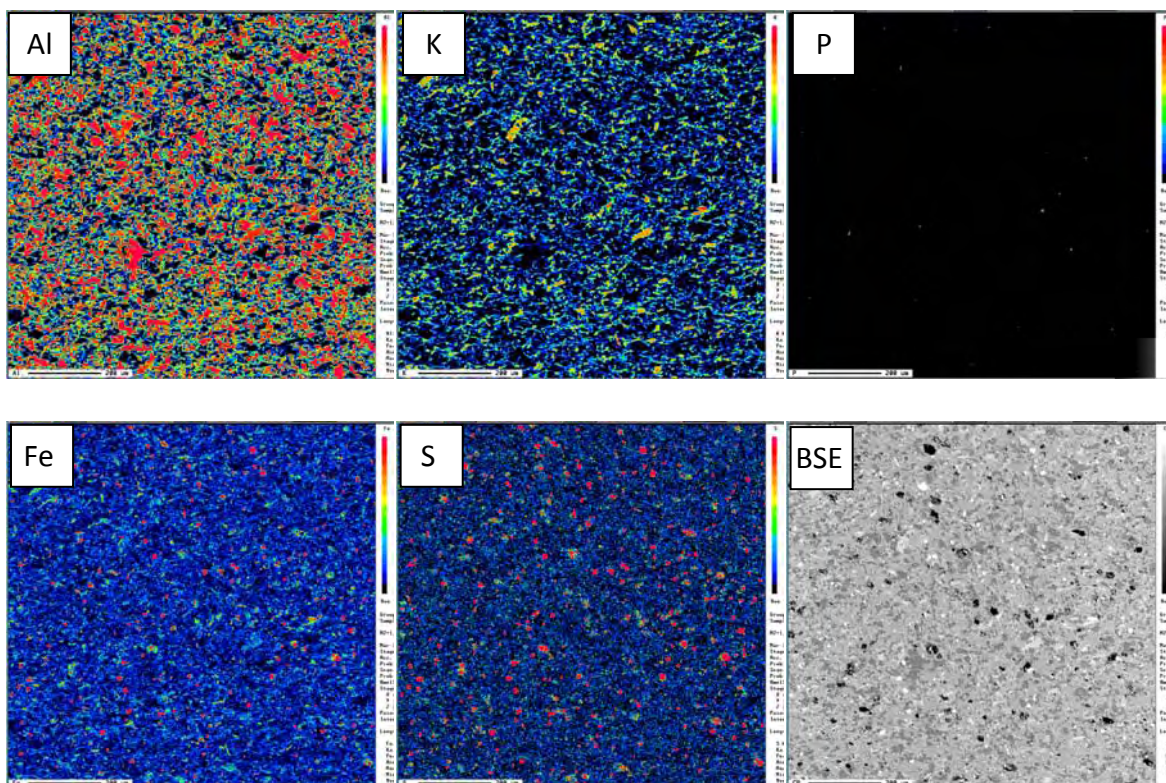

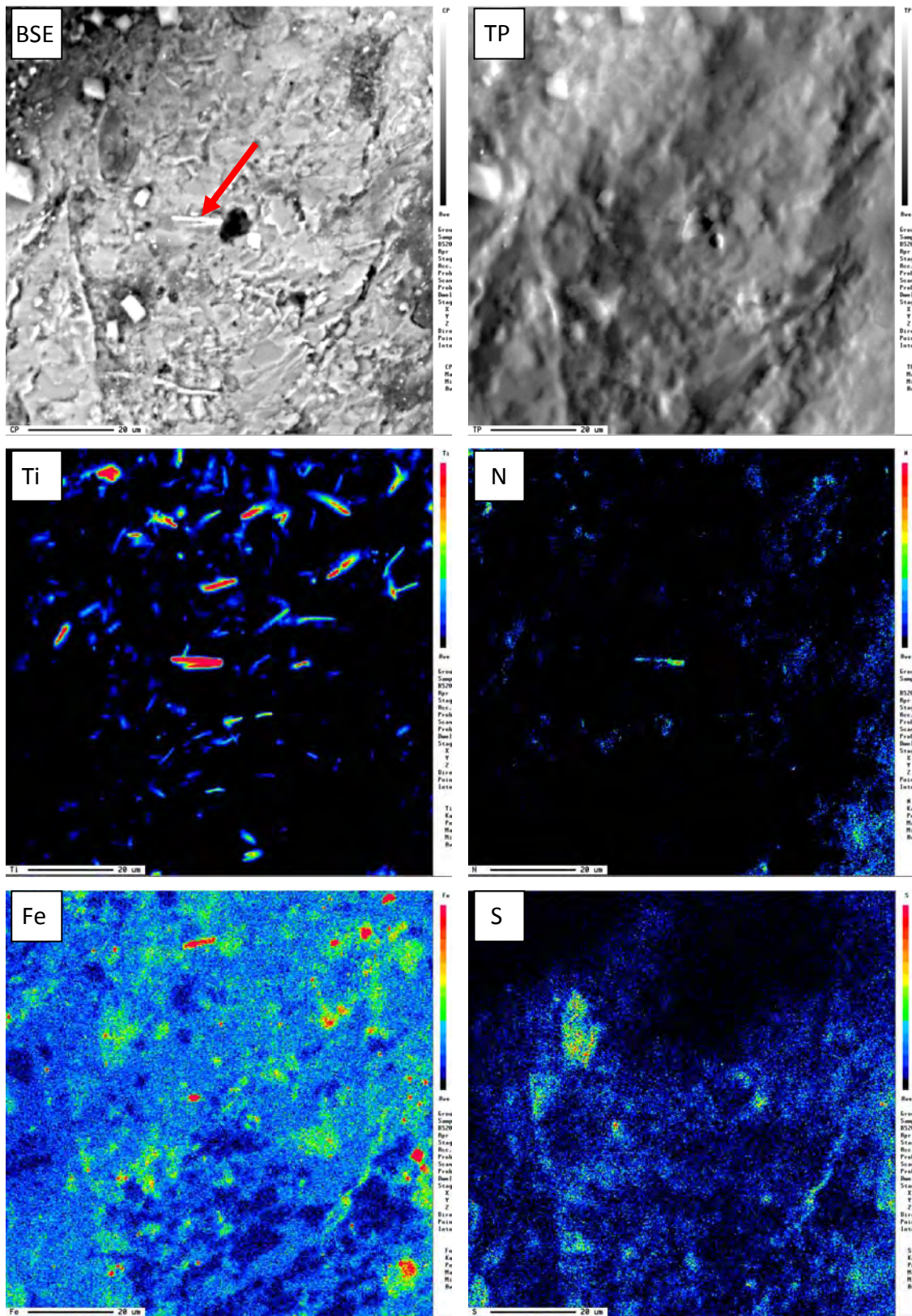Figure 46: EMP element mapping (Al, K, P, Fe S, and BSE) of bleached black slate (M3) control sample

Figure 47: EMP element mapping of black slate surface (BS 208) with hyphal structure; **A)** composition scan (BSE), red arrow = hyphae; **B)** topology scan; **C)** titanium; **D)** nitrogen; **E)** iron; **F)** sulfur; scale bars = 20 μm
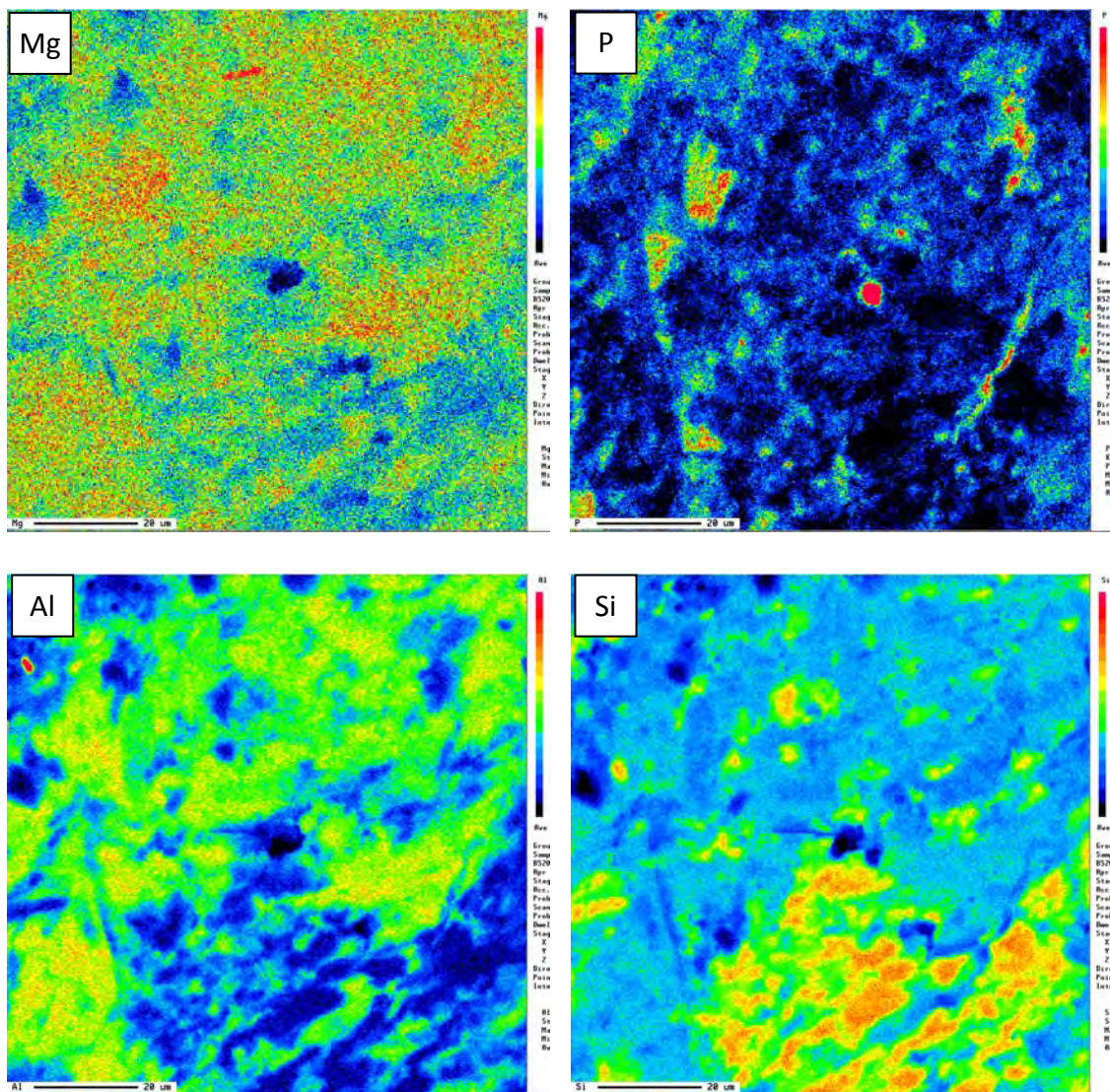
Figure 48: EMP element mapping of black slate surface (BS 208) with hyphal structure; **A)** magnesium; **B)** phosphorus; **C)** aluminum; **D)** silicium; scale bars = 20 μm
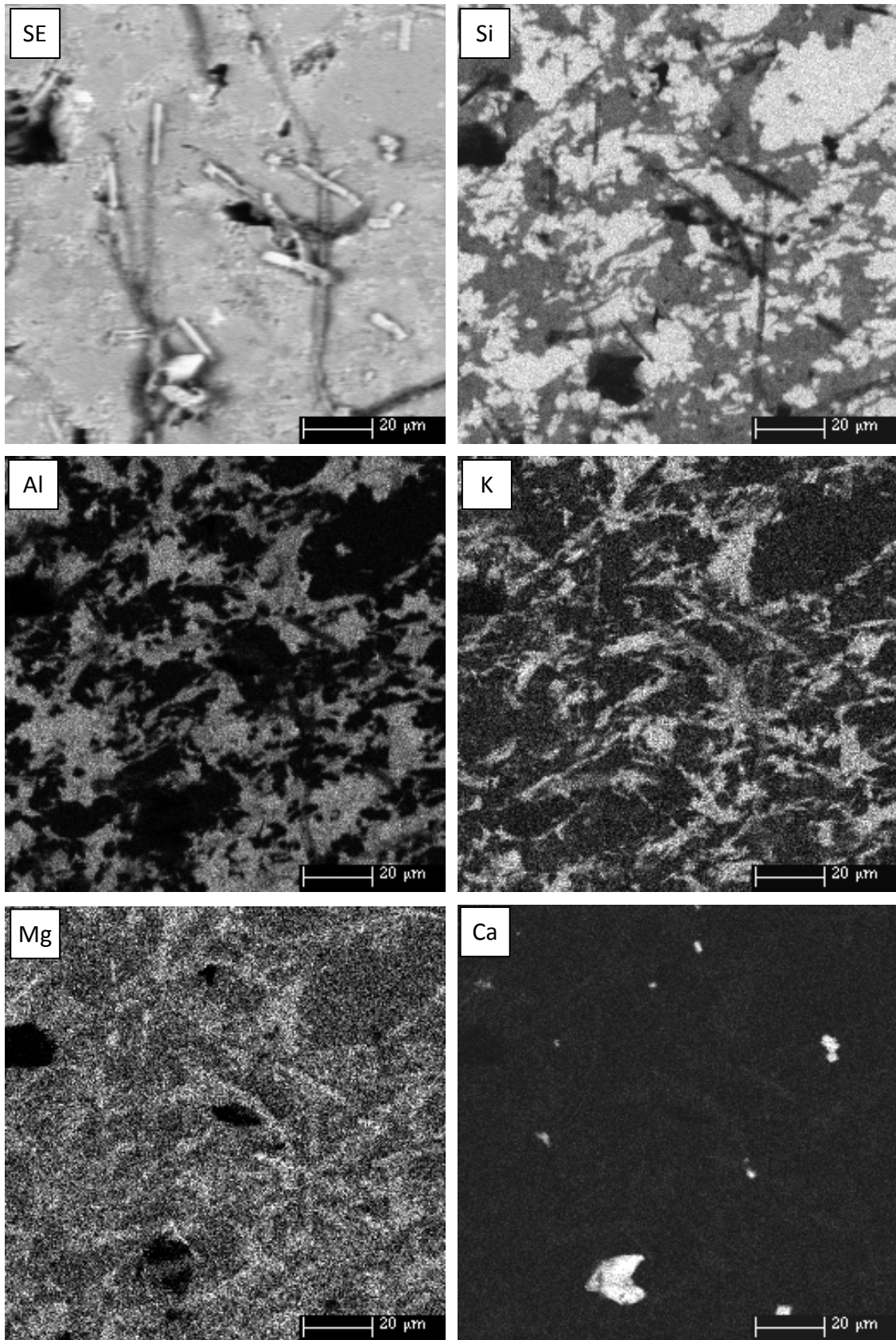
Figure 49: EMP element mapping (SE, Si, Al, K, Mg, Ca) of bleached black slate sample (M3); scale bars = 20 µm
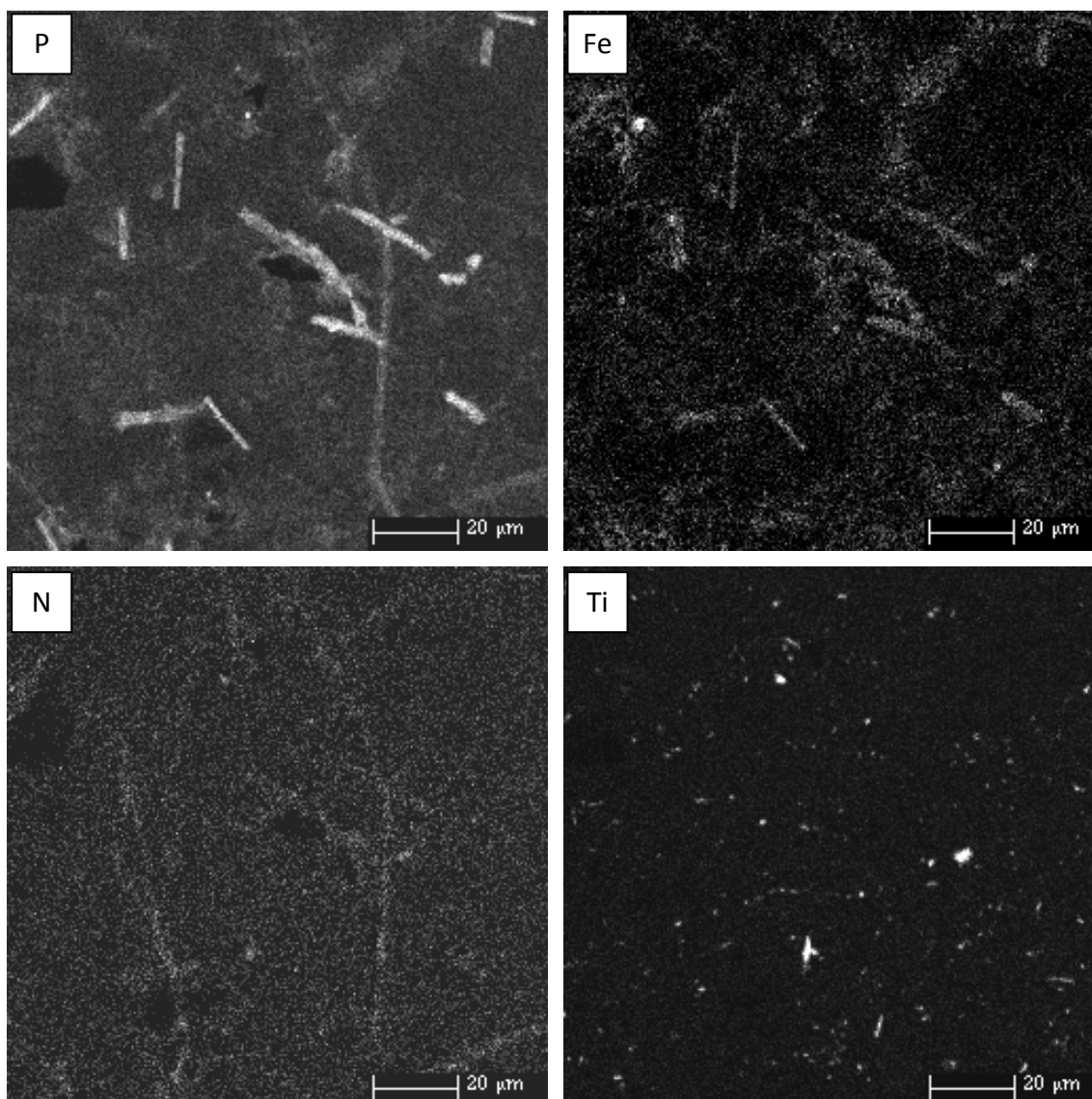
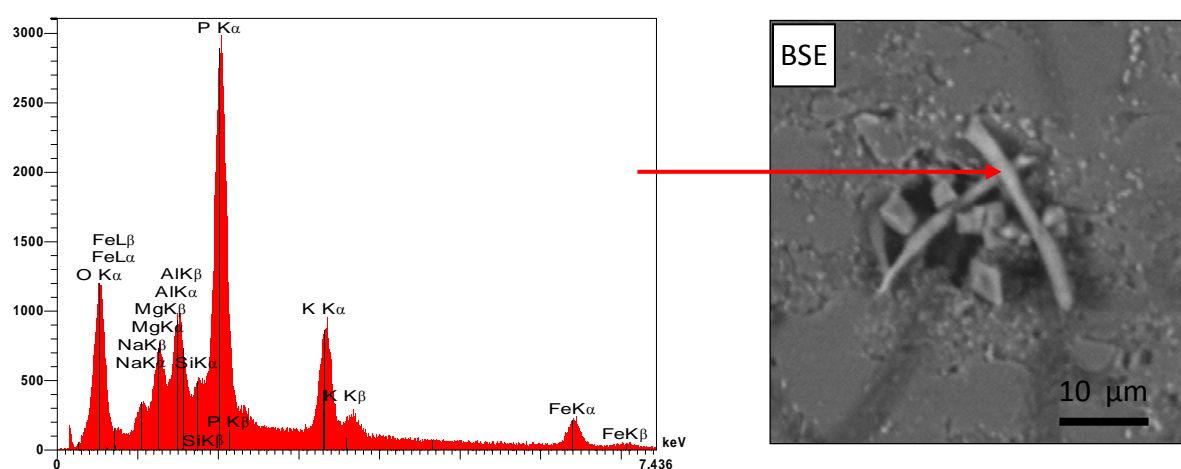Figure 50: EMP element mapping (P, Fe, N, Ti) of bleached black slate sample (M3); scale bars = 20 μm

Figure 51: EDX measurement of hyphae on black slate surface (M3)

Discussion:

Black slate consists of aluminum, potassium and silicium rich minerals. The light colors of BSE-image suggest light material or pore spaces. Therfore, unbleached black slate seems to contain more light elements such as carbon. On bleached black slate (M3) iron and sulfur often occurred together. Iron and sulfur combinations are typical pyrite minerals (Craig et al., 1998; McConville et al., 2000; Schieber, 2002; Wilkin and Barnes, 1997). With optical microscopy and SEM analyses complete and dissolved sulphide minerals were determined. Thus, pyrite loss coincides with or precedes organic carbon loss (Petsch et al., 2000). Phosphorus was hardly distributed on both black slates.

In contrast to control samples, incubated black slate samples with remained hyphae showed other element distributions. Hyphae contained phosphorus, potassium, and small amounts of magnesium which the fungus could accumulate from growth media.

As iron occurred only in rock materials, *Schizophyllum commune* was able to dissolve and accumulate this element. Iron influences many aspects of cell function on various biochemical levels. Iron plays an important role in iron dependent regulations of proteins in iron metabolism, oxidative stress and antioxidant defense mechanism, energy metabolism, cell cycle, and other biochemical processes (Templeton and Liu, 2003). Cytochromes, catalases, peroxidases, iron-sulfur proteins (such as ferredoxin, oxygenases, NADH dehydrogenase) are associated with iron (Madigan et al., 2001). Fungal iron accumulation supports biochemical pathways and black slate alteration. It is suggested that iron was not dissolved from pyrite (still remained) because experiments by Wengel et al. (2006) showed that heavy metal release was not due to pyrite oxidation. Possibly, iron has originated from iron oxides (due to earlier pyrite degradation) or chlorite.

Further nitrogen was found at hyphal areas (Figure 51). Nitrogen as light element is hardly detectable because it shows the same signals as titanium. In this case, titanium can be excluded due to its missing signals (Figure 50). Figure 47 shows that at hyphal area titanium and nitrogen were found. But nitrogen was only enriched at hyphal area. This portends to authenticity of nitrogen presence. In contrast to hyphae, more nitrogen was found at areas where hyphae were removed (Figure 50). This indicates fungal proteins,

such as hydrophobins or exoenzymes, on the rock surface. Hydrophobins are responsible for fungal surface adhesion (Peddireddi, 2008; Wessels, 1993; Whiteford and Spanu, 2002). Extracellular enzymes like laccases are able to degrade carbonaceous components (Fakoussa and Hofrichter, 1999; Hofrichter et al., 1997a; Hofrichter et al., 1999; Theuerl and Buscot, 2010; Wengel et al., 2006). These proteins may have remained on surface due to mycelial removal.

Furthermore, a few calcium bearing aggregations were found near hyphae. The shapes of calcium minerals were similar to crystals and found biominerals. Due to calcium absence in growth media, calcium is suggested to originate from black slate. Formation of biominerals due to fungal colonization is more likely than calcite precipitation. Biomineralization is indicated by very short distance between fungal hyphae and calcium rich minerals.

Since no amounts of silicium and aluminum were found in fungal hyphae, fungus did not dissolve these elements from rock material. Although Figure 51 shows amounts of aluminum and silicium, it must be assumed that these elements were signals from black slate underground.

Results: Graphite

Figure 51 shows the analyzed hyphae on graphite sample. In contrast to titanium and sulfur, nitrogen and phosphorus showed significant signals at hyphal area. A line scan over graphite and hyphal surfaces (Figure 53, Table 6) did show nitrogen increasing to 4.84 %. Potassium (1 %), phosphorus (0.68 %) and, to a lower extent, of sodium (0.33 %) and sulfur (0.33 %) also increased (Figure 54). Additional spot scans (Table 7) showed higher amounts of nitrogen (3.12 %), potassium (0.53 %), phosphorus (0.4 %), sulfur (0.18 %) and sodium (0.22 %) on hyphae. Minor amounts of magnesium (0.1 %) and no amounts of calcium, iron, aluminum and silicium were detected.
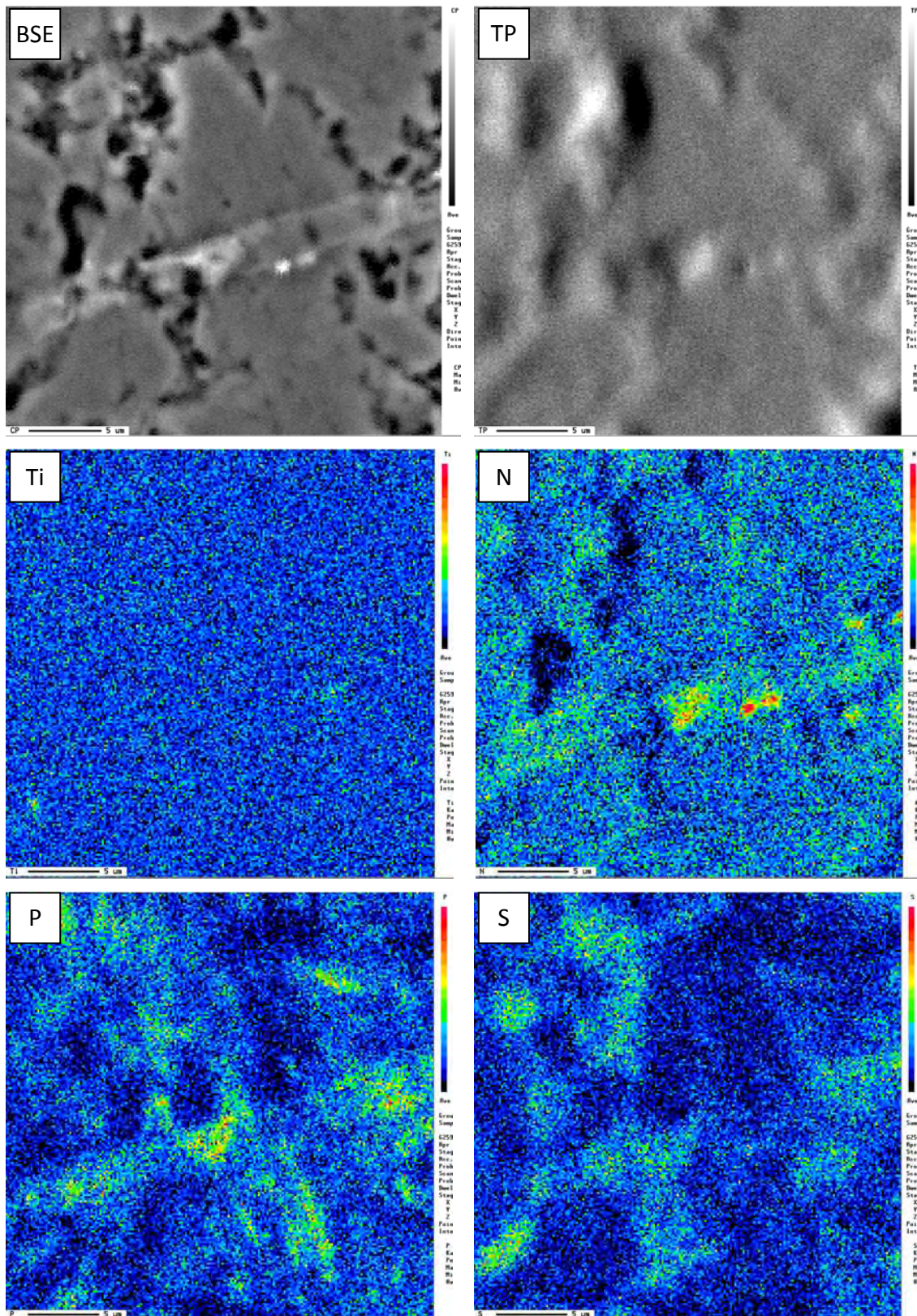
Figure 52: EMP element mapping of graphite surface (259) with hyphal structure, A) composition scan (BSE), B) topology scan, C) titanium, D) nitrogen, E) phosphorus, F) sulfur

Table 6: EMP line scan (25 measuring points) of graphite surface (259) showing mass percent (wt. %) of detected elements (N, K, P, S, Na, Mg and Ca), grey color marks the hyphal area

| No.	N	K	P	S	Na	Mg	Ca
1	0.39	0.28	0.39	0.09	0.09	0.06	0.01
2	0.00	0.21	0.20	0.12	0.08	0.04	0.01
3	0.58	0.16	0.18	0.07	0.04	0.03	0.01
4	0.81	0.16	0.14	0.08	0.06	0.02	0.01
5	1.29	0.31	0.25	0.24	0.09	0.06	0.00
6	1.59	0.47	0.29	0.39	0.11	0.08	0.00
7	0.68	0.49	0.32	0.40	0.16	0.07	0.03
8	0.51	0.24	0.15	0.16	0.11	0.06	0.00
9	0.00	0.23	0.24	0.10	0.09	0.04	0.00
10	0.01	0.19	0.22	0.11	0.06	0.03	0.01
11	0.00	0.27	0.33	0.14	0.12	0.06	0.00
12	0.90	0.18	0.16	0.10	0.06	0.04	0.01
13	0.00	0.22	0.15	0.21	0.07	0.02	0.00
14	0.00	0.18	0.10	0.13	0.05	0.01	0.01
15	0.60	0.17	0.13	0.14	0.09	0.02	0.00
16	0.21	0.16	0.15	0.11	0.05	0.02	0.00
17	2.00	0.15	0.14	0.11	0.07	0.02	0.02
18	4.43	0.70	0.51	0.28	0.24	0.07	0.01
19	4.84	1.00	0.68	0.33	0.33	0.10	0.01
20	2.00	0.33	0.29	0.16	0.13	0.07	0.00
21	0.25	0.12	0.14	0.09	0.05	0.03	0.00
22	0.00	0.08	0.13	0.07	0.04	0.04	0.01
23	0.00	0.08	0.16	0.07	0.03	0.03	0.00
24	0.32	0.32	0.44	0.10	0.13	0.06	0.00
25	0.00	0.20	0.29	0.09	0.08	0.03	0.00
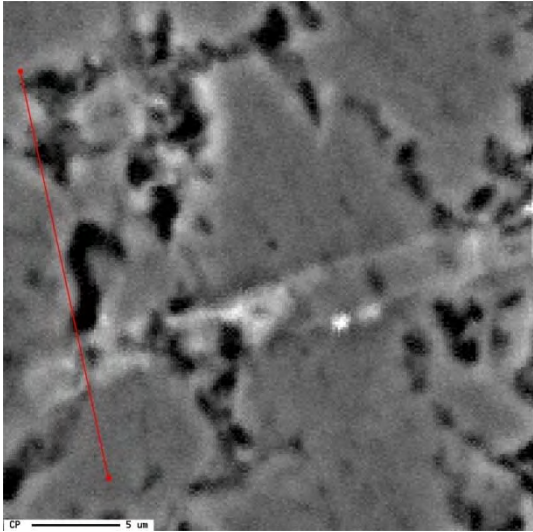
Figure 53: composition scan (BSE) of graphite sample (259), red line marks EMP line scan; scale bar = 5 µm
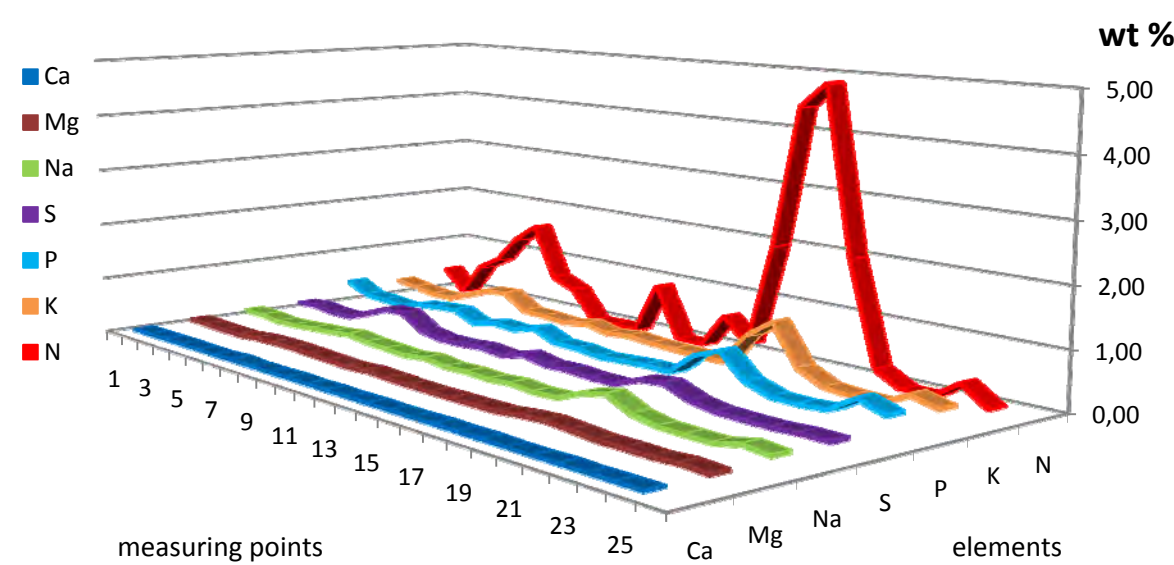

Figure 54: line scan of graphite sample (259, Figure 53) show mass percent of N, K, P, S, Na, Mg and Ca

Table 7: EMP single scans (spots) of blank graphite surface (259) and hyphae showing mass percent (wt. %) of detected elements (N, K, P, S, Na, Mg, Ca, Fe, Al, Si and carbon)

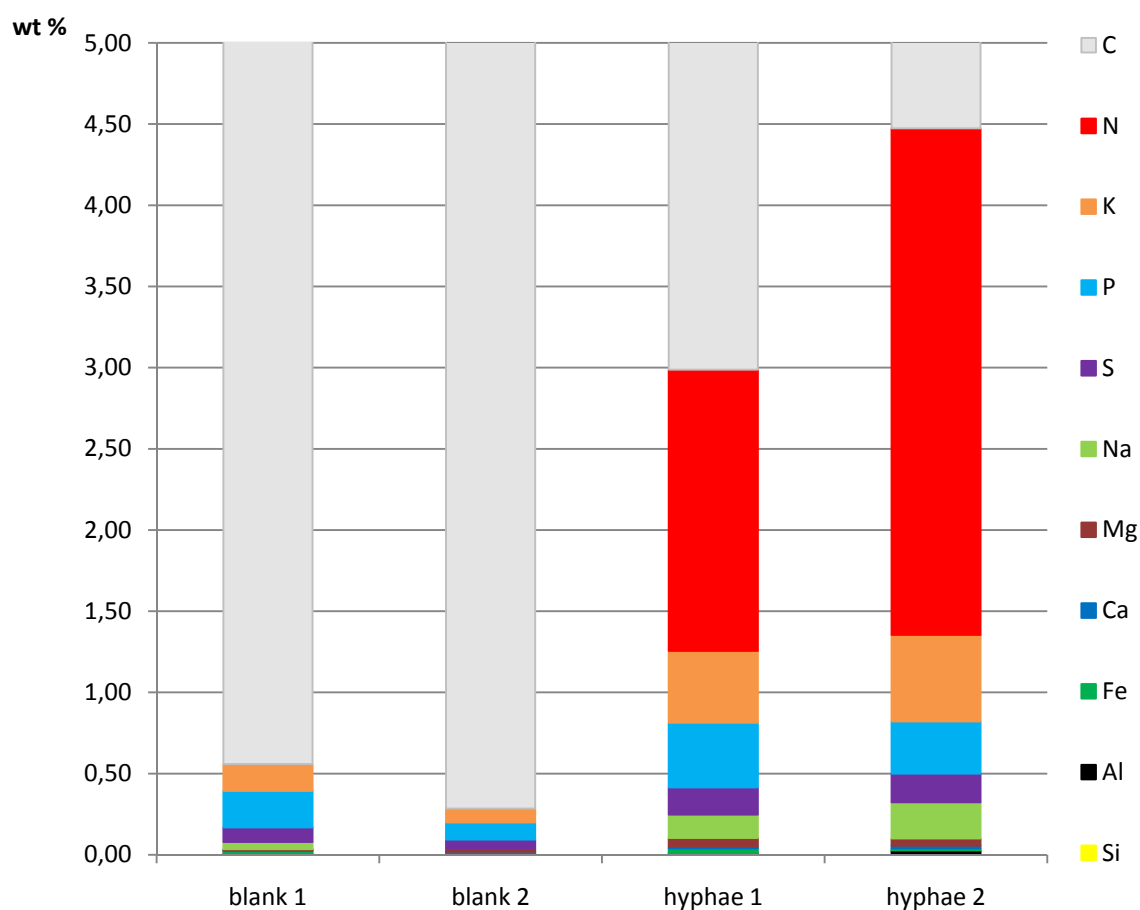|	N	K	P	S	Na	Mg	Ca	Fe	Al	Si	C
blank 1	0.00	0.17	0.22	0.09	0.04	0.01	0.01	0.02	0.01	0.00	99.44
blank 2	0.00	0.09	0.11	0.05	0.00	0.02	0.01	0.00	0.01	0.00	99.71
hyphae 1	1.73	0.44	0.40	0.17	0.14	0.05	0.01	0.00	0.00	0.01	97.04
hyphae 2	3.12	0.53	0.32	0.18	0.22	0.04	0.01	0.01	0.02	0.00	95.55

Figure 55: single spot scans of graphite (259) and hyphal surface show mass percent of N, K, P, S, Na, Mg, Ca, Fe, Al, Si and carbon

Discussion:

The absence of aluminum, silicium, iron, titanium and calcium elucidate graphite purity. Magnesium, sulfur, phosphorus, potassium and nitrogen were added to CYM. These elements were found in different concentrations on graphite and hyphal surfaces. In contrast to graphite surface, the amounts of nitrogen, phosphorus, potassium and sulfur were much higher on hyphae. In spite of lower element concentrations determined on graphite surface, their presences indicate fungal activity. Proteins like hydrophobins and exoenzymes are suggested to remain on surface eminently. Nitrogen, as a main component of proteins (Berg et al., 2007), is the main proof for presence of peptides. Proteins can be associated with phosphorus and sulfur supplementary. Amounts of sodium are unusual because sodium was neither a component of the investigated graphite sample nor added to the medium. Thus, an impurity of one of growth medium components is possible.

4. Summary and Conclusions

Black slate and graphite surfaces were analyzed for the effect of fungal colonization with *Schizophyllum commune*. The complex yeast media (CYM), as a nutrient supply, initialized fungal growth. Fungal aerial mycelia grew over all incubated rock samples subsequently. The complete colonization of the rock material indicated rock attraction to the fungus (Catcheside and Mallett, 1991; Wengel et al., 2006). After three months of incubation the mycelia mats were removed and surface topology and chemistry were analyzed.

Surface Topology:

Surface topology analyzing methods showed an affinity of the fungus to grow and remain on rough surfaces. The hyphae covered large areas (Figure 17 B), coated quartz, clay and other minerals, and grew into nearly all pores bigger than the hyphal diameter. Pores and valleys were colonized very frequently. Comparing black slate and graphite samples, most hyphae stuck on unpolished black slate surfaces, followed by polished bleached and polished unbleached black slates. The rock surface morphology with edges, corners and pits, which is caused by minerals and pores, supported fungal adhesion. Due to its smooth rock surface, the least remaining hyphae were observed on polished graphite samples. Although hyphae preferred rough structures, a few hyphae were found sticking to smooth black slate and graphite surface areas. Thus, adhering forces (Emerson et al., 2006) and organic excretions like hydrophobins (Linder et al., 2005; Scholtmeijer et al., 2004; Wessels, 1993) are suggested to be involved in fungal sticking on rock surfaces as well.

Due to fungal colonization, roughness parameters (R_a, R_q, R_t and F) of rock surfaces changed (Figure 26). In contrast to graphite surfaces, black slates got a smoother surface due to fungal incubation. However, the found values were influenced by rock material loss and fungal presence. Therefore, it is concluded that roughness parameters are inapplicable as long as microorganisms remain.

With vertical scanning interferometric microscopy, fungally induced etch pits were found on all incubated rock samples. This proves microbial impact on rock alteration. Comparing black slate and graphite surfaces, more etch pits were found on graphite samples. In

contrast to etch pits on black slates (Figure 30 and 31), graphite (Figure 29) had a more elongated morphology comparable to hyphae structures. These etch pits achieved up to 30 µm in length, with interruptions even up to 150 µm (Figure 29). The higher etch pit frequency on graphite surfaces is caused on the one hand by higher carbon availability and on the other hand by homogeneity and softness of pressed graphite rods (Figure 39 B). The softness of graphite surfaces and carbon availability allowed fungal hyphae to grow into the surface over longer distances (Figure 29, 39 B). The minor carbon ratio and hardness of mineral grains of black slates prevented uniform rock alteration by *Schizophyllum commune* (Figure 39 A). In spite of minor etch pit frequency of black slate, the average etch pit width (4.19 ± 1.37 µm) and depth (200.6 ± 91.8 nm) were more clear on black slate surfaces. The average width of etch pits on graphite amounted 3.81 ± 0.71 µm and the average depth value was 182.6 ± 75.4 nm. But both width and depth minima and maxima were equal on black slate and graphite samples. Thus the etch pit widths and depths seemed to be less influenced by carbon availability. Because etch pits occurred more frequently on graphite, volume measurements were performed. The average volume value of etch pits on graphite surfaces resulted in $3 ± 0.3 × 10^7$ $nm^3/µm^2$. During three months of incubation about 0.03 $µm^3/µm^2$ rock material was removed. However, this value was achieved under laboratory conditions. In nature, fungi are depended on environmental conditions like temperature, water and nutrient availability, and other rival organisms (Madigan et al., 2001).

The comparison of a characteristic area showed that etch pits were not empty (Figure 32). Apparently empty etch pits were filled with hyphae (Figure 38 E). They lay in their own etch pits. Thus fungal hyphae are able to create their own roughness which leads to better adhering on surface. It is supposed that in spite of mechanical mycelia removal, remaining hyphae stuck in the rock surface. This suggestion is supported by found etch pits surrounding remaining hyphae. Figure 39 illustrates etch pits with hyphae inside. Therefore determined depth and volume values are minimum values.

The etch pit morphology showed similarities to hyphal morphology (Figure 14). Especially etch pit widths suit to fungal hyphae diameters of 2 – 5 µm. Etch pits with lateral

branches and small etch pits around hyphae, which remained on rock surfaces, is further proof of fungal induced etch pits.

Based on fungal capability to excrete organic carbon degrading enzymes, biochemical alteration of rock samples is most likely. *Schizophyllum commune* is able to excrete laccase, an unspecific oxidase, which is able to degrade lignin (Arora and Sharma, 2010; Boyle et al., 1992; De Vries et al., 1986; Hirai et al., 2008; Ko et al., 2001; Leonowicz et al., 2001; Leonowicz et al., 1999; Sharma and Kuhad, 2008; Theuerl and Buscot, 2010). It is assumed that enzymes like fungal laccases are able to dissolve carbon fractions of rocks (Fakoussa and Hofrichter, 1999; Hofrichter et al., 1997a; Wengel et al., 2006). Thus, fungal induced etch pits are suggested to be created by activity of carbon degrading enzymes. The elongated morphology of some etch pits concludes an equal degradation due to enzymatic activity. Hence, rock carbon availability seems to influence etch pit morphology.

During incubation, the fungal hyphae grew with elongated morphology and side branches (Essig, 1920; Weber, 1993). Small lateral structures were found on some hyphae (Figure 15). On one side, the structures created various numbers of elongated excretions and attached to their environment like rock surface or other hyphae (Figure 16 A). This leads to the conclusion that these structures are important for fungal interaction with their environment. Otherwise the lateral structures were able to form bubble-like structures on their tips (Figure 16 B). These bubbles shriveled and collapsed. The obviously altered lateral structures broke up finally. It is assumed that the bubbles might be excretions as well. If the distance between small lateral structures and their neighborhood is too long, excretions are not able to establish a connection with minerals or fungus. They create bubbles instead of filamentous structures. Afterwards the bubbles shrivel due to disuse and the whole lateral structures secede. The appearance of small lateral structures after one month of incubation suggests that they are not necessary for spreading but convenient and helpful to support fungal live. Essig (1920) described lateral projections without any rock material presence. That implies that black slates or graphite are not the

only critical factor to induce lateral structures. The nutrient availability of environment (e.g. nutrient agar media, wood, nutrient containing rocks) may play a rather role.

Surface Chemistry:

Black slate and graphite samples were analyzed by surface chemistry determining methods. Unbleached black slate was characterized by a TOC content of 6.17 % wt. In contrast to that, bleached samples contained 0.48 % wt organic carbon. This indicates oxidative weathering of used bleached black slates.

XPS surveys showed an increase of nitrogen on all investigated and incubated black slate and graphite samples. Furthermore, the carbon ratio increased on both black slate samples (M2 and M3) due to fungal incubation. The Increase of carbon and nitrogen indicates fungal presence and fungal excretions (Adams, 2004; De Vries et al., 1993; Hatamoto et al., 1999; Liers et al., 2007; Linder et al., 2005; Scholtmeijer et al., 2004; van Wetter et al., 2000; Wessels, 1993; Whiteford and Spanu, 2002). With EMP analyses the distribution of nitrogen was determined. Minor amounts of nitrogen were found on fungal hyphae and major amounts were distributed at areas where hyphae were removed (Figure 49). The amounts of nitrogen are suggested to indicate the presence of fungal proteins such as hydrophobins and extracellular enzymes. In addition, fungal hyphae were enriched with carbon, phosphorus, minor amounts of magnesium, potassium and sulfur which the fungus could accumulate from the growth media. Fungal accumulations of iron were only found on hyphae which remained on black slate surfaces. As iron occurred only in black slate material, *Schizophyllum commune* was able to dissolve and accumulate this element from rock material. Iron influences many aspects of metabolism and cell functions on various biochemical levels. Thus, iron accumulation supports fungal life and indicates fungal rock alteration as well.

In contrast to control samples, newly formed minerals were found on incubated black slate and graphite surfaces. These biominerals had amorphous or crystalline shapes. On one side, the minerals found (Figure 20) consisted of phosphorus, magnesium and small amounts of potassium (Table 1). In one case small amounts of sodium were also found. The measured mineral seemed to be a kind of magnesium phosphate with further trace

elements like potassium and sodium. As the phosphorus and magnesium rich biominerals were found between rock surface and hyphae, it must be assumed that biomineralization took place outside of fungal cell walls. Magnesium, phosphorus and potassium were added to fungal growth media.

Calcium containing biominerals were found on black slate samples (Figure 49). Due to calcium absence in growth media, calcium is suggested to originate from black slate. Formation of biominerals due to fungal colonization is more likely to appear than calcite precipitation. Biomineralization is indicated by very short distance between fungal hyphae and calcium rich minerals.

Different oxidations states of black slates influenced fungal colonization and adhering due to its roughness. But the stronger silicification of used bleached samples does not allow quantitative comparisons to fungal activity due to carbon availability.

5. References

Adams D J (2004) Fungal cell wall chitinases and glucanases, *Microbiology-Sgm*, **150**, 2029-2035.

Adeyemi A O and Gadd G M (2005) Fungal degradation of calcium-, lead- and silicon-bearing minerals, *Biometals*, **18**, 269-281.

Alastuey A, Garcia-Sanchez A, Lopez F and Querol X (1999) Evolution of pyrite mud weathering and mobility of heavy metals in the Guadiamar valley after the Aznalcollar spill, south-west Spain, *Science of the Total Environment*, **242**, 41-55.

Allaby M (2008) *Dictionary of Earth Science*, 3rd ed., Oxford University Press, New York.

Altermann W, Bohmer C, Gitter F, Heimann F, Heller I, Lauchli B and Putz C (2009) Defining biominerals and organominerals: Direct and indirect indicators of life. Perry et al., Sedimentary Geology, 201, 157-179, *Sedimentary Geology*, **213**, 150-151.

Arora D S and Sharma R K (2010) Ligninolytic Fungal Laccases and Their Biotechnological Applications, *Applied Biochemistry and Biotechnology*, **160**, 1760-1788.

Baldrian P (2003) Interactions of heavy metals with white-rot fungi, *Enzyme and Microbial Technology*, **32**, 78–91.

Barbour M E, O'Sullivan D J, Jenkinson H F and Jagger D C (2007) The effects of polishing methods on surface morphology, roughness and bacterial colonisation of titanium abutments, *Journal of Materials Science-Materials in Medicine*, **18**, 1439-1447.

Barker W W, Welch S A, Chu S and Banfield J F (1998) Experimental observations of the effects of bacteria on aluminosilicate weathering, *American Mineralogist*, **83**, 1551-1563.

Bartnicki-Garcia S and Lippman E (1972) The Bursting Tendency of Hyphal Tips of Fungi: Presumptive Evidence for a Delicate Balance between Wall Synthesis and Wall Lysis in Apical Growth, *Journal of General Microbiology*, **73**, 487-500.

Bennett P C, Hiebert F K and Choi W J (1996) Microbial colonization and weathering of silicates in a petroleum-contaminated groundwater, *Chemical Geology*, **132**, 45-53.

Berg A and Banwart S A (2000) Carbon dioxide mediated dissolution of Ca-feldspar: implications for silicate weathering, *Chemical Geology*, **163**, 25-42.

Berg J M, Tymoczko J L and Stryer L (2007) *Stryer Biochemie*, 6.ed., Spektrum Akademischer Verlag, Heidelberg, Berlin, Oxford.

Berner R A (2003) The long-term carbon cycle, fossil fuels and atmospheric composition, *Nature*, **426**, 323-326.

Bolton E W, Berner R A and Petsch S T (2006) The weathering of sedimentary organic matter as a control on atmospheric O-2: II. Theoretical modeling, *American Journal of Science*, **306**, 575-615.

Boßelmann F (2007) Charakterisierung biogener Mineralien zum Verständnis der Biomineralisation und Anwendung dieser Prinzipien auf die Kristallisation verschiedener calciumbasierter Materialien. Universität Duisburg-Essen, Duisburg-Essen, (Thesis)

Boyle C D, Kropp B R and Reid I D (1992) Solubilization and Mineralization of Lignin by White Rot Fungi, *Applied and Environmental Microbiology*, **58**, 3217-3224.

Brehm U, Gorbushina A and Mottershead D (2005) The role of microorganisms and biofilms in the breakdown and dissolution of quartz and glass, *Palaeogeography Palaeoclimatology Palaeoecology*, **219**, 117-129.

Brill H (1994) Allgemeine Schutzmaßnahmen vor biogener Materialzerstörung, *Werkstoffe und Korrosion*, **45**, 147-151.

Burford E P, Fomina M and Gadd G M (2003) Fungal involvement in bioweathering and biotransformation of rocks and minerals, *Mineralogical Magazine*, **67**, 1127-1155.

Burford E P, Hillier S and Gadd G M (2006) Biomineralization of fungal hyphae with calcite (CaCO3) and calcium oxalate mono- and dihydrate in carboniferous limestone microcosms, *Geomicrobiology Journal*, **23**, 599-611.

Burkhardt E M, Meisser S, Merten D, Büchel G and Küsel K (2009) Heavy metal retention and microbial activities in geochemical barriers formed in glacial sediments subjacent to a former uranium mining leaching heap, *Chemie Der Erde-Geochemistry*, **69**, 21-34.

Buss H L, Lüttge A and Brantley S L (2007) Etch pit formation on iron silicate surfaces during siderophore-promoted dissolution, *Chemical Geology*, **240**, 326-342.

Carlsson E and Büchel G (2005) Screening of residual contamination at a former uranium heap leaching site, Thuringia, Germany, *Chemie Der Erde-Geochemistry*, **65**, 75-95.

Catcheside D E A and Mallett K J (1991) Solubilization of australian lignites by fungi and other microorganisms, *Energy & Fuels*, **5**, 141-145.

Chertov O, Gorbushina A and Deventer B (2004) A model for microcolonial fungi growth on rock surfaces, *Ecological Modelling*, **177**, 415-426.

Cooke W B (1961) The genus Schizophyllum, *Mycologia*, **53**, 575-599

Craig J R, Vokes F M and Solberg T N (1998) Pyrite: physical and chemical textures, *Mineralium Deposita*, **34**, 82-101.

Crawford D L and Crawford R L (1980) Microbial Degradation of Lignin, *Enzyme and Microbial Technology*, **2**, 11-22.

Davis K J and Lüttge A (2005) Quantifying the relationship between microbial attachment and mineral surface dynamics using vertical scanning interferometry (VSI), *American Journal of Science*, **305**, 727-751.

Davis S A, Dujardin E and Mann S (2003) Biomolecular inorganic materials chemistry, *Current Opinion in Solid State & Materials Science*, **7**, 273-281.

de los Rios A, Camara B, del Cura M A G, Rico V J, Galvan V and Ascaso C (2009) Deteriorating effects of lichen and microbial colonization of carbonate building rocks in the Romanesque churches of Segovia (Spain), *Science of the Total Environment*, **407**, 1123-1134.

De Vries O M H, Fekkes M P, Wosten H A B and Wessels J G H (1993) Insoluble Hydrophobin Complexes in the Walls of Schizophyllum-Commune and Other Filamentous Fungi, *Archives of Microbiology*, **159**, 330-335.

De Vries O M H, Kooistra W and Wessels J G H (1986) Formation of extracellular laccase by Schizophyllum commune dikaryon, *Journal of General Microbiology*, **132**, 2817-2826.

Dean J F D and Eriksson K E L (1992) Biotechnological modification of lignin structure and composition in forest trees, *Holzforschung*, **46**, 135-147.

Dempsey G P and Beever R E (1979) Electron microscopy of the rodlet layer of Neurospora crassa conidia, *Journal of Bacteriology*, **140**, 1050-1062.

Devries O M H and Wessels J G H (1972) Release of Protoplasts from Schizophyllum commune by a Lytic Enzyme Preparation from Trichoderma viride, *Journal of General Microbiology*, **73**, 13-&.

Dold B, Blowes D W, Dickhout R, Spangenberg J E and Pfeifer H R (2005) Low molecular weight carboxylic acids in oxidizing porphyry copper tailings, *Environmental Science & Technology*, **39**, 2515-2521.

Dong H L, Fredrickson J K, Kennedy D W, Zachara J M, Kukkadapu R K and Onstott T C (2000) Mineral transformation associated with the microbial reduction of magnetite, *Chemical Geology*, **169**, 299-318.

Dutton M V, Evans C S, Atkey P T and Wood D A (1993) Oxalate production by Basidiomycetes, including the white-rot species Coriolus versicolor and Phanerochaete chrysosporium, *Applied Microbiology and Biotechnology*, **39**, 5-10.

Eger G (1970) Effect of Some N-Compounds on Growth of Mycelium and Formation of Primordia in Basidiomycete Pleurotus Spec from Florida, *Archiv für Mikrobiologie*, **74**, 160-&.

Ehrlich H, Koutsoukos P G, Demadis K D and Pokrovsky O S (2008) Principles of demineralization: Modern strategies for the isolation of organic frameworks Part I. Common definitions and history, *Micron*, **39**, 1062-1091.

Emerson R J, Bergstrom T S, Liu Y T, Soto E R, Brown C A, McGimpsey W G and Camesano T A (2006) Microscale correlation between surface chemistry, texture, and the adhesive strength of Staphylococcus epidermidis, *Langmuir*, **22**, 11311-11321.

Essig F M (1920) The morphology, development and economic aspects of Schizophyllum commune Fries. University of California, (Thesis)

Evangelou V P (1995) *Pyrite oxidation and its control*, CRC Press, Boca Raton New York London Tokio.

Fakoussa R M and Hofrichter M (1999) Biotechnology and microbiology of coal degradation, *Applied Microbiology and Biotechnology*, **52**, 25-40.

Fischer C (2002) Oberflächenquantifizierung an Schwarzpeliten unterschiedlicher Verwitterungsgrade. Friedrich-Schiller-Universität, Jena, (Thesis)

Fischer C and Gaupp R (2004) Multi-scale rock surface area quantification - a systematic method to evaluate the reactive surface area of rocks, *Chemie Der Erde-Geochemistry*, **64**, 241-256.

Fischer C and Gaupp R (2005) Change of black shale organic material surface area during oxidative weathering: Implications for rock-water surface evolution, *Geochimica Et Cosmochimica Acta*, **69**, 1213-1224.

Fischer C, Karius V and Thiel V (2007) Organic matter in black slate shows oxidative degradation within only a few decades, *Journal of Sedimentary Research*, **77**, 355-365.

Fischer C and Lüttge A (2007) Converged surface roughness parameters - A new tool to quantify rock surface morphology and reactivity alteration, *American Journal of Science*, **307**, 955-973.

Fischer C, Schmidt C, Bauer A, Gaupp R and Heide K (2009) Mineralogical and geochemical alteration of low-grade metamorphic black slates due to oxidative weathering, *Chemie Der Erde-Geochemistry*, **69**, 127-142.

Folk R L (2005) Nannobacteria and the formation of framboidal pyrite: Textural evidence, *Journal of Earth System Science*, **114**, 369-374.

Fomina M, Ritz K and Gadd G M (2000) Negative fungal chemotropism to toxic metals, *Fems Microbiology Letters*, **193**, 207-211.

Fouad H K and El-Rakaiby R M (2009) Environmental Geochemistry for Heavy Metals and Uranium Potentiality in Oil Shale Sediments, Quseir, Red Sea, Egypt, *Journal of Applied Scienes Research*, **5**, 914-921.

Fowler T J, DeSimone S M, Mitton M F, Kurjan J and Raper C A (1999) Multiple Sex Pheromones and Receptors of a Mushroom-producing Fungus Elicit Mating in Yeast *Molecular Biology of the Cell*, **10**, 2559–2572.

Fowler T J and Mitton M F (2000) Scooter, a new active transposon in Schizophyllum commune, has disrupted two genes regulating signal transduction, *Genetics*, **156**, 1585-1594.

Fratesi S E, Lynch F L, Kirkland B L and Brown L R (2004) Effects of SEM preparation techniques on the appearance of bacteria and biofilms in the carter sandstone, *Journal of Sedimentary Research*, **74**, 858-867.

Fritsche W, Hofrichter M and Ziegenhagen D (1999) Biodegradation of Coals and Lignite. In: *Biochemical Principles and Mechanisms of Biosynthesis and Biodegradation of Polymers* (ed Steinbüchel A). Wiley-VCH Weinheim, pp. 265-271

Fuchs G and Schlegel H G (2007) *Allgemeine Mikrobiologie*, 8.ed., Georg Thieme Verlag, Stuttgart.

Gadd G M (2007) Geomycology: biogeochemical transformations of rocks, minerals, metals and radionuclides by fungi, bioweathering and bioremediation, *Mycological Research*, **111**, 3-49.

Gadd G M (2010) Metals, minerals and microbes: geomicrobiology and bioremediation, *Microbiology-Sgm*, **156**, 609-643.

Giannantonio D J, Kurth J C, Kurtis K E and Sobecky P A (2009) Effects of concrete properties and nutrients on fungal colonization and fouling, *International Biodeterioration & Biodegradation*, **63**, 252-259.

Gleeson D B, Clipson N, Melville K, Gadd G M and McDermott F P (2005) Characterization of fungal community structure on a weathered pegmatitic granite, *Microbial Ecology*, **50**, 360-368.

Glombitza C, Mangelsdorf K and Horsfield B (2009) A novel procedure to detect low molecular weight compounds released by alkaline ester cleavage from low maturity coals to assess its feedstock potential for deep microbial life, *Organic Geochemistry*, **40**, 175-183.

Gorbushina A A, Krumbein W E, Hamman C H, Panina L, Soukharjevski S and Wollenzien U (1993) Role of black fungi in color-change and biodeterioration of antique marbles, *Geomicrobiology Journal*, **11**, 205-221.

Grawunder A, Lonschinski M, Merten D and Büchel G (2009) Distribution and bonding of residual contamination in glacial sediments at the former uranium mining leaching heap of Gessen/Thuringia, Germany, *Chemie Der Erde-Geochemistry*, **69**, 5-19.

Green F, Clausen C A, Larsen M J and Highley T L (1992) Immuno-scanning electron microscopic localization of extracellular wood-degrading enzymes within the fibrillar sheath of the brown-rot fungus Postia placenta, *Canadian Journal of Microbiology*, **38**, 898-904.

Haferburg G, Kloess G, Schmitz W and Kothe E (2008) "Ni-struvite" - A new biomineral formed by a nickel resistant Streptomyces acidiscabies, *Chemosphere*, **72**, 517-523.

Hagedorn F and Machwitz M (2007) Controls on dissolved organic matter leaching from forest litter grown under elevated atmospheric CO2, *Soil Biology & Biochemistry*, **39**, 1759-1769.

Hatamoto O, Sekine H, Nakano E and Abe K (1999) Cloning and expression of a cDNA encoding the laccase from Schizophyllum commune, *Bioscience Biotechnology and Biochemistry*, **63**, 58-64.

Heilmann-Clausen J and Boddy L (2005) Inhibition and stimulation effects in communities of wood decay fungi: Exudates from colonized wood influence growth by other species, *Microbial Ecology*, **49**, 399-406.

Heuse T, Erdtmann B-D and Kraft P (1994) Early Ordovician microfossils (acritarchs, chitinozoans) and graptolites from the Schwarzburg Anticline, Thuringia (Germany), *Veröffentlichungen des Naturhistorischen Museums Schleusingen*, **9**, 41-68.

Hiebert F K and Bennett P C (1992) Microbial Control of Silicate Weathering in Organic-Rich Ground-Water, *Science*, **258**, 278-281.

Hirai H, Kashima Y, Hayashi K, Sugiura T, Yamagishi K, Kawagishi H and Nishida T (2008) Efficient expression of laccase gene from white-rot fungus Schizophyllum commune in a transgenic tobacco plant, *Fems Microbiology Letters*, **286**, 130-135.

Hoffland E, Giesler R, Jongmans T and van Breemen N (2002) Increasing feldspar tunneling by fungi across a north Sweden podzol chronosequence, *Ecosystems*, **5**, 11-22.

Hoffland E, Kuyper T W, Wallander H, Plassard C, Gorbushina A A, Haselwandter K, Holmstrom S, Landeweert R, Lundstrom U S, Rosling A, Sen R, Smits M M, van Hees P A and van Breemen N (2004) The role of fungi in weathering, *Frontiers in Ecology and the Environment*, **2**, 258-264.

Hofrichter M, Bublitz F and Fritsche W (1997a) Fungal attack on coal II. Solubilization of low-rank coal by filamentous fungi, *Fuel Processing Technology*, **52**, 55-64.

Hofrichter M, Bublitz F and Fritsche W (1997b) Fungal attack on coal: I. Modification of hard coal by fungi, *Fuel Processing Technology*, **52**, 43-53.

Hofrichter M, Ziegenhagen D, Sorge S, Ullrich R, Bublitz F and Fritsche W (1999) Degradation of lignite (low-rank coal) by ligninolytic basidiomycetes and their manganese peroxidase system, *Applied Microbiology and Biotechnology*, **52**, 78-84.

Huang P M, Wang M K and Chiu C Y (2005) Soil mineral-organic matter-microbe interactions: Impacts on biogeochemical processes and biodiversity in soils, *Pedobiologia*, **49**, 609-635.

Jaffe L A, Peucker-Ehrenbrink B and Petsch S T (2002) Mobility of rhenium, platinum group elements and organic carbon during black shale weathering, *Earth and Planetary Science Letters*, **198**, 339-353.

Jafri R and Hassan W (2008) Micro Electromechanical Systems Fabrication Processes, *Journal of Engineering and Sciences*, **2**, 54-58.

Jakubick A T, Gatzweiler R, Mager D and Robertson A M (1997) The Wismut waste rock pile remediation programme of the Ronneburg district, Germany. In: *Proceedings of the Fourth International Conference on Acid Mine Drainage*, Vancouver, BC, Canada, pp. 1285-1301.

Jarosz-Wilkolazka A and Gadd G M (2003) Oxalate production by wood-rotting fungi growing in toxic metal-amended medium, *Chemosphere*, **52**, 541-547.

Johnson D, Warner R and Shih A J (2007) Surface Roughness and Material Removal Rate in Machining Using Microorganisms, *Journal of Manufacturing Science and Engineering*, **129**, 223-227.

Jongmans A G, vanBreemen N, Lundstrom U, vanHees P A W, Finlay R D, Srinivasan M, Unestam T, Giesler R, Melkerud P A and Olsson M (1997) Rock-eating fungi, *Nature*, **389**, 682-683.

Kalinowski B E, Liermann L J, Givens S and Brantley S L (2000) Rates of bacteria-promoted solubilization of Fe from minerals: a review of problems and approaches, *Chemical Geology*, **169**, 357-370.

Kim J, Dong H L, Seabaugh J, Newell S W and Eberl D D (2004) Role of microbes in the smectite-to-illite reaction, *Science*, **303**, 830-832.

Ko E M, Leem Y E and Choi H T (2001) Purification and characterization of laccase isozymes from the white-rot basidiomycete Ganoderma lucidum, *Applied Microbiology and Biotechnology*, **57**, 98-102.

Koenigs J W (1974) Production of hydrogen peroxide by wood-rotting fungi in wood and its correlation with weight loss, depolymerization, and pH changes *Archives of Microbiology*, **99**, 129-145.

Koestler R J (2002) Biodeterioration of stone in tropical environments: An overview, *Journal of the American Institute for Conservation*, **41**, 98-102.

Kolo K, Keppens E, Preat A and Claeys P (2007) Experimental observations on fungal diagenesis of carbonate substrates, *Journal of Geophysical Research-Biogeosciences*, **112**, 20.

Kothe E (2007) Pilze. In: *Allgemeine Mikrobiologie* (ed Fuchs G). Thieme, Stuttgart, pp. 57-96.

Kothe E, Bergmann H and Büchel G (2005) Molecular mechanisms in bio-geo-interactions: From a case study to general mechanisms, *Chemie der Erde - Geochemistry*, **65**, 7-27.

Kulkarni S, Syed A, Singh S, Gaikwad A, Patil K, Vijayamohanan K, Ahmad A and Ogale S (2008) Silicate nanoparticles by bioleaching of glass and modification of the glass surface, *Journal of Non-Crystalline Solids*, **354**, 3433-3437.

Lee J U and Fein J B (2000) Experimental study of the effects of Bacillus subtilis on gibbsite dissolution rates under near-neutral pH and nutrient-poor conditions, *Chemical Geology*, **166**, 193-202.

Leonowicz A, Cho N S, Luterek J, Wilkolazka A, Wojtas-Wasilewska M, Matuszewska A, Hofrichter M, Wesenberg D and Rogalski J (2001) Fungal laccase: properties and activity on lignin, *Journal of Basic Microbiology*, **41**, 185-227.

Leonowicz A, Matuszewska A, Luterek J, Ziegenhagen D, Wojtas-Wasilewska M, Cho N S, Hofrichter M and Rogalski J (1999) Biodegradation of lignin by white rot fungi, *Fungal Genetics and Biology*, **27**, 175-185.

Li W, Zhou P-P, Jia L-P, Yu L-J, Li X-L and Zhu M (2009) Limestone dissolution induced by fungal mycelia, acidic materials, and carbonic anhydrase from fungi, *Mycopathologia*, **167**, 37-46.

Liers C, Ullrich R, Pecyna M, Schlosser D and Hofrichter M (2007) Production, purification and partial enzymatic and molecular characterization of a laccase from the wood-rotting ascomycete Xylaria polymorpha, *Enzyme and Microbial Technology*, **41**, 785-793.

Lilly W W, Wallweber G J and Lukefahr T A (1992) Cadmium absorption and its effects on growth and mycelial morphology of the basidiomycete fungus, Schizophyllum commune, *Microbios*, **72**, 227-237.

Linder M B, Szilvay G R, Nakari-Setala T and Penttila M E (2005) Hydrophobins: the protein-amphiphiles of filamentous fungi, *Fems Microbiology Reviews*, **29**, 877-896.

Littke R (1993) *Deposition, Diagenesis and Weathering of Organic Matter-Rich Sediments*, Springer-Verlag Berlin, Heidelberg.

Littke R, Klussmann U, Krooss B and Leythaeuser D (1991) Quantification of Loss of Calcite, Pyrite, and Organic-Matter Due to Weathering of Toarcian Black Shales and Effects on Kerogen and Bitumen Characteristics, *Geochimica Et Cosmochimica Acta*, **55**, 3369-3378.

Lower S K, Hochella M F and Beveridge T J (2001) Bacterial recognition of mineral surfaces: Nanoscale interactions between Shewanella and alpha-FeOOH, *Science*, **292**, 1360-1363.

Lundell T K, Makela M R and Hilden K (2010) Lignin-modifying enzymes in filamentous basidiomycetes - ecological, functional and phylogenetic review, *Journal of Basic Microbiology*, **50**, 5-20.

Lüttge A, Bolton E W and Lasaga A C (1999) An interferometric study of the dissolution kinetics of anorthite: The role of reactive surface area, *American Journal of Science*, **299**, 652-678.

Lüttge A and Conrad P G (2004) Direct observation of microbial inhibition of calcite dissolution, *Applied and Environmental Microbiology*, **70**, 1627-1632.

Madigan M T, Martinko J M and Parker J (2001) *Brock Mikrobiologie*, Spektrum Akademischer Verlag, Heidelberg, Berlin.

Mann S (2001) *Biomineralization: Principles and Concepts in Bioinorganic Materials Chemistry*, Oxford University Press, Oxford.

Matlakowska R and Sklodowska A (2009) The culturable bacteria isolated from organic-rich black shale potentially useful in biometallurgical procedures, *Journal of Applied Microbiology*, **107**, 858-866.

Mayer L M (2005) Extent of coverage of mineral surfaces by organic matter in marine sediments (vol 63, pg 207, 1999), *Geochimica Et Cosmochimica Acta*, **69**, 1375-1375.

McConville P, Boyce A J, Fallick A E, Harte B and Scott E M (2000) Sulphur isotope variations in diagenetic pyrite from core plug to sub-millimetre scales, *Clay Minerals*, **35**, 303-311.

McGraw-Hill (2004) *McGraw-Hill Concise Encyclopedia of Science & Technology*, 5.ed., McGraw-Hill Professional, New York.

Merten D, Geletneky J, Bergmann H, Haferburg G, Kothe E and Büchel G (2005) Rare earth element patterns: A tool for understanding processes in remediation of acid mine drainage, *Chemie der Erde - Geochemistry*, **65**, 97-114.

Mikushkin V M, Sysoev S E and Gordeev Y S (2004) Standardless XPS method for determining the chemical composition of multiphase compounds and its application to studies of InP plasma oxide nanofilms *Physics of the Solid State*, **46**, 1830-1835.

Mingram B, Hoth P and Harlov D E (2003) Nitrogen potential of Namurian shales in the North German Basin, *Journal of Geochemical Exploration*, **78-79**, 405-408.

Mingram B, Hoth P, Luders V and Harlov D (2005) The significance of fixed ammonium in Palaeozoic sediments for the generation of nitrogen-rich natural gases in the North German Basin, *International Journal of Earth Sciences*, **94**, 1010-1022.

Modl C, Wormann H and Amelung W (2007) Contrasting effects of different types of organic material on surface area and microaggregation of goethite, *Geoderma*, **141**, 167-173.

Paananen A, Vuorimaa E, Torkkeli M, Penttila M, Kauranen M, Ikkala O, Lemmetyinen H, Serimaa R and Linder M B (2003) Structural hierarchy in molecular films of two class II hydrophobins, *Biochemistry*, **42**, 5253-5258.

Peddireddi S (2008) Hydrophobins in wood biology and biotechnology. Georg-August-Universität Göttingen, (Thesis)

Perry C C, Patwardhan S V and Deschaume O (2009) From biominerals to biomaterials: the role of biomolecule-mineral interactions, *Biochemical Society Transactions*, **37**, 687-691.

Perry R S, Mcloughlin N, Lynne B Y, Sephton M A, Oliver J D, Perry C C, Campbell K, Engel M H, Farmer J D, Brasier M D and Staley J T (2007) Defining biominerals and organominerals: Direct and indirect indicators of life, *Sedimentary Geology*, **201**, 157-179.

Petsch S T, Berner R A and Eglinton T I (2000) A field study of the chemical weathering of ancient sedimentary organic matter, *Organic Geochemistry*, **31**, 475-487.

Petsch S T, Edwards K J and Eglinton T I (2005) Microbial transformations of organic matter in black shales and implications for global biogeochemical cycles, *Palaeogeography Palaeoclimatology Palaeoecology*, **219**, 157-170.

Petsch S T, Eglinton T I and Edwards K J (2001) C-14-dead living biomass: Evidence for microbial assimilation of ancient organic carbon during share weathering, *Science*, **292**, 1127-1131.

Phillips L E and LappinScott H M (1997) Enrichment and characterisation of sulfate-reducing bacteria from sandstone rock cores from the UK Continental shelf, *Fems Microbiology Reviews*, **20**, 415-423.

Pokorny R, Olejnikova P, Balog M, Zifcak P, Holker U, Janssen M, Bend J, Hofer M, Holiencin R, Hudecova D and Varecka L (2005) Characterization of microorganisms isolated from lignite excavated from the Zahorie coal mine (southwestern Slovakia), *Research in Microbiology*, **156**, 932-943.

Ralph J P, Graham L A and Catcheside D E A (1996) Extracellular oxidases and the transformation of solubilised low rank coal by wood-rot fungi, *Applied Microbiology and Biotechnology*, **46**, 226-232.

Ranogajec J, Markov S, Kiurski J, Radeka M and Ducman V (2008) Microbial Deterioration of Clay Roofing Tiles as a Function of the Firing Temperature, *Journal of the American Ceramic Society*, **91**.

Raper C A and Fowler T J (2004) Why Study Schizophyllum?, *Fungal Genetics Newsletter*, **51**, 30-36.

Raper J R and Miles P G (1958) The genetics of Schizophyllum commune, *Genetics*, **43**, 530-546.

Rayner A D M (1991) The challenge of the individualistic mycelium, *Mycologia*, **83**, 48-71.

Rezacova V, Hrselova H, Gryndlerova H, Miksik I and Gryndler M (2006) Modifications of degradation-resistant soil organic matter by soil saprobic microfungi, *Soil Biology & Biochemistry*, **38**, 2292-2299.

Riding R (2000) Microbial carbonates: the geological record of calcified bacterial-algal mats and biofilms, *Sedimentology*, **47**, 179-214.

Riva S (2006) Laccases: blue enzymes for green chemistry, *Trends in Biotechnology*, **24**, 219-226.

Roden E E and Zachara J M (1996) Microbial reduction of crystalline iron(III) oxides: Influence of oxide surface area and potential for cell growth, *Environmental Science & Technology*, **30**, 1618-1628.

Rumbold C (1910) Les champignons destructeurs du bois, *Annales de la Science Agronomique*, **5**.

Sanchez C, Tellez-Tellez M, Diaz-Godinez G and Moore D (2004) Simple staining detects ultrastructural and biochemical differentiation of vegetative hyphae and fruit body initials in colonies of Pleurotus pulmonarius, *Letters in Applied Microbiology*, **38**, 483-487.

Santelli C M, Welch S A, Westrich H R and Banfield J F (2001) The effect of Fe-oxidizing bacteria on Fe-silicate mineral dissolution, *Chemical Geology*, **180**, 99-115.

Saul J M (2009) Did detoxification processes cause complex life to emerge?, *Lethaia*, **42**, 179-184.

Schieber J (2002) Sedimentary pyrite: A window into the microbial past, *Geology*, **30**, 531-534.

Schilling J S and Jellison J (2007) Extraction and translocation of calcium from gypsum during wood biodegradation by oxalate-producing fungi, *International Biodeterioration & Biodegradation*, **60**, 8-15.

Schlegel G (1995) Silur. In: *Geologie von Thüringen* (ed Seidel G). Schweizerbart, Stuttgart, pp. 111-121.

Schmidt C M (2004) DEGAS - Untersuchungen zur Verwitterung von Schwarzpeliten. Friedrich-Schiller-Universität, Jena, (Thesis)

Scholtmeijer K, Janssen M I, van Leeuwen M B M, van Kooten T G, Hektor H and Wosten H A B (2004) The use of hydrophobins to functionalize surfaces, *Bio-Medical Materials and Engineering*, **14**, 447-454.

Schuren F H J (1999) Atypical interactions between thn and wild-type mycelia of Schizophyllum commune, *Mycological Research*, **103**, 1540-1544.

Schüring J (1996) Die Verwendung von Steinkohlenbergematerial im Deponiebau im Hinblick auf die Pyritverwitterung und die Eignung als geochemische Barriere. Universität Bremen, Bremen, (Thesis)

Schwalb M N and Miles P G (1967) Morphogenesis of Schizophyllum commune .I. Morphological variation and mating behavior of thin mutation, *American Journal of Botany*, **54**, 440-&.

Sharma K K and Kuhad R C (2008) Laccase: enzyme revisited and function redefined *Indian Journal of Microbiology*, **48**, 309-316.

Siegbahn K (1982) Electron-Spectroscopy for Atoms, Molecules, and Condensed Matter, *Science*, **217**, 111-121.

Siegel D, Fischer C, Kothe E, Lüttge A and Gaupp R (2009) Fungal weathering of black shale and graphite surfaces, *Geochimica Et Cosmochimica Acta*, **73**, A1220-A1220.

Silva-Stenico M E, Vengadajellum C J, Janjua H A, Harrison S T L, Burton S G and Cowan D A (2007) Degradation of low rank coal by Trichoderma atroviride ES11, *Journal of Industrial Microbiology & Biotechnology*, **34**, 625-631.

Simkiss K (1977) Biomineralization and Detoxification, *Calcified Tissue Research*, **24**, 199-200.

Sinsabaugh R L and Findlay S (1995) Microbial-production, enzyme-activity, and carbon turnover in surface sediments of the Hudson river estuary, *Microbial Ecology*, **30**, 127-141.

Skinner H C W (2005) Biominerals, *Mineralogical Magazine*, **69**, 621-641.

Snieskiene V and Juronis V (2001) Distribution of the fungus Schizophyllum commune Fr. in plantings of trees in the Kaunas City, *Biologija*, **3**, 45-47.

Solis-Fernandez P, Paredes J I, Cosio A, Martinez-Alonso A and Tascon J M D (2010) A comparison between physically and chemically driven etching in the oxidation of graphite surfaces, *Journal of Colloid and Interface Science*, **344**, 451-459.

Staley J T, Palmer F and Adams J B (1982) Microcolonial fungi - common inhabitants on desert rocks, *Science*, **215**, 1093-1095.

Sterflinger K (2000) Fungi as geologic agents, *Geomicrobiology Journal*, **17**, 97-124.

Stevenson F J (1961) Chemical state of the nitrogen in rocks, *Geochimica Et Cosmochimica Acta*, **26**, 797-809.

Sunde M, Kwan A H Y, Templeton M D, Beever R E and Mackay J P (2008) Structural analysis of hydrophobins, *Micron*, **39**, 773-784.

Szurowski H (1985) Katalog der Gesteinseigenschaften Teil I und II. SDAG Wismut, Gera, pp. 165.

Takano M, Hayashi N and Kuroda K (2008) Selective staining and visualization of hyphal sheath of a white-rot fungus Phanerochaete crassa WD1694 with phloxine B, *Journal of Wood Science*, **54**, 76-80.

Templeton D M and Liu Y (2003) Genetic regulation of cell function in response to iron overload or chelation, *Biochimica Et Biophysica Acta-General Subjects*, **1619**, 113-124.

Theuerl S and Buscot F (2010) Laccases: toward disentangling their diversity and functions in relation to soil organic matter cycling, *Biology and Fertility of Soils*, **46**, 215-225.

Thomas T R (1999) *Rough Surfaces*, Second.ed., Imperial College Press, London.

TLUG Geologische Karte von Thüringen. Thüringer Landesanstalt für Umwelt und Geologie.

Torkkeli M, Serimaa R, Ikkala O and Linder M (2002) Aggregation and Self-Assembly of Hydrophobins from Trichoderma reesei: Low-Resolution Structural Models, *Biophysical Journal*, **83**, 2240-2247.

Tugrul A (2004) The effect of weathering on pore geometry and compressive strength of selected rock types from Turkey, *Engineering Geology*, **75**, 215-227.

Tuttle M L W, Breit G N and Goldhaber M B (2009) Weathering of the New Albany Shale, Kentucky: II. Redistribution of minor and trace elements, *Applied Geochemistry*, **24**, 1565-1578.

van der Vegt W, van der Mei H C, Wosten H A B, Wessels J G H and Busscher H J (1996) A comparison of the surface activity of the fungal hydrophobin SC3p with those of other proteins, *Biophysical Chemistry*, **57**, 253-260.

van Peer A F, Muller W H, Boekhout T, Lugones L G and Wosten H A B (2009) Cytoplasmic Continuity Revisited: Closure of Septa of the Filamentous Fungus Schizophyllum commune in Response to Environmental Conditions, *Plos One*, **4**.

van Wetter M A, Wosten H A B, Sietsma J H and Wessels J G H (2000) Hydrophobin gene expression affects hyphal wall composition in Schizophyllum commune, *Fungal Genetics and Biology*, **31**, 99-104.

Verrecchia E P, Dumont J L and Verrecchia K E (1993) Role of calciumoxalate biomineralization by fungi in the formation of calcretes - a case-study from Nazareth, Israel., *Journal of Sedimentary Petrology*, **63**, 1000-1006.

Visscher P T and Stolz J F (2005) Microbial mats as bioreactors: populations, processes, and products, *Palaeogeography Palaeoclimatology Palaeoecology*, **219**, 87-100.

Wang X (2004) Insight into the interfacial self-assembly and structural changes of hydrophobins. University of Groningen, Groningen, (Thesis)

Warscheid T and Braams J (2000) Biodeterioration of stone: a review, *International Biodeterioration & Biodegradation*, **46**, 343-368.

Weber H (1993) *Allgemeine Mykologie*, Gustav-Fischer-Verlag Jena, Stuttgart.

Wengel M, Kothe E, Schmidt C M, Heide K and Gleixner G (2006) Degradation of organic matter from black shales and charcoal by the wood-rotting fungus Schizophyllum commune and release of DOC and heavy metals in the aqueous phase, *Science of the Total Environment*, **367**, 383-393.

Wessels J G H (1993) Wall growth, protein excretion and morphogenesis in fungi, *New Phytologist*, **123**, 397-413.

Wessels J G H, Devries O M H, Asgeirsdottir S A and Schuren F H J (1991) Hydrophobin genes involved in formation of aerial hyphae and fruit bodies in Schizophyllum, *Plant Cell*, **3**, 793-799.

White A F and Brantley S L (2003) The effect of time on the weathering of silicate minerals: why do weathering rates differ in the laboratory and field?, *Chemical Geology*, **202**, 479-506.

Whiteford J R and Spanu P D (2002) Hydrophobins and the interactions between fungi and plants, *Molecular Plant Pathology*, **3**, 391-400.

Wilkin R T and Barnes H L (1997) Formation processes of framboidal pyrite, *Geochimica Et Cosmochimica Acta*, **61**, 323-339.

Wilkin R T, Barnes H L and Brantley S L (1996) The size distribution of framboidal pyrite in modern sediments: An indicator of redox conditions, *Geochimica Et Cosmochimica Acta*, **60**, 3897-3912.

Wismut (1994) Sanierungskonzept Standort Ronneburg.-Stand Dezember 1994. In: *Internal Report*. Wismut GmbH, Chemnitz.

Wösten H A B and de Vocht M L (2000) Hydrophobins, the fungal coat unravelled, *Biochimica Et Biophysica Acta-Reviews on Biomembranes*, **1469**, 79-86.

Wösten H A B, Ruardy T G, Vandermei H C, Busscher H J and Wessels J G H (1995) Interfacial self-assembly of a Schizophyllum commune hydrophobin into an insoluble amphipathic protein membrane depends on surface hydrophobicity, *Colloids and Surfaces B-Biointerfaces*, **5**, 189-195.

Wösten H A B, Schuren F H J and Wessels J G H (1994) Interfacial self-assembly of a hydrophobin into an amphipathic protein membrane mediates fungal attachment to hydrophobic surfaces, *Embo Journal*, **13**, 5848-5854.

Yamaguchi K E (2003) Evolution of the geochemical cycles of redox-sensitive elements, *Frontier Research on Earth Evolution*, **1**, 249-252.

Zhao J and Kwan H S (1999) Characterization, molecular cloning, and differential expression analysis of laccase genes from the edible mushroom Lentinula edodes, *Applied and Environmental Microbiology*, **65**, 4908-4913.

Zhuang J and Yu G R (2002) Effects of surface coatings on electrochemical properties and contaminant sorption of clay minerals, *Chemosphere*, **49**, 619-628.

Acknowledgements

their help and fruitful discussions during my PhD time and Kelli Gatewood for proof-reading.
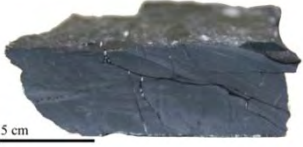
And I cannot end without thanking my family, on whose constant encouragement and love I have relied throughout my time as a PhD student. This thesis is dedicated to my husband, my sister and my parents.

Appendix

Origin/Source	Abbr.	No	Surface	Incubated	VSI	REM	Others
Morassina mine, Schmiedefeld	M2	**77**	polished [1]	S.c. 4-39	x		
black slate (6.2 wt % TOC)	M2	**78**	polished [1]	Control	x		
	M2	**79**	polished [1]	S.c. 4-39	x		
	M2	**80**	polished [1]	S.c. 4-39	x		XPS
	M2	**81**	polished [1]	S.c. 4-39	x		
	M2	**82**	polished [1]	S.c. 4-39	x		
	M2	**83**	polished [1]	S.c. 4-39	x	x	Critical point drying
	M2	**113**	polished [1]	Control	x		XPS
dump, Schmiedefeld	M3	**85**	polished [1]	S.c. 4-39	x		AFM, EMP
black slate (0.5 wt % TOC)	M3	**86**	polished [1]	S.c. 4-39	x	x	Lysozym
	M3	**87**	polished [1]	S.c. 4-39	x	x	
	M3	**88**	polished [1]	S.c. 4-39	x	x	Plasma etching
	M3	**89**	polished [1]	S.c. 4-39	x		XPS
	M3	**90**	polished [1]	S.c. 4-39	x		
	M3	**91**	polished [1]	S.c. 4-39	x		EMP
	M3	**92**	polished [1]	Control	x	x	AFM
	M3	**93**	polished [1]	S.c. 4-39		x	Critical point drying
	M3	**112**	polished [1]	Control	x		XPS
graphite rods (PLANO GmbH)	G	**100**	polished [2]	S.c. 4-39	x		XPS
(impurities < 2 ppm)	G	**101**	polished [2]	S.c. 4-39	x	x	Hydrogen peroxide
	G	**102**	polished [2]	S.c. 4-39	x		
	G	**103**	polished [2]	S.c. 4-39	x	x	
	G	**104**	polished [2]	S.c. 4-39		x	Critical point drying
	G	**105**	polished [2]	Control	x	x	
	G	**118**	polished [2]	Control	x		XPS
	G	**119**	polished [2]	Control			Plasma etching
	G	**256**	polished [2]	S.c. 4-39	x	x	Caylase
	G	**259**	polished [2]	S.c. 4-39			EMP
	G	**260**	polished [2]	S.c. 4-39	x	x	Lysozym
Creunitz/Schmiedefeld	BS	**200**	polished [3]	Control	x		
black slate – bleached/unbleached	BS	**208**	polished [3]	S.c. 4-39			EMP
	BS	**215**	polished [3]	S.c. 4-39	x	x	

[1] T. Beckmann, Schwulper-Lagesbüttel
[2] S. Bergmann, IGW Jena
[3] H. Schulze, BGI Bayreuth

A2: Plasma Etching (IPHT, Jena)

Black slate (88) 20 min O_2 RIE
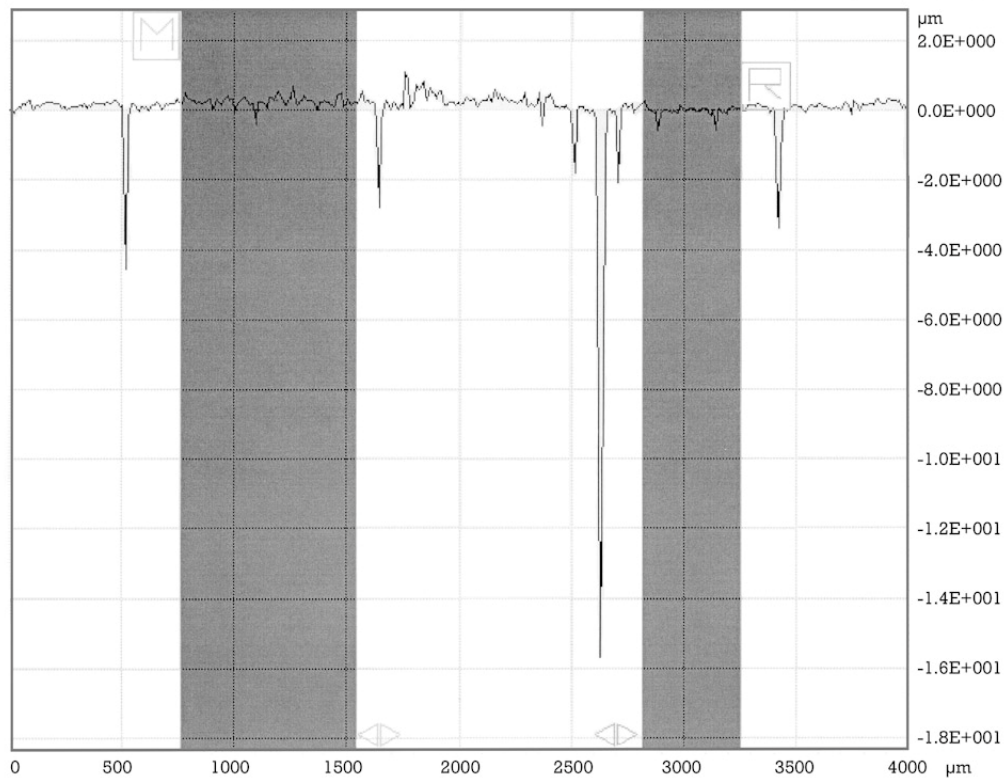
Scan Routine	1
Scan Type	Standard Scan
Time of Scan	23.10.2008
Data File Name	..\Dektak32\..
Scan ID	0
Stylus Type	Radius: 5 µm
Location	108632 µm, 108873 µm, 0,0 °
Scan Length	4000 µm
Resolution	0,889 µm /sample
Stylus Force	7 mg
Number of Points	4500
Duration	15 sec
Meas Range	1 mm
Profile	Hills&Valleys
R. Cursor	3255 µm
R. Cursor Width	443 µm
M. Cursor	759 µm
M. Cursor Width	787 µm
Cursor ASH	"-0,27 µm
Cursor Distance	"-24696 µm
Display Range	Auto
Display Date Type	Raw
Ash Result	**269,4 nm**

Graphite (119) 20 min O₂ RIE
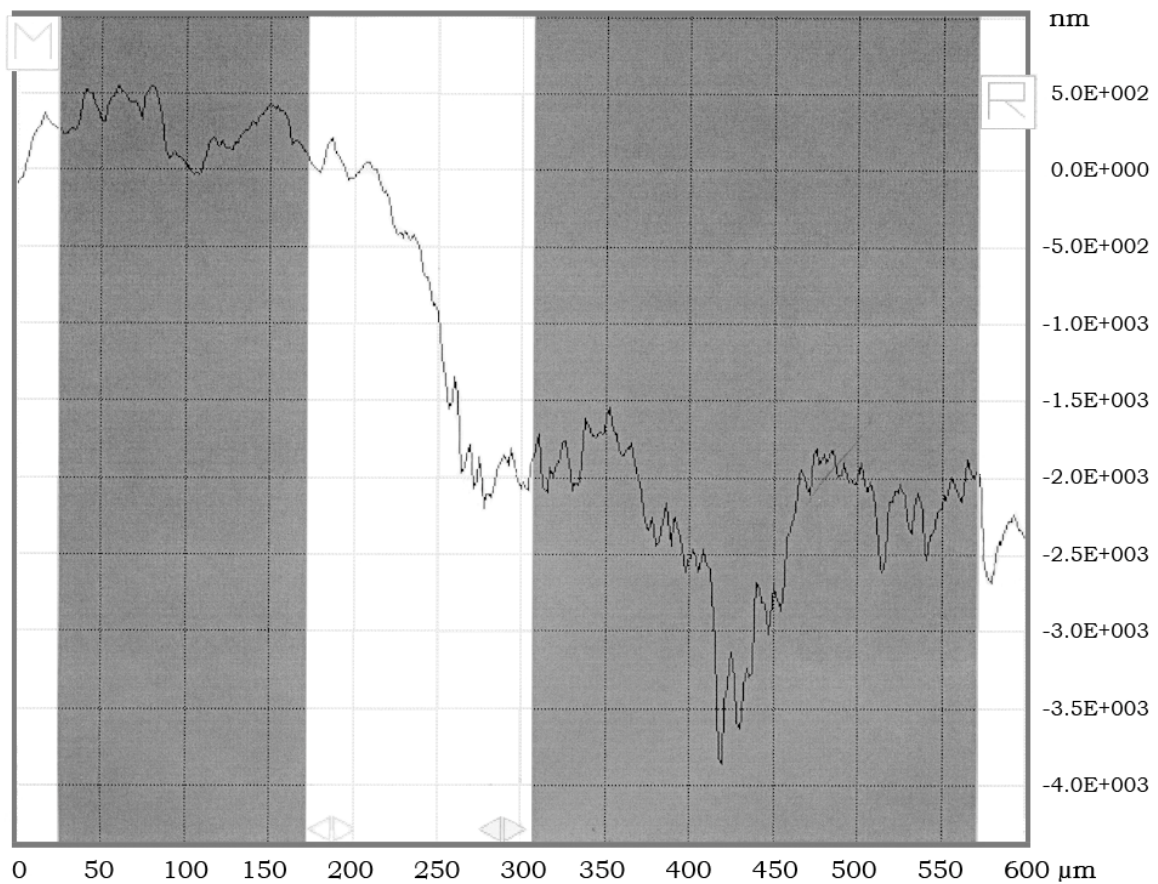
Scan Routine	1
Scan Type	Standard Scan
Time of Scan	23.10.2008
Data File Name	..\Dektak32\..
Scan ID	0
Stylus Type	Radius: 5 µm
Location	108632 µm, 108873 µm, 0,0 °
Scan Length	600 µm
Resolution	0,133 µm /sample
Stylus Force	3 mg
Number of Points	4500
Duration	15 sec
Meas Range	1 mm
Profile	Hills&Valleys
R. Cursor	572 µm
R. Cursor Width	266 µm
M. Cursor	24 µm
M. Cursor Width	149 µm
Cursor ASH	"-2542 µm
Cursor Distance	"-547 µm
Display Range	Auto
Display Date Type	Raw
Ash Result	**2541,8 nm**

A3: Elemental Analysis of Carbon and Nitrogen (C, N) with VarioMAX

sample	parameter	result [wt %]	Weight (mg)	heated
black slate M2-01	C	under range	249.10	Yes
black slate M2-02	C	under range	249.80	Yes
black slate M2-03	C	under range	245.20	Yes
black slate unbleached		under range		
black slate M2-04	C	6.00	256.30	No
black slate M2-05	C	6.31	244.80	No
black slate M2-06	C	6.19	242.90	No
black slate unbleached		6.16		
black slate M3-07	C	under range	259.20	Yes
black slate M3-08	C	under range	248.10	Yes
black slate M3-09	C	under range	247.80	Yes
black slate bleached		under range		
black slate M3-10	C	0.47	242.50	No
black slate M3-11	C	0.47	259.10	No
black slate M3-12	C	0.51	252.70	No
black slate bleached		0.48		

sample	parameter	result [wt %]	Weight (mg)	heated
black slate M2-01	N	under range	249.10	Yes
black slate M2-02	N	under range	249.80	Yes
black slate M2-03	N	under range	245.20	Yes
black slate unbleached		under range		
black slate M2-04	N	0.13	256.30	No
black slate M2-05	N	0.13	244.80	No
black slate M2-06	N	0.13	242.90	No
black slate unbleached		0.13		
black slate M3-07	N	0.09	259.20	Yes
black slate M3-08	N	0.10	248.10	Yes
black slate M3-09	N	0.10	247.80	Yes
black slate bleached		0.10		
black slate M3-10	N	0.13	242.50	No
black slate M3-11	N	0.13	259.10	No
black slate M3-12	N	0.13	252.70	No
black slate bleached		0.13		

A4: SEM – Framboidal Pyrite /Radiolarian Test?
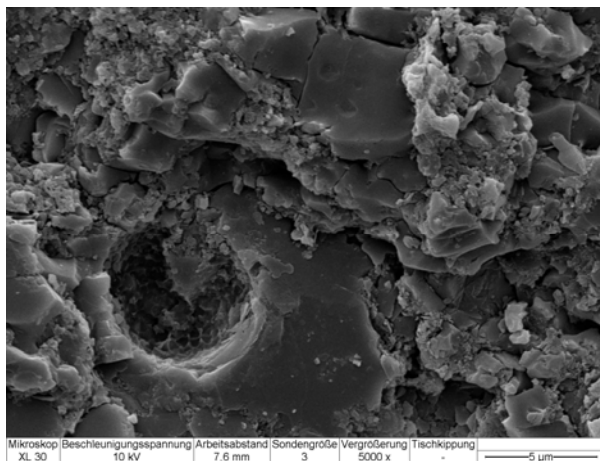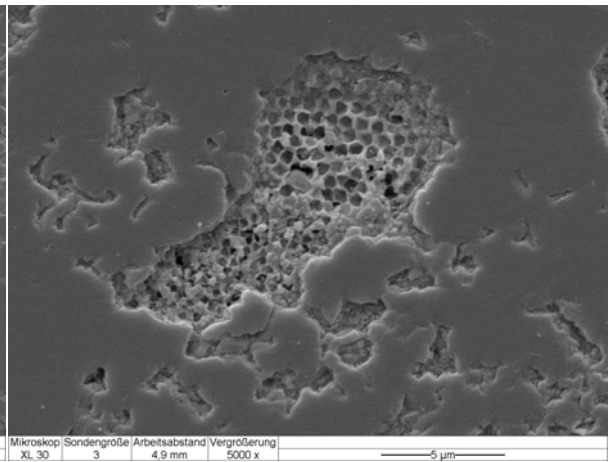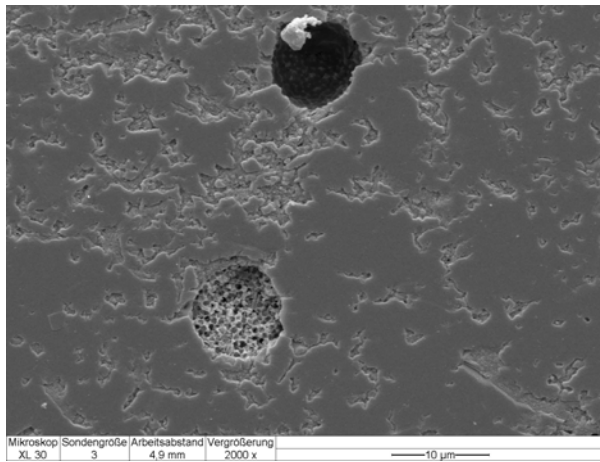
A5: SEM – Mycelial Mat/ Hyphal Net of *Schizophyllum commune*
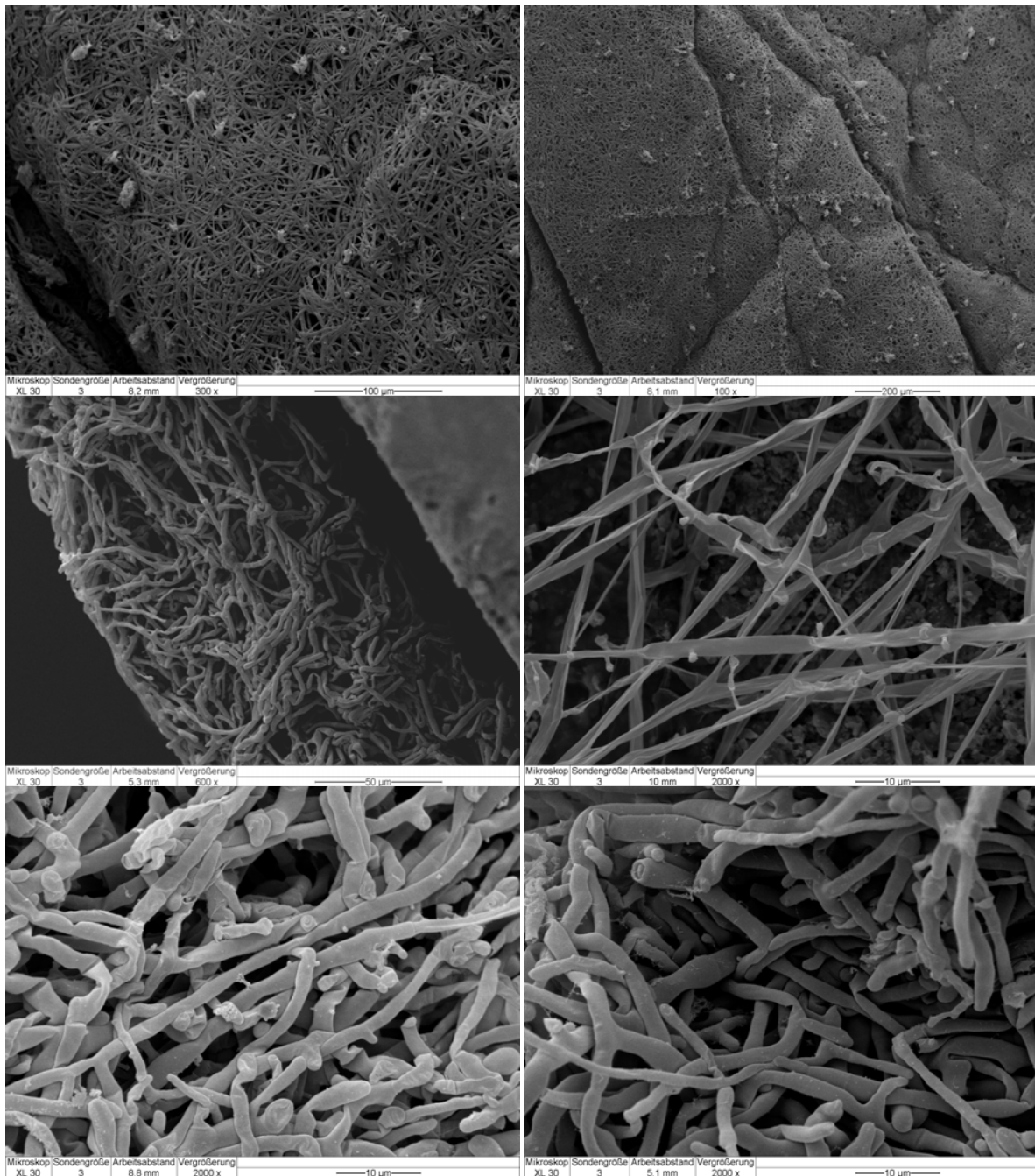
A6: SEM – Hyphal Growth of *Schizophyllum commune* on Rock Surfaces (Critical Point Dried)
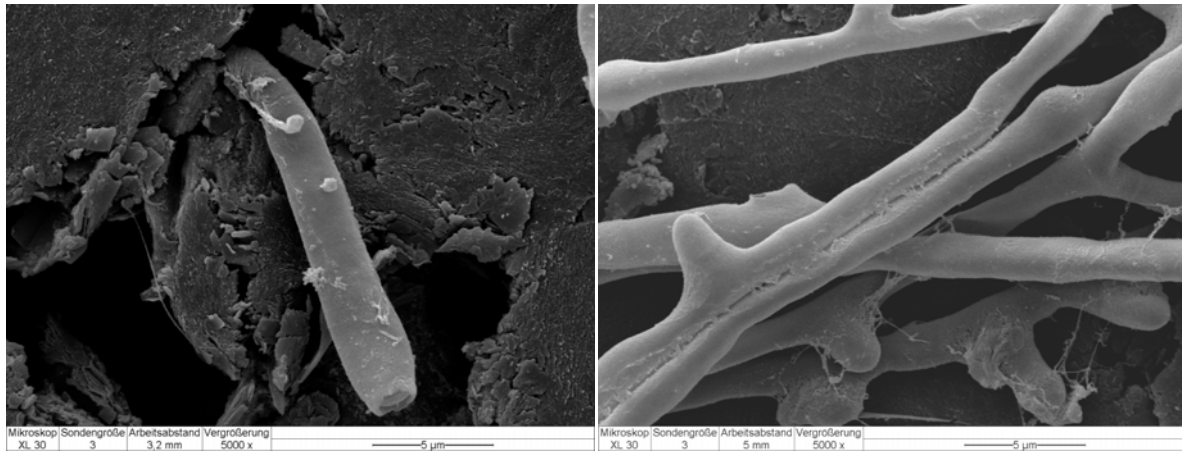
A7: SEM – Hyphal Growth of *Schizophyllum commune* on Rock Surfaces
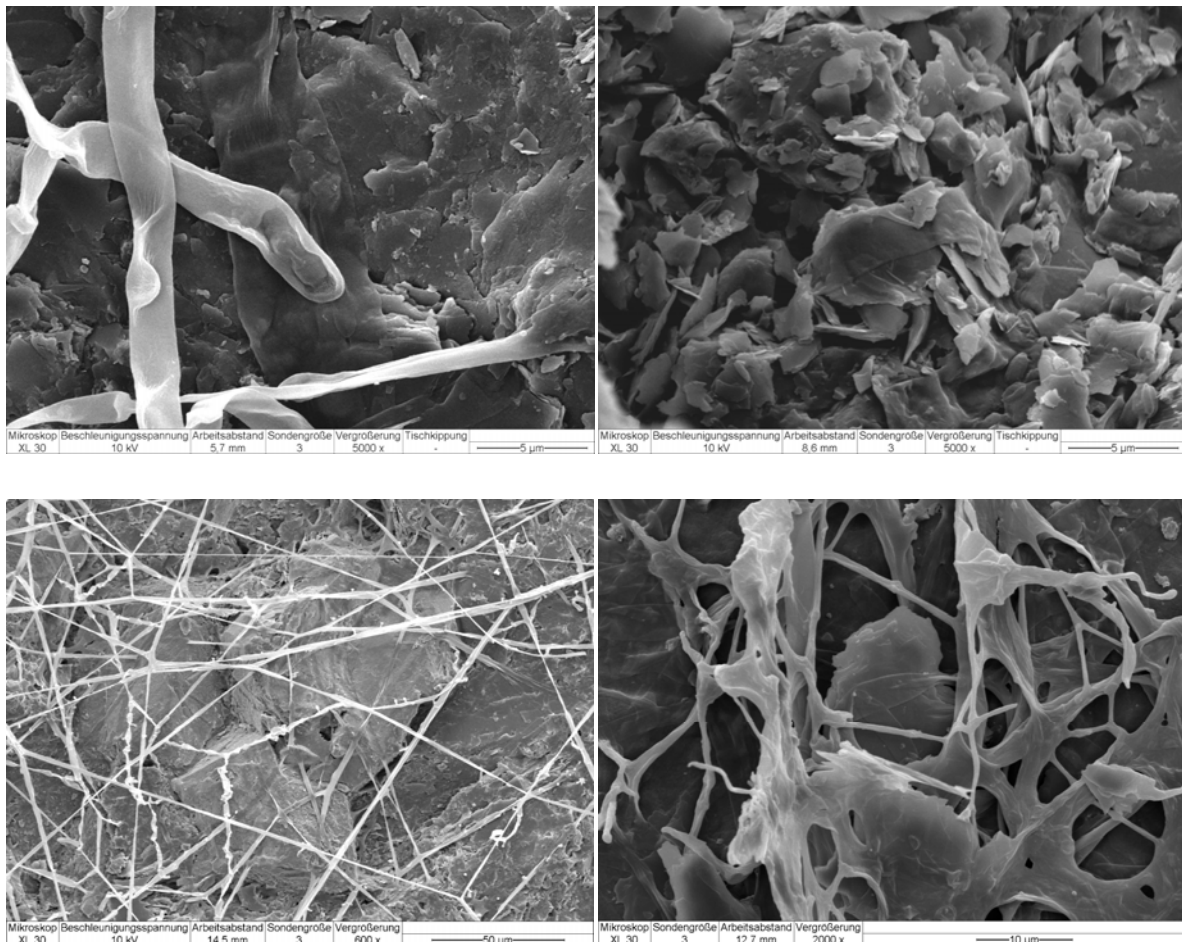
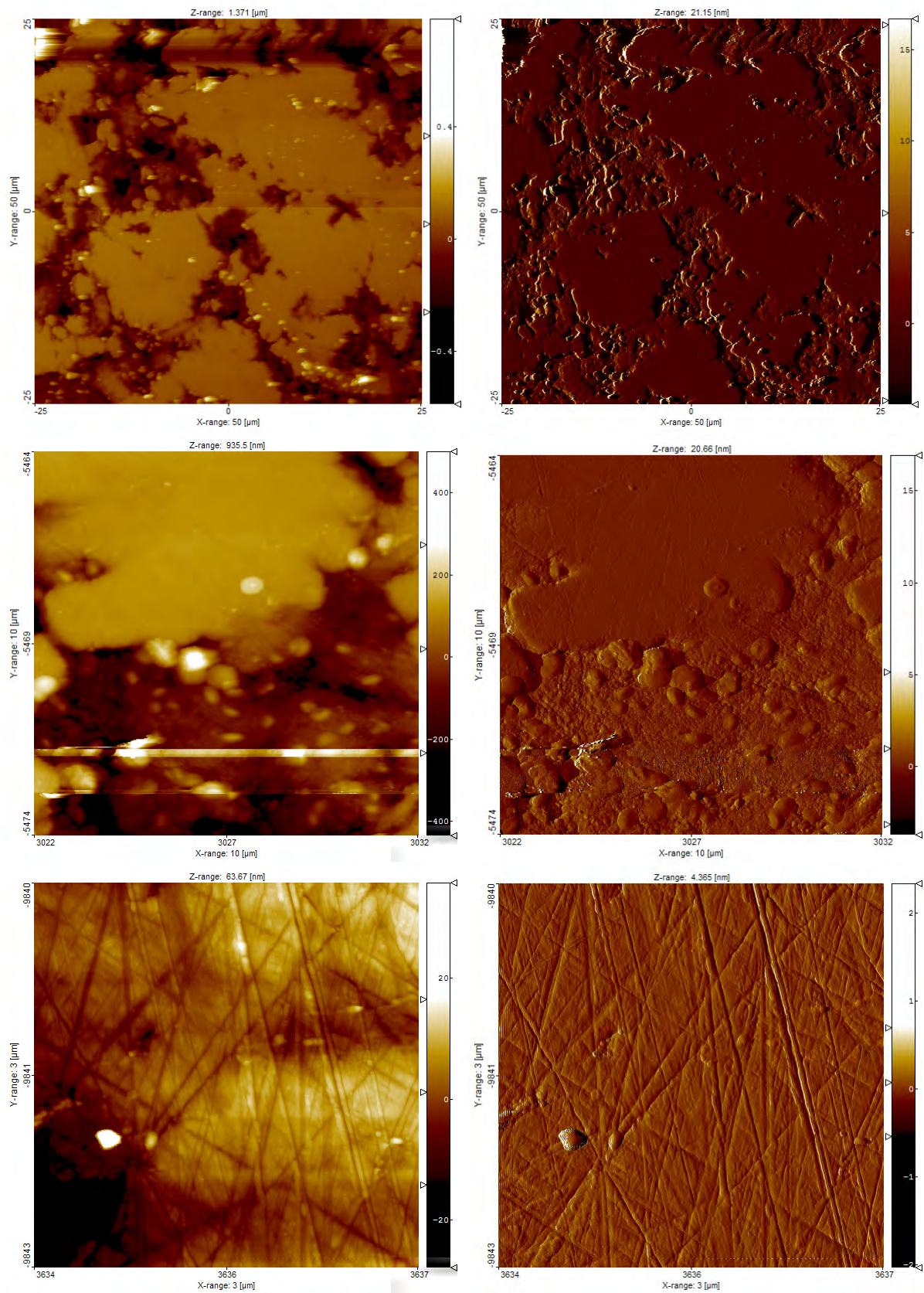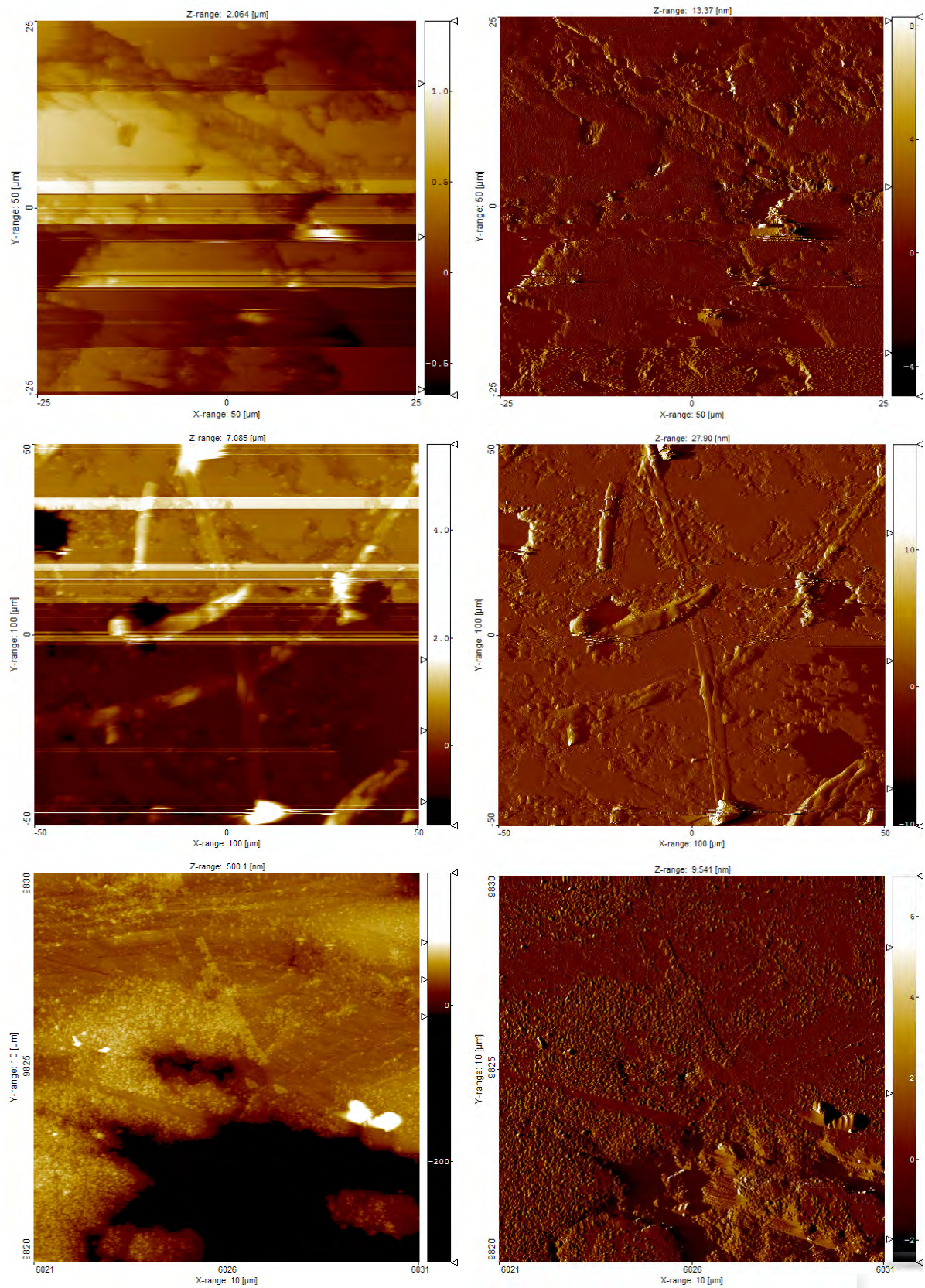## A8: SEM – Hyphal Growth of *Schizophyllum commune* into Pores
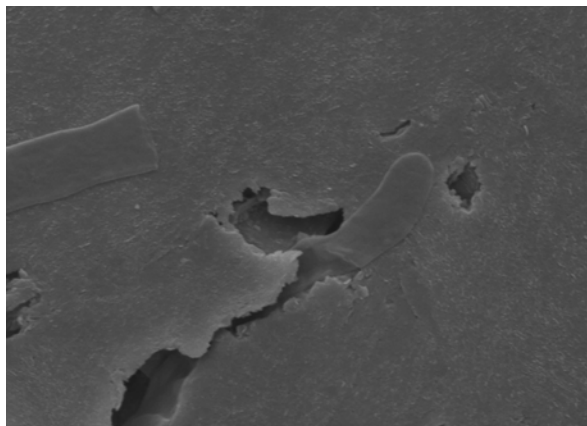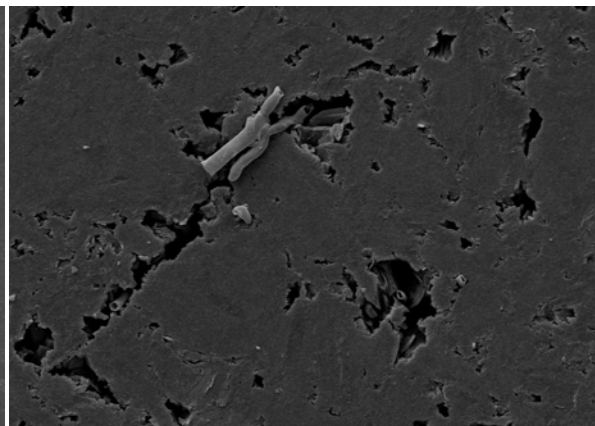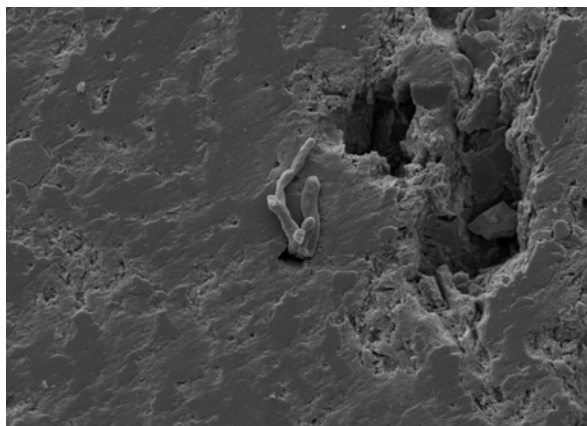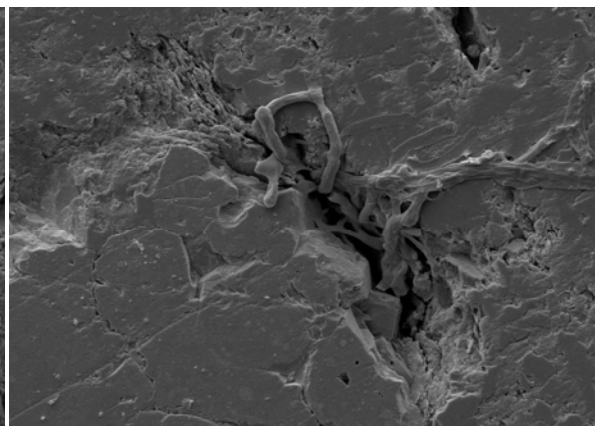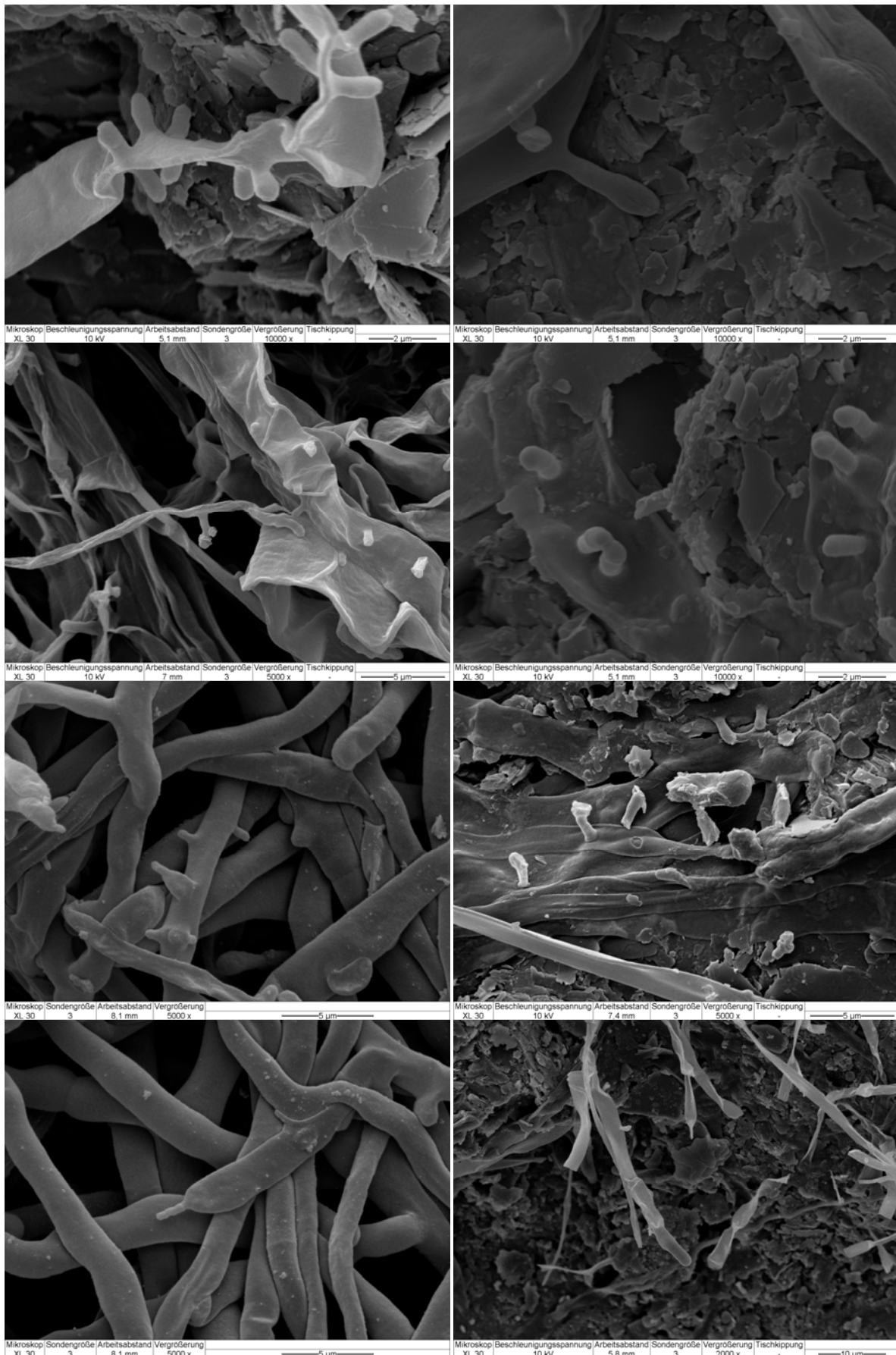
A10: SEM – Small Lateral Structures with Excretions
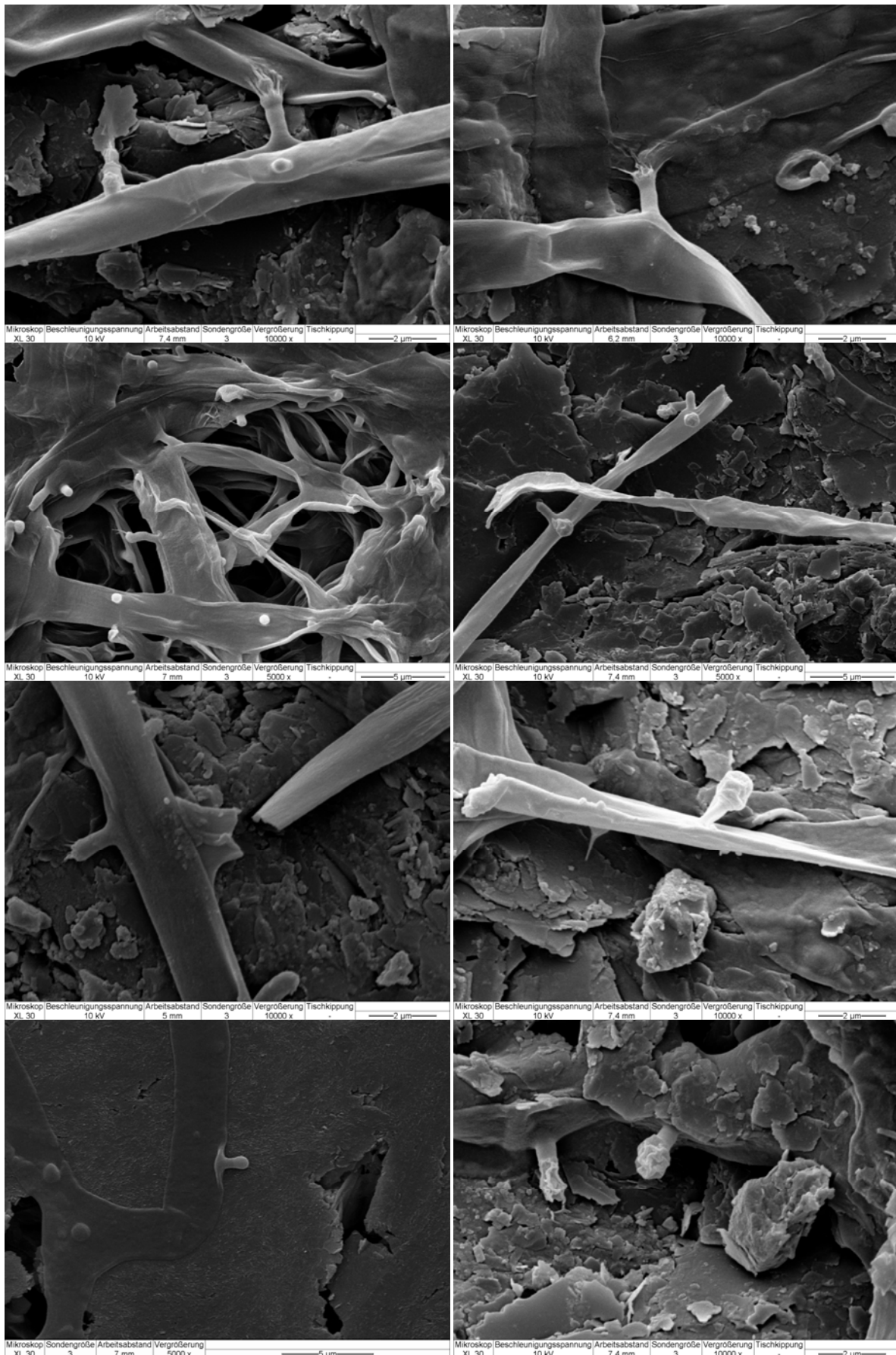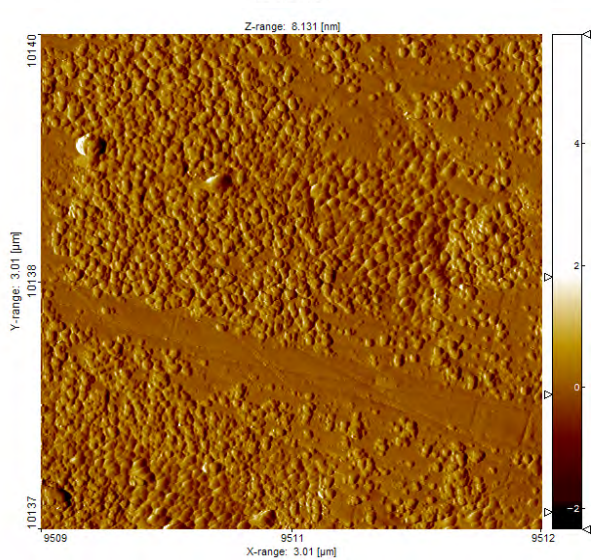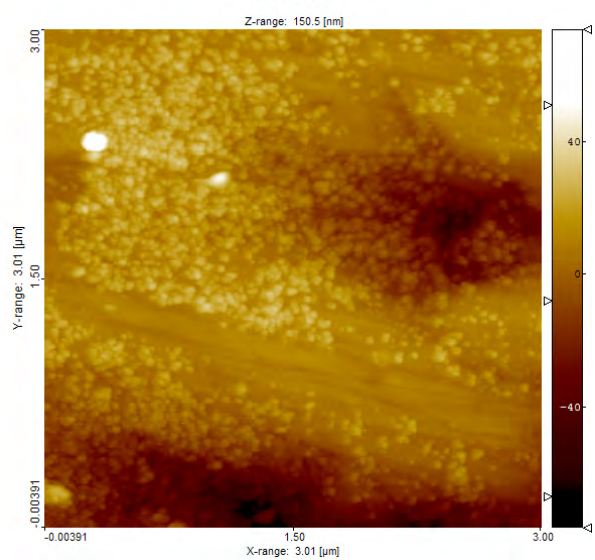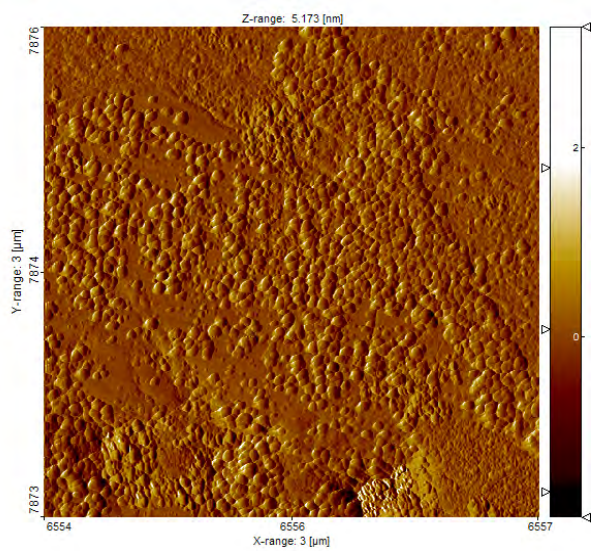
A11: SEM – Small Lateral Structure Excretions

Mikroskop	Beschleunigungsspannung	Arbeitsabstand	Sondengröße	
XL 30	20 kV	5,4 mm	3	—1 µm—
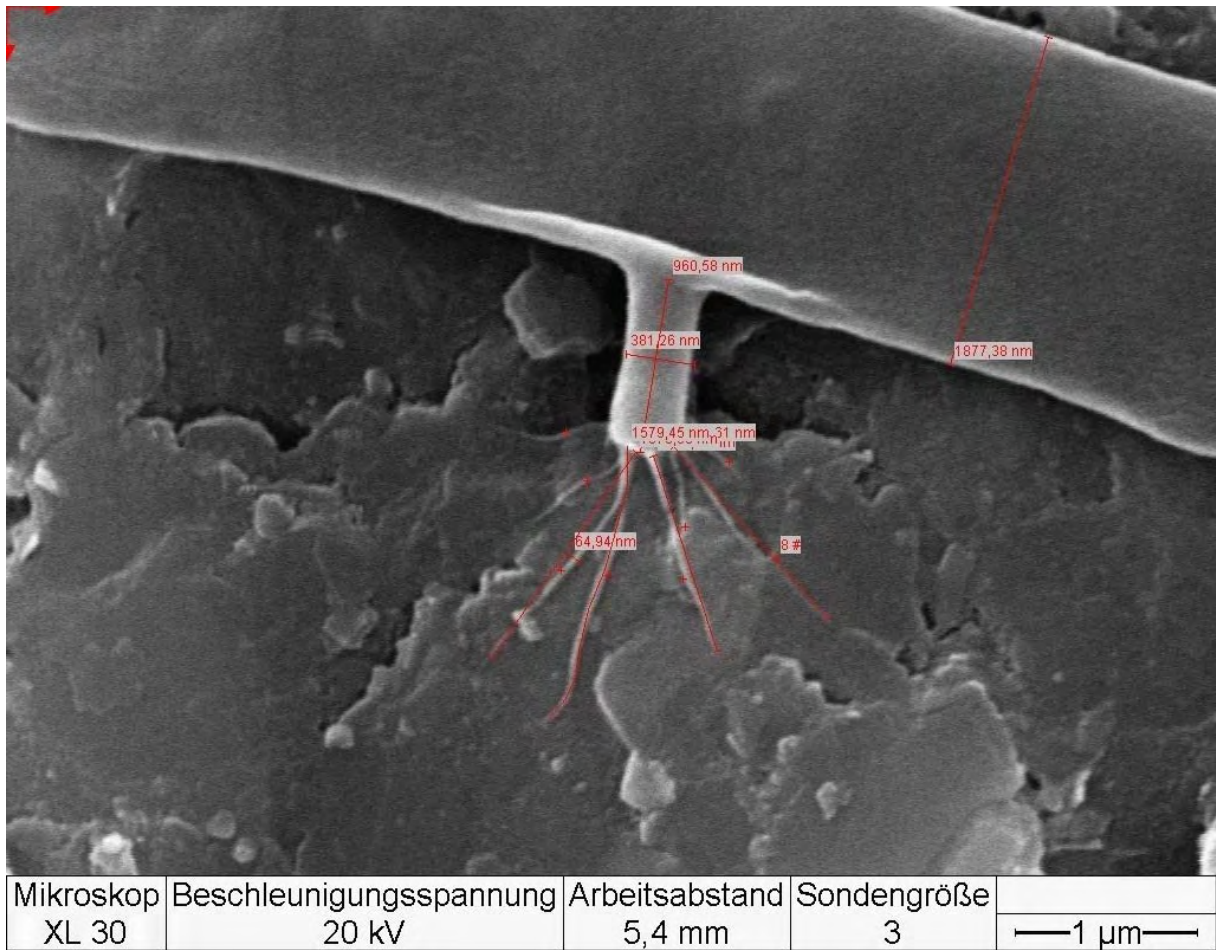
A12: AFM – M3 Control Sample

A13: AFM – M3 Incubated Sample
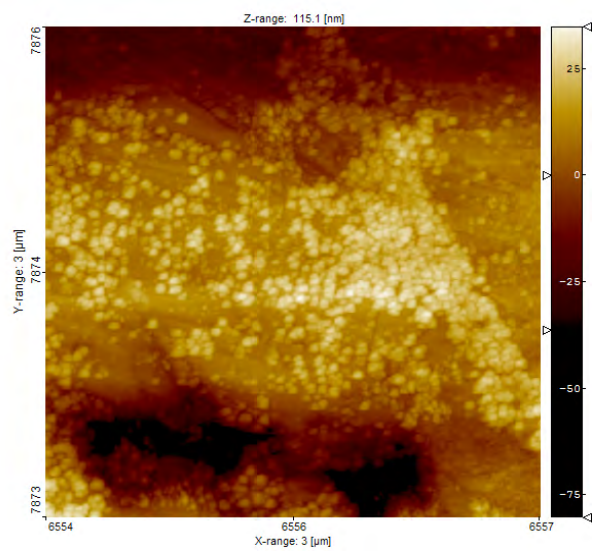
A14: Roughness Parameters

|	Ra	Rq	Rv	Rp	F	Rt
G 105 AV	64,1	152,5	-4788	3537	3,79	8325
G 118 AV	91,0	186,8	-5478	5094	3,39	10572
G Control AV	**77,6**	**169,7**	**-5133**	**4316**	**3,59**	**9449**
SD	19,0	24,3	487,9	1101,0	0,3	1588,9
G 100 AV	139,0	350,0	-5964	3742	8,43	9706
G 100p AV	145,9	361,6	-6345	5784	38,62	12129
G 101 AV	153,4	414,6	-6126	6284	47,01	12409
G 101g AV	98,1	168,8	-3348	2843	2,79	6191
G 103 AV	88,6	247,6	-6224	5317	7,19	11540
G Sample AV	**125,0**	**308,5**	**-5601**	**4794**	**20,81**	**10395**
SD	29,5	98,8	1267,4	1448,0	20,4	2575,3
M2 78 AV	91,6	162,8	-3501	1247	2,73	4747
M2 113 AV	140,8	264,5	-5879	5200	32,86	11078
M2 Control AV	**116,2**	**213,7**	**-4690**	**3223**	**17,80**	**7913**
SD	34,7	71,9	1681,5	2795,0	21,3	4476,5
M2 79 AV	86,1	186,7	-5670	4768	8,91	10438
M2 80 AV	64,4	133,8	-4777	4240	4,24	9017
M2 81 AV	96,9	202,3	-5269	4449	23,21	9718
M2 82 AV	92,6	166,7	-5247	4800	7,11	10047
M2 Sample AV	**85,0**	**172,4**	**-5241**	**4564**	**10,87**	**9805**
SD	14,4	29,6	365,4	268,1	8,5	602,4
M3 92 AV	237,0	472,3	-6460	6000	44,76	12460
M3 112 AV	269,1	483,4	-5940	5930	51,07	11869
M3 Control AV	**253,1**	**477,8**	**-6200**	**5965**	**47,91**	**12165**
SD	22,7	7,9	368,2	49,4	4,5	417,5
M3 85 AV	265,0	521,6	-6213	6165	80,59	12378
M3 86 AV	172,3	230,3	-3398	1350	6,32	4748
M3 87 AV	206,9	432,1	-6469	5684	44,71	12153
M3 88 AV	159,8	332,3	-6324	5622	35,39	11945
M3 88 RIE AV	157,0	220,0	-3236	5424	5,67	8659
M3 89 AV	216,1	484,9	-6436	6023	56,55	12459
M3 91 AV	218,3	425,2	-6060	5879	25,87	11940
M3 Sample AV	**199,3**	**378,0**	**-5448**	**5164**	**36,44**	**10612**
SD	38,9	119,8	1463,1	1700,4	27,0	2905,5

A15: Influence of Hydrogen Peroxide to Fungal Etch Pit Depth (graphite)
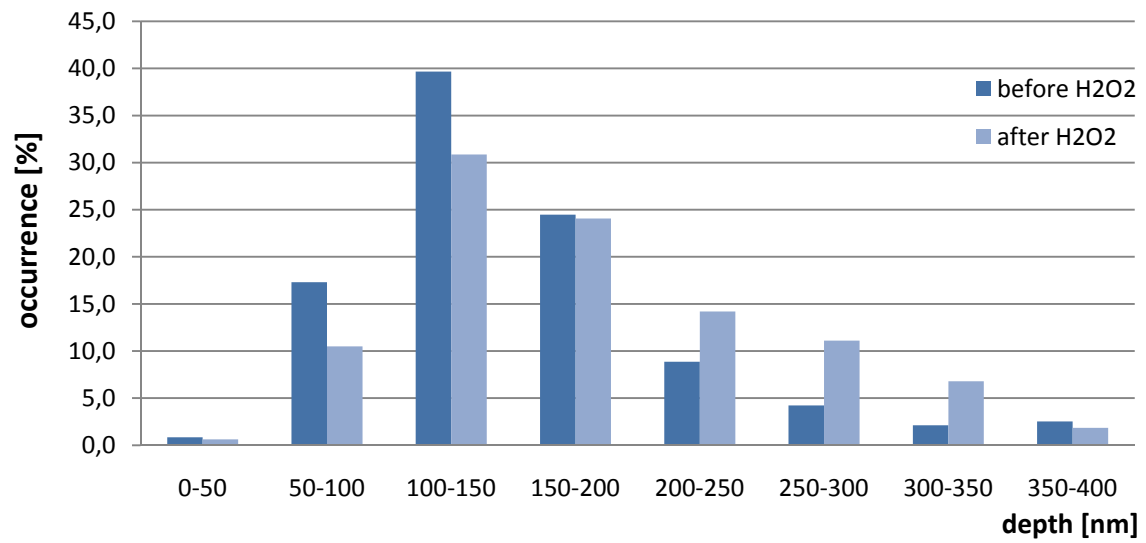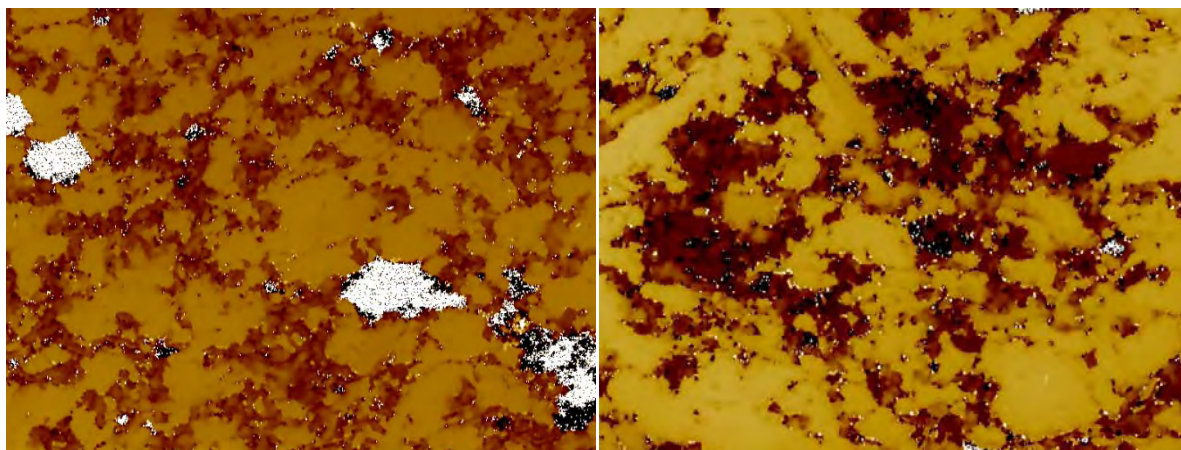
A16: VSI – Black Slate M2 Control Samples (160 x 120 nm)
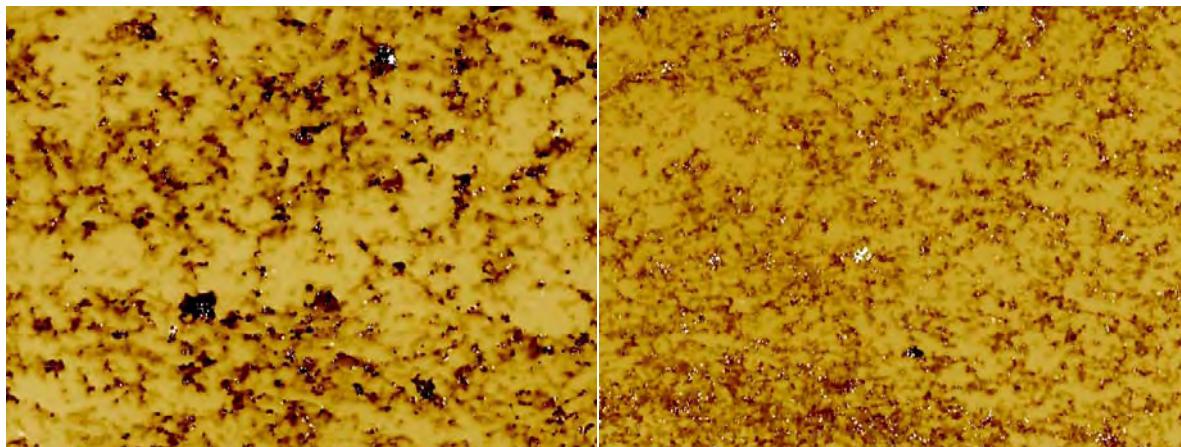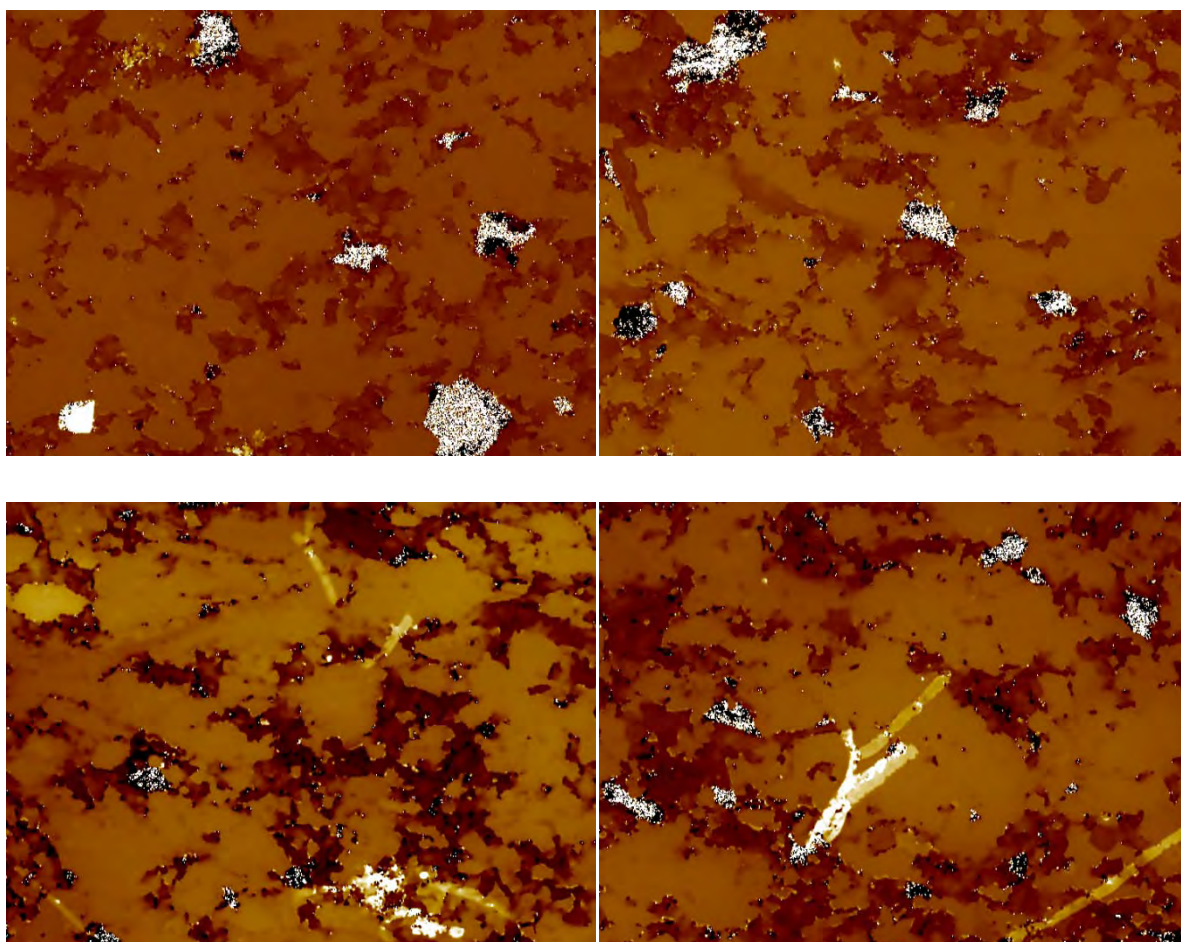

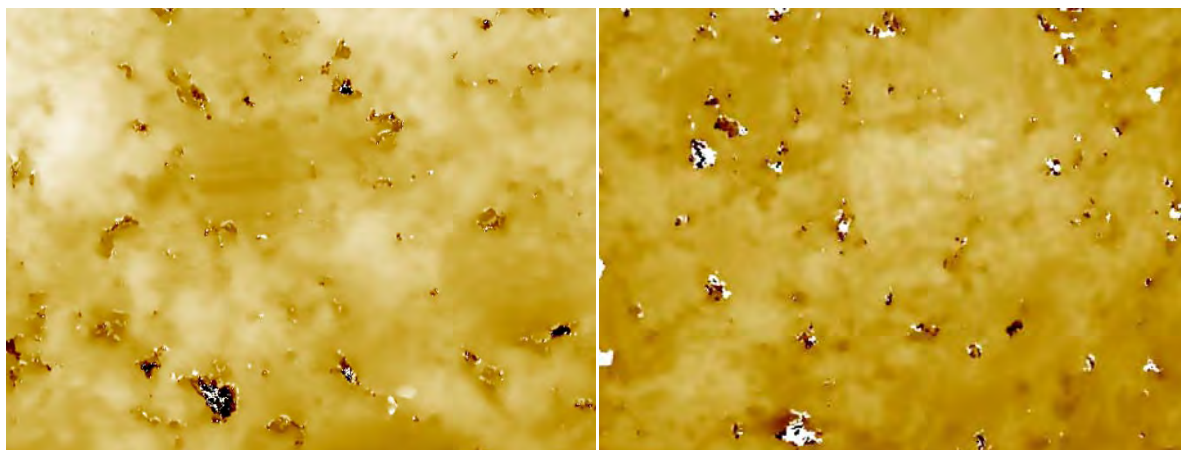**A17: VSI – Black Slate M2 Incubated Samples** (160 x 120 nm)
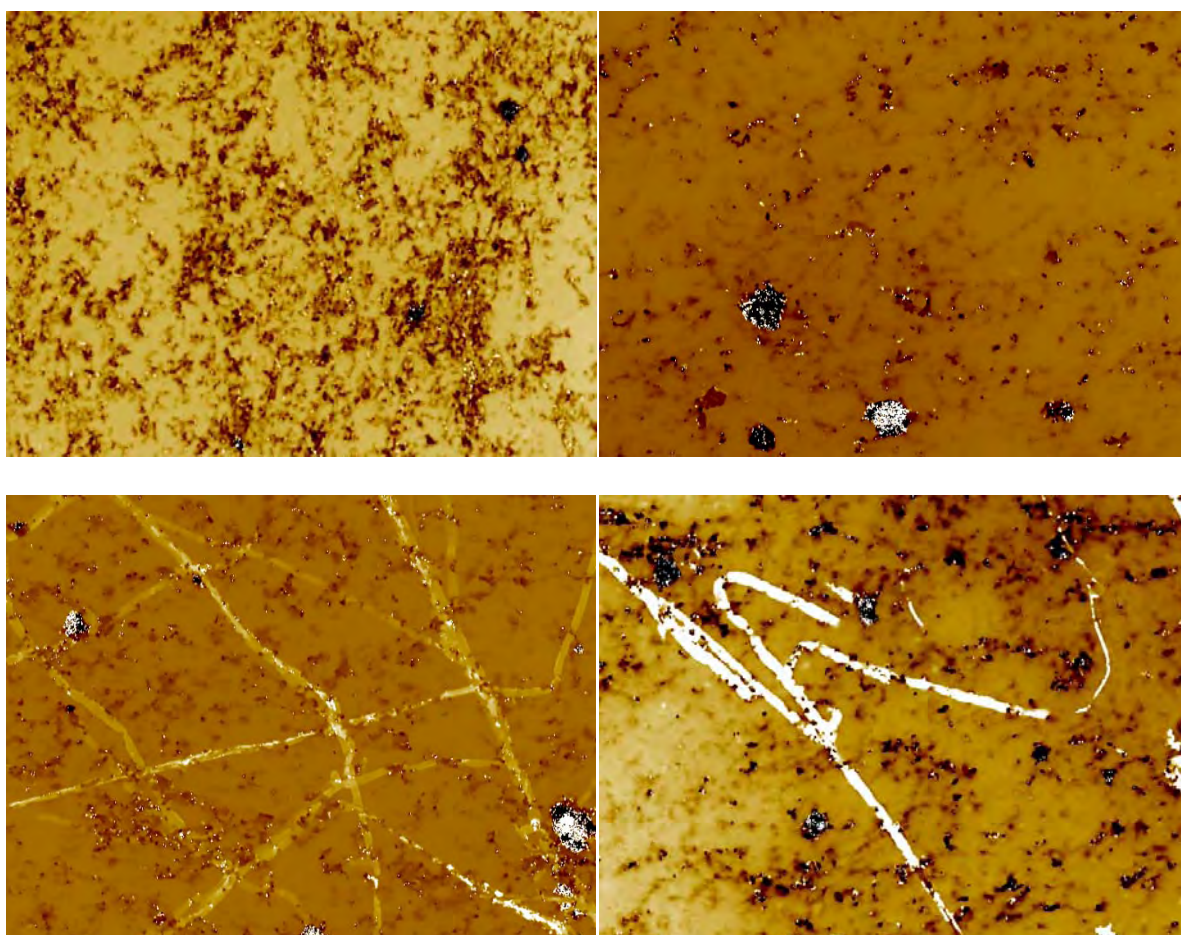
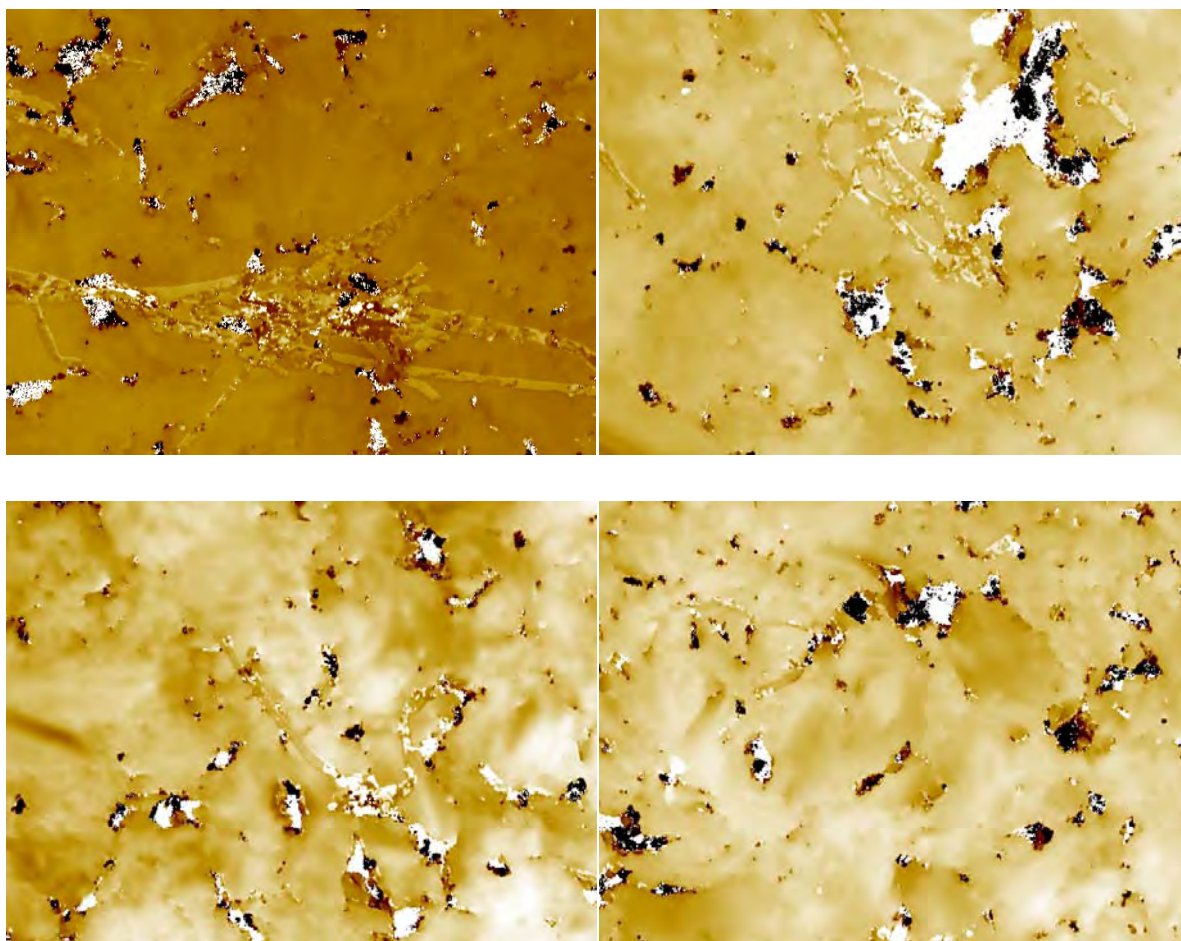**A18: VSI – Black Slate M3 Control Samples** (160 x 120 nm)

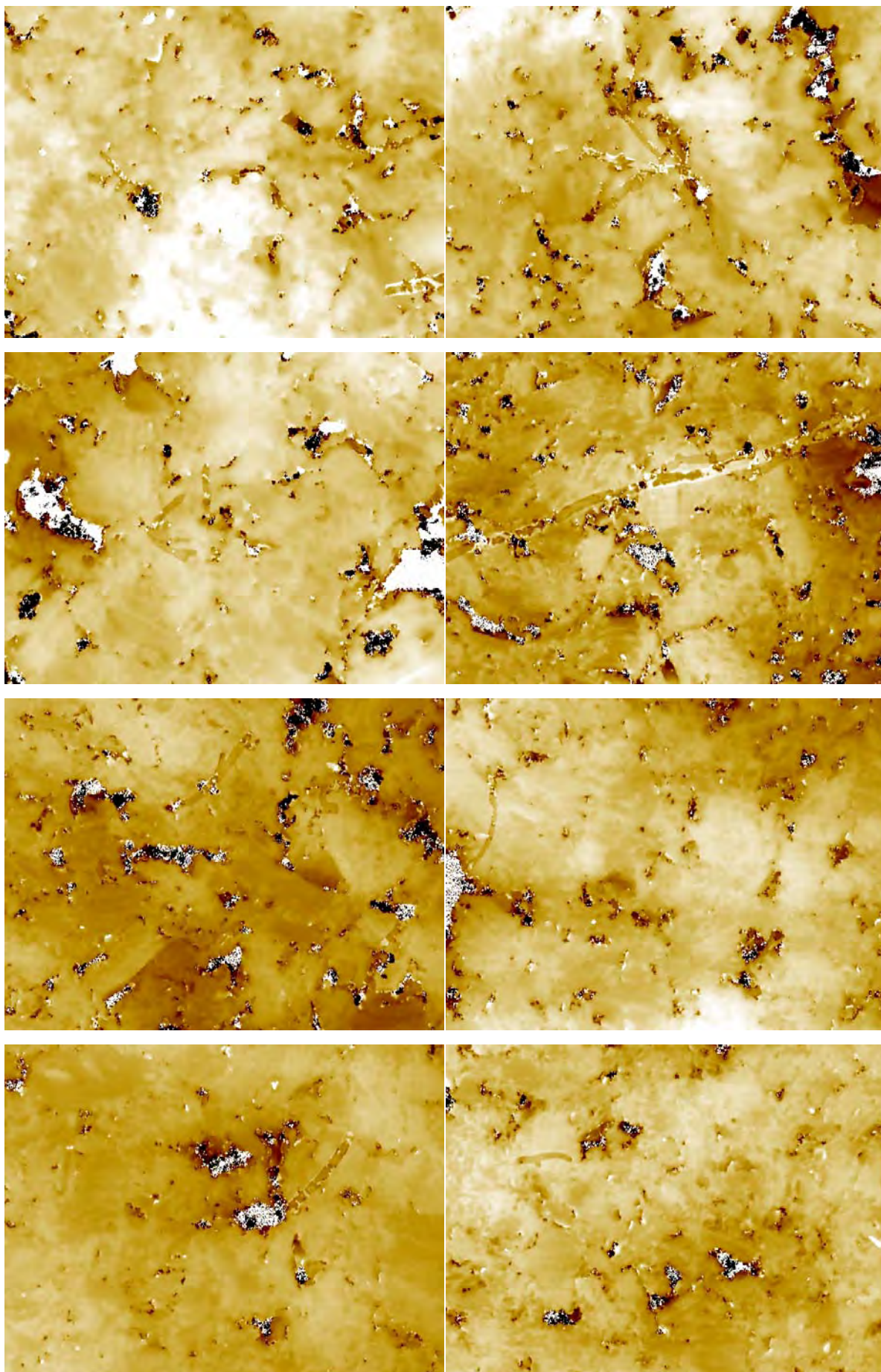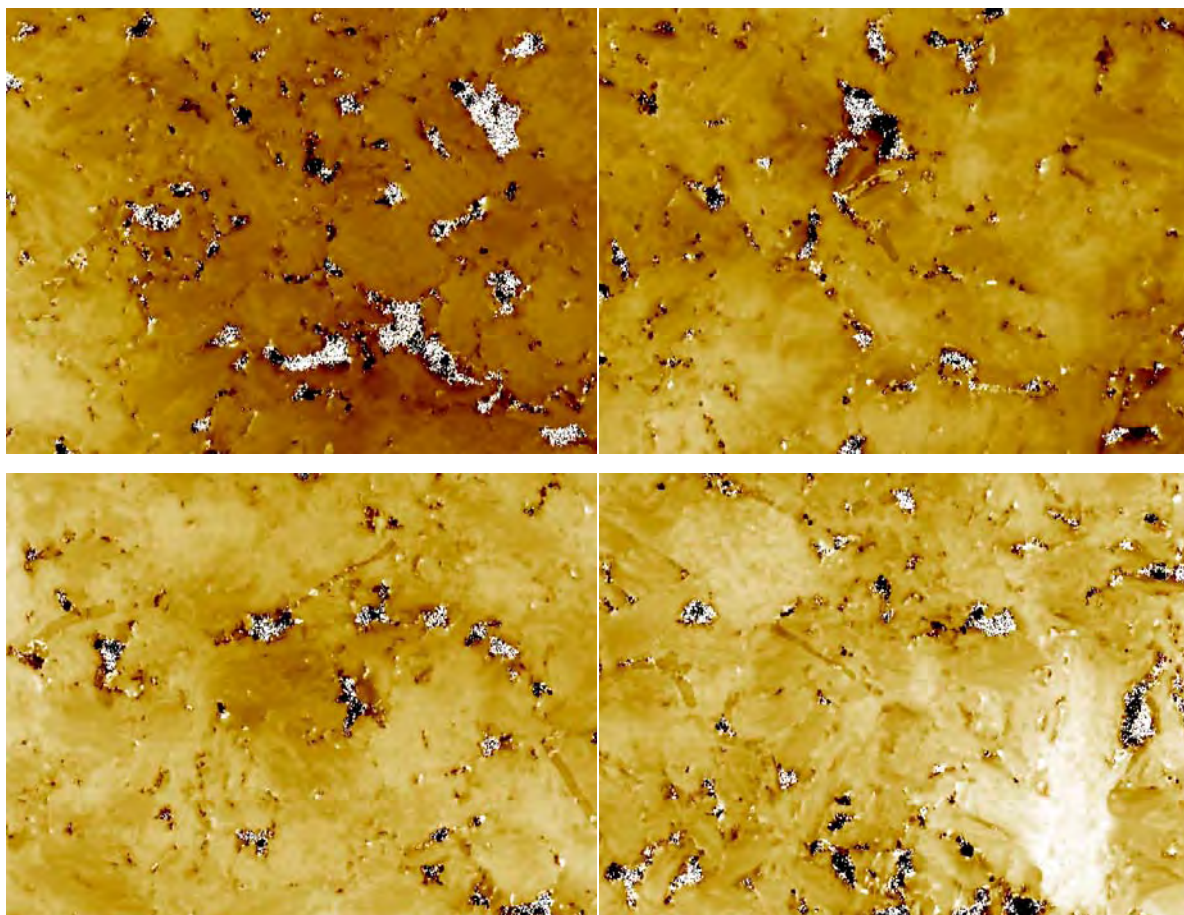**A19: VSI – Black Slate M3 Incubated Samples** (160 x 120 nm)

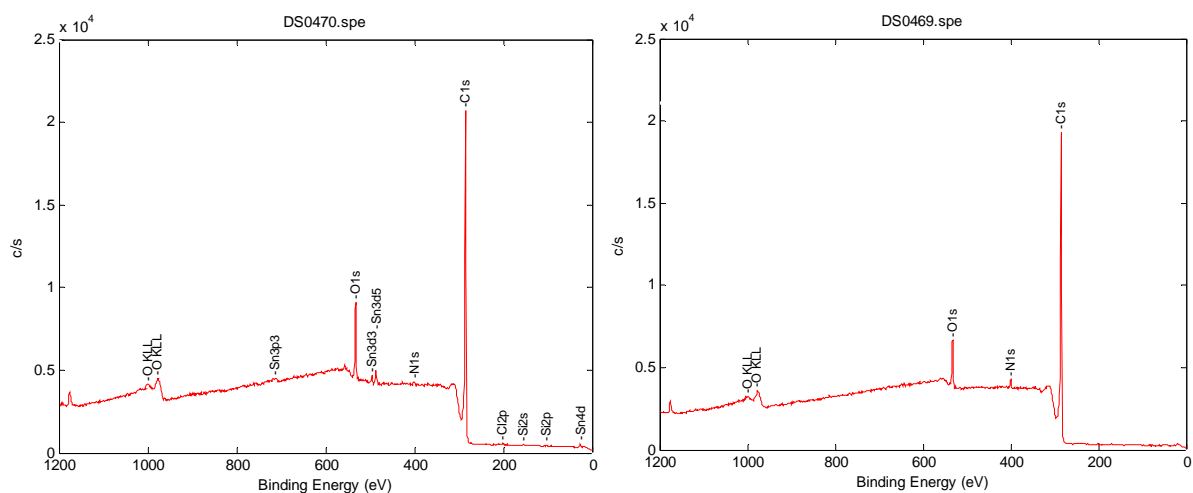**A20: VSI – Graphite Control Samples** (160 x 120 nm)
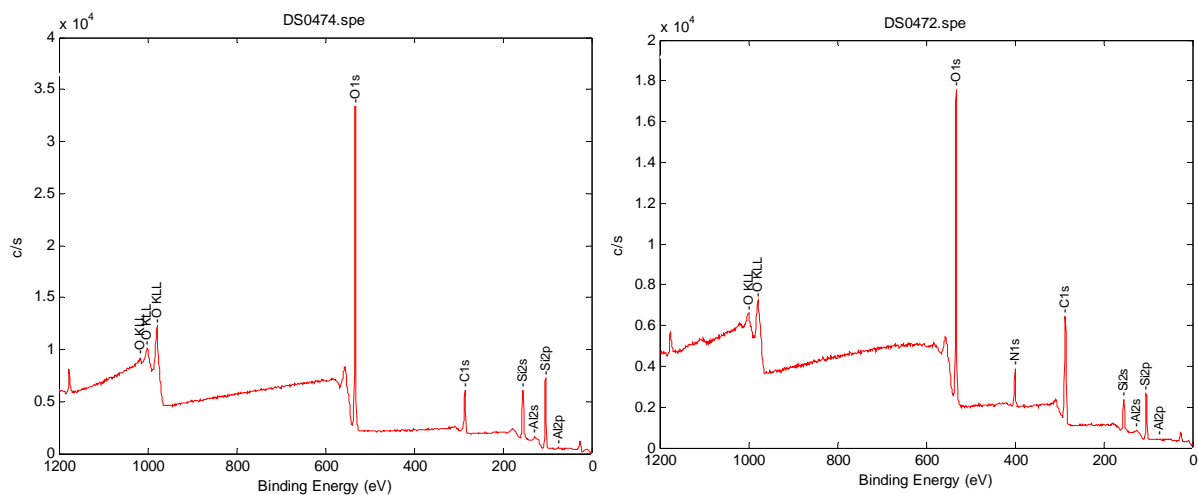

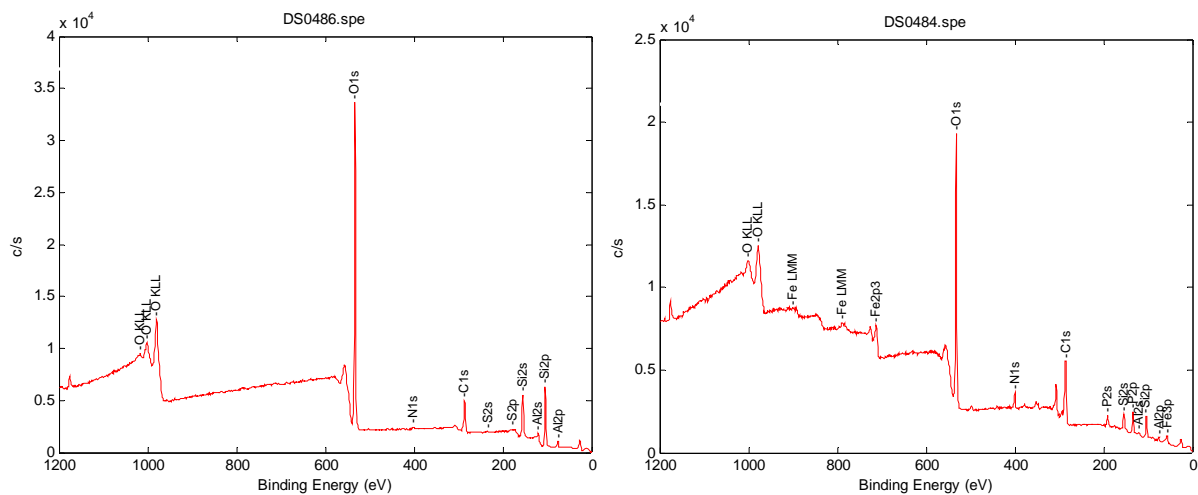**A21: VSI – Graphite Incubated Samples** (160 x 120 nm)

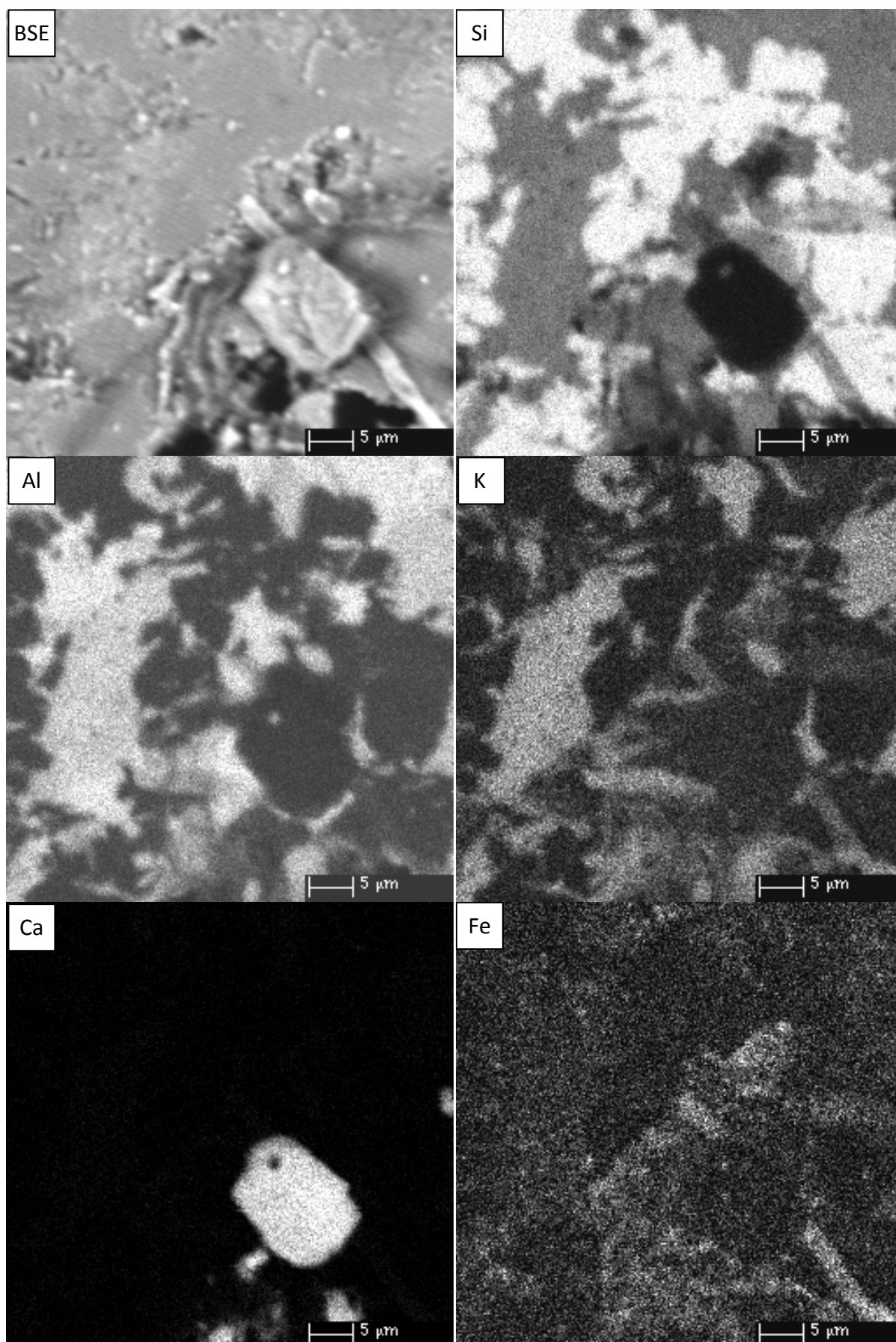## A22: XPS Spectra of Graphite control and incubated sample

A23: XPS Spectra of Black Slate (M2) control and incubated sample
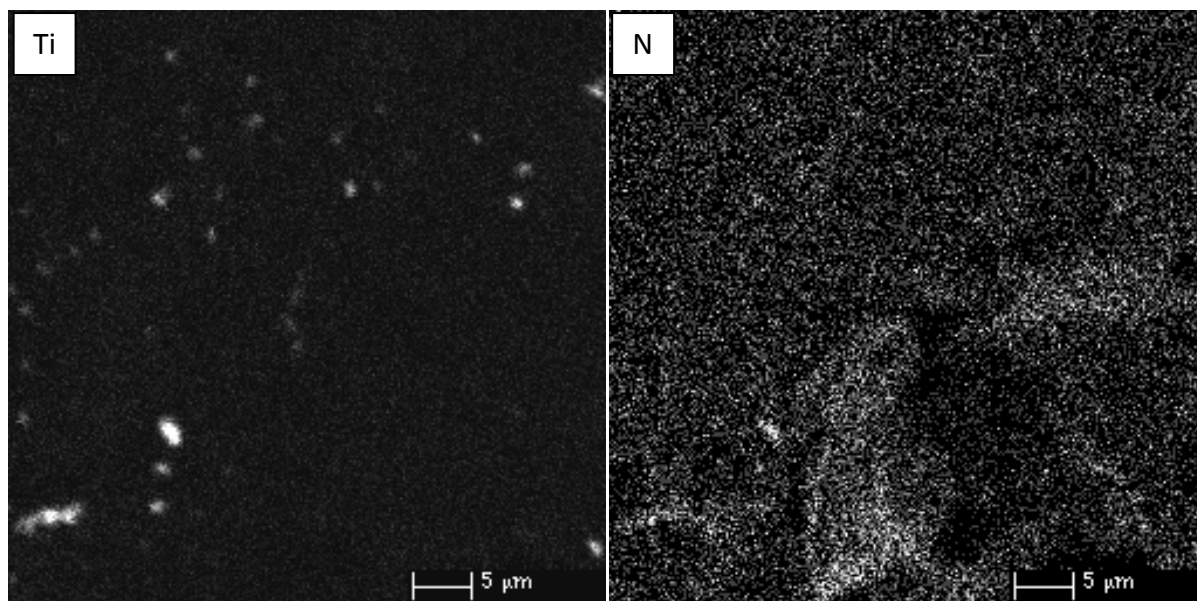

A24: XPS Spectra of Black Slate (M2) control and incubated sample

A25: EMP – Element Mapping of Black Slate M3 (85)

Selbständigkeitserklärung

Ich erkläre, dass ich die vorliegende Arbeit selbständig und unter Verwendung der angegebenen Hilfsmittel, persönlichen Mitteilungen und Quellen angefertigt habe.

Jena, 27. Mai 2010